Dissertation
submitted to the
Combined Faculties for the Natural Sciences and for Mathematics
of the Ruperto Carola University of
Heidelberg, Germany
for the degree of
Doctor of Natural Sciences

presented by:


| | |
|---|---|
| Diplom-Physicist: | Klaus Borkenstein |
| born in: | Aachen |


Oral examination: November 7th, 2001

# Modeling and computer simulation of tumor growth and tumor response to radiotherapy

Referees: Prof. Dr. Wolfgang Schlegel
Prof. Dr. Josef Bille

## Zusammenfassung

### Modellierung und Computersimulation des Tumorwachstums und der Tumorantwort auf Strahlentherapie

Gegenwärtig werden in der Strahlentherapie Gesamtdosis und Fraktionierungsschema der geplanten Bestrahlung vom Strahlentherapeuten anhand seiner klinischen Erfahrung ausgewählt. Diese Erfahrungswerte sollen um eine computersimulierte Tumorantwort auf Bestrahlung ergänzt werden, die auf biologischen Zusammenhängen basiert. Ziel der Arbeit ist die Entwicklung und Implementierung eines radiobiologischen Modells auf zellulärer Ebene, das die dreidimensionale Computersimulation von Tumoren klinisch relevanter Größe ermöglicht. Simulationen von Tumorproliferation und Tumorantwort auf Strahlentherapie anhand des entwickelten Modells erlauben es, den Einfluss einzelner radiobiologischer Größen auf das Tumorverhalten zu untersuchen. Simuliertes ungestörtes Tumorwachstum wird verglichen mit entsprechenden experimentell ermittelten Wachstumskurven in vivo. Für unterschiedliche radiobiologische Parameter, wie etwa Zellzykluszeit, Wachstumsfraktion und Strahlenempfindlichkeit, werden Gesamtdosen angegeben, die bei konventioneller und bei beschleunigter Fraktionierung appliziert werden müssen, um Tumorkontrolle zu erreichen.

## Abstract

### Modeling and computer simulation of tumor growth and tumor response to radiotherapy

In radiotherapy, total dose and time-dose patterns are currently chosen according to the clinical expertise of the radiation oncologist. To aid radiation oncologists in the treatment planning process, it is important to quantitatively assess tumor response to irradiation. The objective of this work is to devise a cellular radiobiological model and to develop three-dimensional simulation methods that allow simulation of tumors with clinically relevant sizes. Simulations of unperturbed tumor proliferation are compared to corresponding experimental growth curves in vivo. The most important radiobiological parameters are identified and their influence on tumor growth and tumor response to irradiation is quantified. Total doses needed by conventional and accelerated fractionation schemes for tumor control are given for different radiobiological parameters, such as cell cycle time, growth fraction and radiosensitivity.

# Contents

# Chapter 1

# Introduction

About 50% of all cancer patients are subject to radiation treatment, either to radiotherapy alone or in combination with surgery or chemotherapy [67]. Radiation oncology aims at maximizing tumor control while minimizing normal tissue complications. Treating cancer patients with radiation is based on the damage radiation induces in cells. Tailoring dose distributions that deliver a high dose to the tumor volume and spare organs at risk as much as possible is of major concern in radiotherapy. This problem is addressed by three-dimensional conformal radiotherapy techniques such as intensity modulated radiotherapy (IMRT) [14, 15].

Finding a dose distribution that is an acceptable trade-off between tumor control and normal tissue complications is based on empirical knowledge and the radiation oncologist's clinical expertise. To further improve treatment outcome it is important to quantitatively assess the biological effect the delivered dose has on the tumor and on normal tissues. In recent years biological models have been proposed to aid radiation oncologists in the decision making process. Radiobiological models aim at predicting probabilities for either tumor control [52, 82, 80, 110] or normal tissue complications [73, 117] based on physical parameters, such as the dose distribution, and biological parameters, such as the radiosensitivity of the tumor.

Current radiobiological models are either derived from biological first principles or from empirical observations [119]. Mechanistic models allow for a more realistic description of tumor behavior, but the simplicity of phenomenological models makes them more appealing for clinical practice. All present models restrict their number of parameters to reduce their complexity [119]. A novel approach to radiobiological modeling and simulating treatment outcome is founded on a cellular description of tumor growth and tumor response to irradiation. Switching to a cellular level allows for the introduction of additional cell biological parameters and processes to those that are usu-

ally accounted for in biological modeling. This approach was first introduced by Düchting et al [41, 42] and Kocher et al [63, 64, 65].

The objective of the work described here is to devise a cellular radiobiological model and to develop three-dimensional computer simulation methods that allow to predict tumor control for different tumor entities and treatment scenarios. In order to be validated by clinical data, a simulation tool must predict tumor control for tumors of clinically relevant sizes. It will be shown that simulating tumor proliferation up to diameters of 12 mm is feasible with the cellular methods presented here.

The model presented in this work takes into account more radiobiological parameters than current models do. This allows for a more realistic description of tumor behavior. Including biological processes such as the oxygenation status of individual cells [102, 96] and tumor angiogenesis [56, 46] is crucial in developing a simulation tool that is capable of predicting tumor control by radiotherapy. It has been pointed out that treatment outcome depends crucially on the time-dose pattern chosen and that strategies have to be employed to account for days off in dose-fractionation schedules [57, 8]. It will be shown that the cellular approach chosen in this work allows to consider time dependent effects throughout the treatment. Current mechanistic models [105, 109, 107, 18, 40] try to account for the time factor in radiotherapy by defining global parameters quantifying effects such as repopulation. Due to the dynamic behavior of tumors in the cellular approach, there is no need to define global parameters to allow for the time factor in tumor response.
The cellular model presented is a tumor model only. No modeling of normal tissue complications is attempted in spite of their significance for treatment outcome.

The cellular approach to biological modeling of tumor growth and tumor response to radiotherapy tries to account for the most important cell biological parameters governing tumor behavior. The complexity of cellular models requires an understanding of the underlying biological mechanisms and the knowledge of the values of the input parameters. The chapters introducing the cellular radiobiological model, chapters 2 to 4, will therefore start out with a brief outline of the biological processes involved. The biological basis of the tumor model will be described from a perspective of modeling, which is a very simplistic one. Complex interactions on a molecular level, such as proteins triggering events like cell death or repair mechanisms, will be reduced to a description of causes and effects.

In section 2.1 the most basic parameters influencing unperturbed tumor growth will be sketched. Simplifying the complex processes of tumor pro-

liferation yields a cellular model that allows computer simulation of tumor growth up to diameters of 12 mm. How to implement this model will be described in section 2.2.

Tumors cannot reach clinically detectable sizes without securing their own blood supply by generation of new vasculature penetrating the tumor [56]. This process is called angiogenesis. The angiogenesis model used to simulate tumor angiogenesis is explained in chapter 3.

Tumor response to radiotherapy is modeled based on the linear-quadratic formalism [70, 27, 34] to calculate survival fractions of cell populations subject to a certain radiation dose. Its biomechanistical rationale is given in chapter 4. It has been shown that fractionating total dose over a certain period of time rather than administering it in one single dose allows escalating total dose and increasing tumor control without increasing normal tissue complications [104, 108, 4]. The radiobiological basis for dose-fractionation patterns will be derived from the parameters of the linear-quadratic model for tumors and normal tissues. Time dependent effects due to the dynamic behavior of tumors can influence treatment outcome of fractionated radiotherapy. The "4 Rs" of radiotherapy [115], repair, repopulation, redistribution and reoxygenation, address these phenomena.

The simulation results presented in chapter 5 demonstrate the relationships between tumor behavior and the model parameters chosen. Three-dimensional computer simulations of tumor growth up to diameters of 12 mm are presented. Tumor response to irradiation is simulated for different radiobiological parameters and two fractionation schemes.

The work presented aims to reduce the gap between radiobiological research and clinical practice by three-dimensional computer simulation of tumor control. It will be shown that simulations of tumor behavior qualitatively agree with experimental data. The computer simulation methods developed in this work aim at identifying the crucial parameters in tumor growth and tumor response to irradiation. Their influence on tumor control will be quantified. Total doses needed for tumor control will be given for different time-dose patterns and various radiobiological parameters.
Validating any model requires comparing predictions based on simulations with corresponding experimental and clinical data. In section 5.3, simulations of tumor growth will be compared to observed growth of Dunning R3327 prostate carcinoma in male Copenhagen rats.
This work is designed to lay the foundations for a future integration of the simulation tool for prediction of tumor response to radiotherapy into clinical practice.

# Chapter 2

# Modeling tumor growth

Current radiobiological models calculate the outcome of radiotherapy by use of a restricted number of global parameters, such as radiosensitivity of tumor cells and clonogenic cell density [52, 82, 80, 110].
A more realistic model of tumor response to irradiation must take into account the dynamic behavior of the tumor. Repair [105], redistribution [18, 100] and repopulation [109, 107, 40] have been modeled but other effects that reflect the dynamic characteristics of tumors such as oxygen supply, re-oxygenation and angiogenesis are not considered. Furthermore, no unified model exists to date. Time dependent effects are modeled separately. The cellular radiobiological model presented here includes the main factors influencing tumor proliferation. Elaborating on tumor growth allows to take into account time dependent effects during radiotherapy in a more realistic way than current radiobiological models do.

In section 2.1 some basic processes governing tumor proliferation will be introduced. Cell proliferation and apoptosis, programmed cell suicide, are discussed in sections 2.1.1.1 to 2.1.1.4. The influence exerted on the tumor by its microenvironment is described in sections 2.1.2 and 2.1.3.
Comparing simulated tumor behavior to experimentally observed tumor proliferation is crucial to validate the cellular model and its implementation into a simulation tool. The tumor system chosen for comparison, the Dunning R3327 prostate tumor system, will be introduced in section 2.1.4.
Based on the main biological processes of tumor proliferation identified in section 2.1, a cellular tumor growth model will be devised in section 2.2. Section 2.2.2 will discuss important aspects of implementing the model to perform computer simulations. Simplifications made to enhance computer perfomance will be pointed out.

## 2.1 The biological basis of tumor growth

Tumor growth is determined by cell proliferation and cell death. Both processes will be described in a very mechanistic manner. This section serves as a background for the tumor growth model devised in section 2.2.

### 2.1.1 Cell proliferation

In normal tissues there is an equilibrium between cell proliferation, determined by the cell cycle time, the growth fraction and the ability to undergo apoptosis (see figure 2.1). The cell cycle duration is the time span between two cell divisions. The growth fraction is defined as the fraction of well oxygenated cells that do actively proliferate. Apoptosis is programmed cell suicide, a phenomenon first described by Kerr et al in 1972 [62].

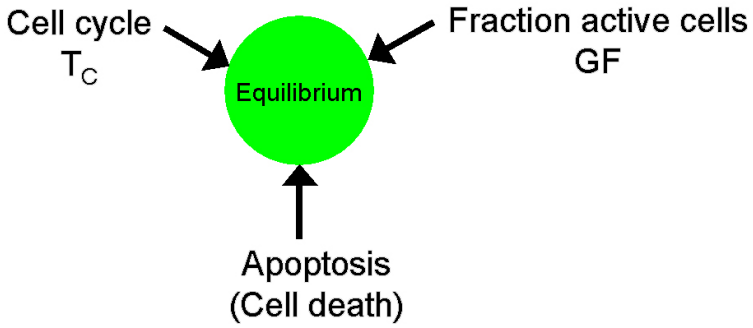


Figure 2.1: *In normal tissues there is an equilibrium between the three factors governing the proliferation and death of cells: The duration $T_C$ of the cell cycle, the growth fraction GF and the ability to undergo apoptosis (programmed cell death).*

#### 2.1.1.1 Cell cycle

Cell division takes place during mitosis (M phase), which only lasts a few hours. Cells spend most of their time in interphase, the time between successive mitoses. Interphase is made up of three phases. Mitosis is followed by the $G_1$ phase (G for gap). During synthesis (S phase), the DNA is duplicated. Synthesis is followed by the $G_2$ phase after which another mitosis takes place. Differences in cell cycle time are mostly due to differences in the duration of $G_1$. Mitosis and $G_2$ usually last only a few hours [35, 55].

Analyzing cell kinetics can be done by feeding cell cultures with agents that are taken up and incorporated into the DNA during S phase. Feeding a pulse of bromodeoxyuridine (BrdUrd) and adding a stain allows to determine

the fraction of cells in synthesis by counting the number of cells that have been labeled by BrdUrd (labeling index LI). This technique also serves to determine the time span $T_S$, during which DNA is duplicated, the time span between synthesis and mitosis, $T_{G_2}$, and the duration of mitosis, $T_M$, itself. If all tumor cells are proliferating, the cell cycle time $T_C$ can be calculated from the labeling index and the duration of synthesis $T_S$:

$$T_C = \lambda \frac{T_S}{LI} ,$$

where $\lambda$ is a factor correcting the fact that cells are not distributed uniformly along the cell cycle because of cell production during mitosis. Hall suggests $\lambda = ln2$ based on the assumption of an exponential distribution of cells in time [55], but $\lambda = 0.8$ is used mostly [101]. In flow cytometry a fluorescent-labeled antibody instead of a staining agent is added. The labeling index LI is determined by passing a suspension of labeled cells through a laser beam and detecting the fluorescence. Flow cytometry allows for much faster estimation of $T_S$ and the cell cycle time $T_C$ than the staining technique does. Table 2.1 lists median cell proliferation parameters for selected human tumor entities measured by flow cytometry.

#### 2.1.1.2 Tumor growth fraction

In normal tissues the majority of cells does not actively proliferate. Only 14% of intestinal epithelial cells are in cell division cycle and only 0.01% of endothelial cells are [56, 46]. Inactive cells are called quiescent cells and are treated as being in an additional phase, termed $G_0$, which follows $G_1$. The fraction of cells that are capable of proliferation and actively do proliferate is defined as the growth fraction, GF. A major cause for the growth disequilibrium observed in tumors is the increase in their growth fraction. The Myc oncogene is frequently associated with activating cells in $G_0$. Its expression is deregulated in many human cancers [12]. Tumors exhibit growth fractions of up to 100% [72], compared to growth fractions of below 20% for all normal tissues. Tumor proliferation is mostly quantified as $T_{pot}$, the potential doubling time. $T_{pot}$ is defined as

$$T_{pot} = \frac{T_C}{GF}.$$

In flow cytometry it is measured as

$$T_{pot} = \lambda \frac{T_S}{LI} ,$$

which equals $T_C$ if all cells capable of mitosis do actually proliferate and GF=100%. It can be seen from table 2.1 that the increasing tumor proliferation (decreasing $T_{pot}$) of less differentiated aneuploid cell lines is mostly due to an increase in growth fraction (corresponding to a higher LI) and only to a lesser extent due to a decrease in $T_S$.

| Tumor | LI [%] | $T_S$ [h] | $T_{pot}$ [d] |
|---|---|---|---|
| HNSCC [47] | 8 | 13.7 | 6.2 |
| diploid | 5 | 13.5 | 7.7 |
| aneuploid | 9.5 | 13.8 | 5.0 |
| HNSCC [113] | 4.9 | 9.9 | 6.4 |
| diploid | 3.9 | 8.9 | 8 |
| aneuploid | 9.3 | 11.5 | 4.2 |
| HNSCC [7] | 9.9 | 9.9 | 5.7 |
| Cervical tumors[13] | 9.5 | 12.1 | 4.4 |
| size<5cm | 9 | 11.7 | 4.9 |
| size>5cm | 11.7 | 12.5 | 4.0 |
| Cervical tumors [113] | 11.6 | 15.8 | 4.5 |
| diploid | 6.1 | 13.8 | 6.9 |
| aneuploid | 16.9 | 16.9 | 4.4 |
| Rectal cancer [103] | 21.2 | 20.7 | 3.3 |
| Rectal cancer [113] | 9 | 13.1 | 3.9 |
| diploid | 8.5 | 11.1 | 5.4 |
| aneuploid | 12 | 15 | 3.5 |
| Lung cancer [113] | 8 | 15.1 | 7.3 |
| diploid | 2.2 | 12.9 | 17 |
| aneuploid | 9.5 | 15.8 | 4.7 |

Table 2.1: *Cell kinetics for selected human tumors. Less differentiated aneuploid tumor cells have higher labeling indices.*

#### 2.1.1.3 Apoptosis

The third mechanism responsible for growth equilibrium in normal tissues is apoptosis, programmed cell suicide. Tissues with a large turnover rate such as mucosa have relatively low cell cycle times and relatively high growth fractions. Equilibrium can only be obtained if there is a mechanism for controlled cell death after a certain number of cell divisions. Besides ensuring equilibrium, apoptosis fulfills two further needs. It is a control mechanism to remove cells that have served their purpose, such as lymphocytes, and

it inhibits mutagenesis. A mammalian genome undergoes about 100,000 modifications per day [91], each carrying a finite probability for DNA damage. It is clear that having a mechanism that controls DNA integrity is of high priority. Apoptosis is triggered by external and internal signals which induce the cell to produce enzymes causing its death.
Deactivation of apoptosis is a main cause for malignant diseases. Mutations to the tumor suppressor gene p53 are observed in more than 50% of human cancers [12, 89]. Transformation to malignant growth is also associated with a class of oncogenes, the bcl-2 family, that inhibit (and promote) apoptosis. The bcl-2 oncogene has been isolated from 70% of human breast, 30-60% of human prostate and 90% of human colo-rectal cancers [31].
With decreasing differentiation, tumor cell lines show decreasing ability to undergo apoptosis. Anaplastic tumors often show no apoptosis at all.
Apoptotic cells lose contact with their neighbors, decrease in size and show condensed chromatin. They fragment into small membrane bound blebs termed apoptotic bodies [62].

Apoptosis is also a response to external injury, such as radiation damage, but this aspect of apoptosis is not considered here. Induction of apoptosis by radiation is located at the transition from $G_2$ to M.

#### 2.1.1.4 Cell cycle checkpoints

Transition from one cycle phase to another is accompanied by the expression of a number of proteins, most notably cyclins and cyclin-dependent kinases. Control mechanisms exist to inhibit cells with chromosome aberrations to pass into the next cycle phase. Thus, mutagenesis is prevented in healthy tissues. Cell cycle checkpoints were defined to describe control mechanisms at the $G_1$-S transition, throughout S phase, and at the $G_2$-M transition [111, 112]. Failing to pass checkpoints causes either cycle phase arrest or cell death [12, 10]. Cells that do not pass the $G_1$-S checkpoint are either arrested for DNA repair or die of apoptosis [12]. Those that do not pass the $G_2$-M checkpoint (also termed the DNA damage checkpoint) usually die of mitotic death, but apoptosis can also be induced at this point. $G_1$ arrest for repair is mediated by the protein p21 which is induced by another protein, p53. p53 is also capable of blocking the transition through synthesis. Inhibition of the complex composed by $p34^{cdc2}$ and cyclin B1 causes a delay at the $G_2$-M transition to enable repair of DNA damage [79]. By deleting specific genes in mutants, loss of checkpoint mechanisms can be induced. Failure of the $G_2$-M DNA damage checkpoint, for instance, can be provoked by deleting the Rad9 gene [86].

### 2.1.2 Oxygenation, hypoxia and necrosis

Cells depend on supply with oxygen and nutrients to survive. Oxygen diffuses from capillaries, which form the microscopic part of the vascular system. Capillaries have diameters from approximately 10 $\mu$m to 20 $\mu$m [71]. Oxygen supply in tissues does not only depend on oxygen diffusion around capillaries but on oxygen consumption, too. Oxygen concentrations around cylindrical vessels and within two-dimensional networks of blood vessels have been modeled by Tannock [102] and by Secomb et al [96]. The results obtained in these publications will be presented briefly.

Assuming radial symmetry, the equation for steady state diffusion around a cylindrical blood vessel is

$$D\frac{1}{r}\frac{d}{dr}(r\frac{dp}{dr}) = kQ_{O_2} \ .$$

$D$ is the diffusion coefficient in $\frac{cm^2}{s}$, $p$ is the oxygen tension $pO_2$ at radius $r$ in mm Hg, $Q_{O_2}$ is the rate of oxygen consumption in $\frac{\mu l}{mg\,h}$ and $k$ is a constant [102]. It is assumed that oxygen consumption does not depend on oxygen concentration. With the blood vessel radius $a$, the blood oxygen tension $p_0$ and the diffusion radius $R$, the diffusion equation must be solved for the following boundary conditions:

- $p$ is equal to the blood oxygen tension adjacent to a capillary (which means $p = p_0$ at $r = a$).
- Both $p$ and the oxygen flow are zero at the diffusion radius (which means $p = \frac{dp}{dr} = 0$ at $r = R$).

Introducing the parameter

$$R_0 = \sqrt{\frac{4Dp_0}{kQ_{O_2}}}$$

the solution to the diffusion equation can be expressed as

$$p = p_0(1 + \frac{r^2 - a^2}{R_0^2} - 2\frac{R^2}{R_0^2}\ln\frac{r}{a}) \ .$$

Typical values for $R_0$ and $a$ have been published by Tannock [102], showing that the term $\frac{a^2}{R_0^2}$ can be neglected. The diffusion radius $R$ at which $p = 0$ is therefore given by

$$R_0^2 = R^2(2\ln\frac{R}{a} - 1) \ .$$

$\frac{R}{R_0}$ is relatively constant for a wide range of diffusion radii. The oxygen tension $p$ at radius $r$ can be calculated by

$$p = p_0 \frac{R^2}{R_0^2}(2 \ln \frac{R}{r} - 1 + \frac{r^2}{R^2}) \ .$$

The parameter $R_0$ involves the diffusion coefficient $D$ and the blood oxygen tension $p_0$ which is lower for venous blood (40 mm Hg) than for arterial blood (100 mm Hg). At 37°C, $D = 2 \times 10^{-5} \frac{cm^2}{s}$ is assumed [102]. Figure 2.2 shows how oxygen tension decreases exponentially with capillary distance. The black curve represents venous blood flow, a capillary size of 20 $\mu$m and a diffusion radius of 150 $\mu$m. The blue and red curves represent arterial blood flow with the same capillary size of 20 $\mu$m and different diffusion radii, $R = 150\,\mu$m (blue) and $R = 180\,\mu$m (red).

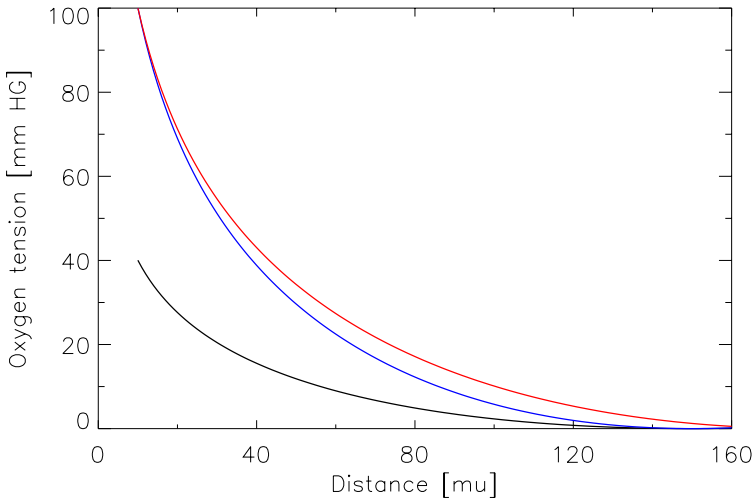


Figure 2.2: *Oxygen tension $pO_2$ around a cylindrical blood vessel for diffusion for venous blood (black curve) and arterial blood (colored curves). The oxygen tension represented by the red curve corresponds to a diffusion radius R of 180 $\mu m$. The diffusion radius chosen in the calculation of the black and blue curves is $R = 150\,\mu m$.*

Simulations of oxygen tension for two-dimensional (random) vessel networks have been performed by Secomb et al based on the diffusion equation

$$D\Delta c = M(c) \text{ [96]}.$$

Again, $D$ is the diffusion coefficient, $c$ is the oxygen concentration and the rate of oxygen consumption is $M$. The concentration $c$ is considered to depend

linearly on oxygen tension $p_{O_2}$. Consumption $M$ is taken to be related to concentration $c$ by Michaelis-Menten kinetics

$$M(c) = M_0 \frac{c}{c + \alpha P_M} ,$$

where $M_0$ is the consumption rate when oxygen is not rate-limiting and $P_M$ is the $pO_2$ at which M falls to $\frac{M_0}{2}$. The boundary condition is $\frac{\partial c}{\partial n} = 0$ for tissue boundaries. The vessels of the random network are considered to have uniform diameter and constant blood flow rate. A typical result of simulations run by Secomb et al for a number of random networks is presented in figure 2.3.

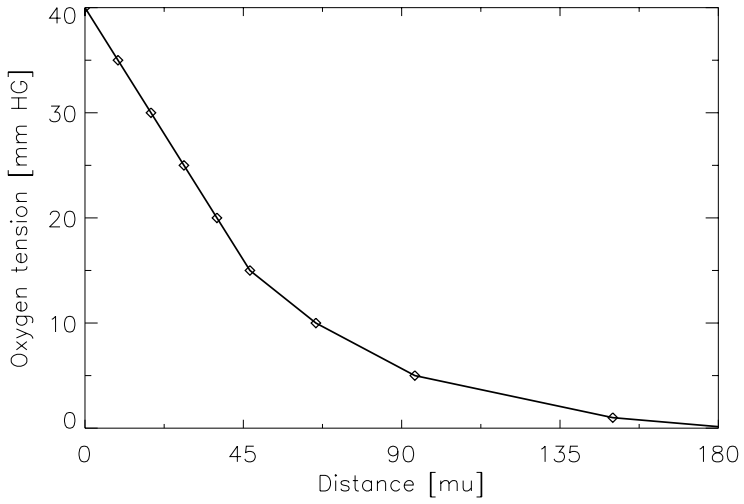


Figure 2.3: *Oxygen concentration (illustrated as oxygen tension $pO_2$ in mm Hg) around vessels for a two-dimensional random network of venous blood vessels according to Secomb et al [96].*

Cells that are well supplied with oxygen are called normoxic. Within the tumor it is the normoxic cells that proliferate. Reduced oxygen tension of 5 to 10 mm Hg forces cells into hypoxia, a state in which they do no longer proliferate [60, 59]. Certain proteins that trigger tumor angiogenesis, however, become overexpressed in hypoxia. Hypoxic cells do not move through the cell cycle and do not undergo apoptosis. At distances of 100 $\mu$m or more from the nearest capillary oxygen levels are considered so low that cells become hypoxic (see figure 2.4). This distance corresponds to about five cell layers [49].

Severe lack of oxygen causes necrosis. Cells that are more than 150 $\mu$m (7-8 cell layers) away from the nearest capillary become necrotic [23]. Necrotic

cells can easily be distinguished histologically from apoptotic cells. Whereas apoptosis effects individual cells, necrosis is usually observed within a whole group of cells. Necrosis is characterized by a loss of membrane integrity which means that necrotic cells release their contents and cause an inflammatory reaction [36, 12].

In addition to the potential doubling time $T_{pot}$ used to describe cell proliferation, the tumor doubling time $T_d$, is defined to quantify tumor growth. $T_d$ takes into account cell loss, which is defined as the fraction of cells unable to proliferate. This fraction comprises dead cells (apoptotic or necrotic) and hypoxic cells. If the fraction of cells lost is termed $\Phi$, $T_d$ is defined as

$$T_d = \frac{T_{pot}}{\Phi}.$$

### 2.1.3 Lysis

Dead cells within a tumor are resorbed by two different mechanisms. Apoptotic cells are rapidly phagocytosed by adjacent cells and macrophages. They are recognized within a few hours and resorbed within around 24 h. Necrotic cells are resorbed by phagocytosis, as well. However, phagocytosis of necrotic cells by macrophages and immune cells happens more slowly than for apoptotic cells [31].

### 2.1.4 The Dunning R3327 tumor system

The tumor system chosen to compare simulated tumor growth with growth curves in vivo was the Dunning R3327 prostate tumor system. This system was chosen for three reasons. Firstly, prostate cancer is the most common cancer among men in Germany. Secondly, it is considered to be a useful animal model for human prostate cancer [61]. Thirdly, its cell kinetics are well known for several different degrees of differentiation [72, 93]. The cell kinetics parameters are presented in table 2.2. Table 2.3 lists the observed tumor volume doubling times and their cell loss $\Phi$. The AT1 subline is anaplastic, the HI subline is moderately well differentiated. Experimental data indicate that these two sublines have a growth fraction of 100% and no apoptotic cells. The well differentiated hormone dependent H subline has a mean volume doubling time of 20 days but has not been compared to simulated tumor growth because so far it is not certain whether the H subline has a tumor growth fraction below 100%. Experimental growth curves were obtained from tumor seeds ($\simeq 8$ mm$^3$) transferred subcutaneously into the distal right thigh of male adult Copenhagen rats. Tumor growth was measured starting from

volumes of about 300 $mm^3$. Experimental tumor volumes were calculated from three orthogonal diameters using the ellipsoid formula

$$V = D_1 \times D_2 \times D_3 \times \frac{\pi}{6} \, . \tag{2.1}$$

| Growth parameters | AT1 | HI | H |
|---|---|---|---|
| $T_S$ [h] | 8 | 10.7 | |
| LI [%] | 7±0.5 | 7±0.5 | 3.7±0.5 |
| $T_C$ [d] | 3.8±0.25 | 7.1 | |
| Growth fraction [%] | 100 | 100 | |
| Apoptotic capacity [%] | 0 | 0 | |

Table 2.2: *Growth parameters for three sublines of the Dunning R3327 prostate tumor system. The AT1 subline is anaplastic, the HI subline is moderately well differentiated. Measuring* $T_S$ *for the highly differentiated H subline is difficult because it consists of two subpopulations with varying DNA content. Data are taken from Lohr et al [72].*

| Tumor behavior | AT1 | HI | H |
|---|---|---|---|
| Volume doubling time $T_D$ [d] | 5.6±0.4 | 10±1.1 | 20 |
| Cell loss $\Phi$ [%] | 15 | 10 | |

Table 2.3: *Observed tumor growth for the three sublines of the Dunning R3327 prostate tumor system according to Lohr et al [72].*

## 2.2 A cellular model for tumor growth

In this section the biological model used to simulate tumor growth is introduced. It has two main characteristics which are motivated by the desire to aid radiation oncologists in their decision making process by simulating tumor response to radiotherapy. Firstly, the model is defined on a three-dimensional rigid cubic lattice to enable fast computer simulations. Secondly, the model must include the main biological factors to be realistic without including too many parameters. Simplification is crucial because on the one hand many biological parameters are known with some uncertainty only and because on the other hand every parameter assigned to the tumor cells increases the computer run time and memory requirements.

The cellular approach chosen for tumor modeling allows for intra-tumor variability in biological parameters, such as $T_C$, to be taken into account. By dealing with every single tumor cell effects that are relevant for treatment outcome, such as blood supply of individual cells and reoxygenation due to cell displacement, can be included in the tumor growth model.

### 2.2.1 Biological parameters

The cellular model is developed along the lines of tumor growth discussed in the previous section 2.1. The following parameters are included in the growth model.

1. The cell cycle time $T_C$ and the four cycle phases.
   $T_C$ is the time between successive cell divisions. Distinguishing the cycle phases is important when taking into account phase dependent parameters, such as radiosensitivities varying within the cell cycle. Typical values for $T_S$ (from which $T_C$ can be calculated) are given in table 2.1 for some human cancers. Table 2.2 lists $T_C$ for an animal model, the Dunning R3327 prostate tumor system in Copenhagen rats.

2. The tumor growth fraction GF.
   GF is defined as the fraction of normoxic cells that do actively proliferate. Tumors exhibit an elevated growth fraction which can reach 100% for tumor cell lines with poor differentiation. Within a tumor, the growth fraction is assumed to be size dependent. Being a control mechanism, it decreases logarithmically with increasing size. In the simulations presented, tumor growth fractions for large tumors are assumed to reach values as low as 75%.

3. Apoptotic capacity.
   The ability to undergo apoptosis is quantified as the fraction $\Phi_{apop}$ of normoxic cells that undergo apoptosis.
   $\Phi_{apop}$ is also size dependent. It increases logarithmically with increasing size to counter uncontrolled growth. In the simulations presented, apoptotic capacity for large tumors is assumed to reach values as high as 25%.

4. Blood supply.
   The microvasculature is modeled by a capillary distribution that is homogenous at the onset of tumor growth. An intercapillary distance of 7 cell layers in every direction is chosen. This represents a normal tissue with no hypoxic cells. Varying the intercapillary distance allows

to model tissues with different degrees of oxygenation. A more realistic capillary system can be modelled by randomly offsetting capillaries by one lattice site.

5. Oxygenation status.
   Oxygen tension $pO_2$ is modeled by a step function. Only normoxic, hypoxic and necrotic cells are distinguished according to their distance to the nearest capillary. This is shown in figure 2.4. Cells within 5 cell layers of a capillary are taken to be normoxic, cells 6 and 7 cell layers away from a capillary are considered to be hypoxic. At capillary distances of 8 and more cell layers, cells become necrotic.

6. Resorption of dead cells.
   Lysis takes longer for necrotic cells than for apoptotic cells. Resorption mechanisms are taken to saturate, prolonging lysis times with ongoing cell death. Lysis times for necrotic cells are taken to increase logarithmically from 72 h for little necrosis to 144 h for large numbers of necrotic cells. For apoptotic cells, there is a logarithmic increase from 24 h to 96 h.

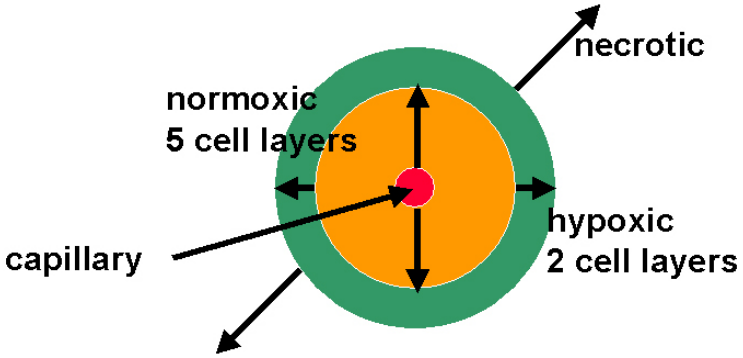


Figure 2.4: *Simplified model for oxygen supply around capillaries. Within a distance of 100 µm (corresponding to 5 cell layers) cells are well supplied with oxygen. They are termed normoxic. At distances between 100 and 150 µm (corresponding to 6 and 7 cell layers) cells turn hypoxic and cells farther away than that die of necrosis.*

### 2.2.2 Implementation

Simulations are performed on a three-dimensional rigid cubic lattice. Each lattice site represents an individual cell with a volume of $(20\ \mu\text{m})^3$, implying

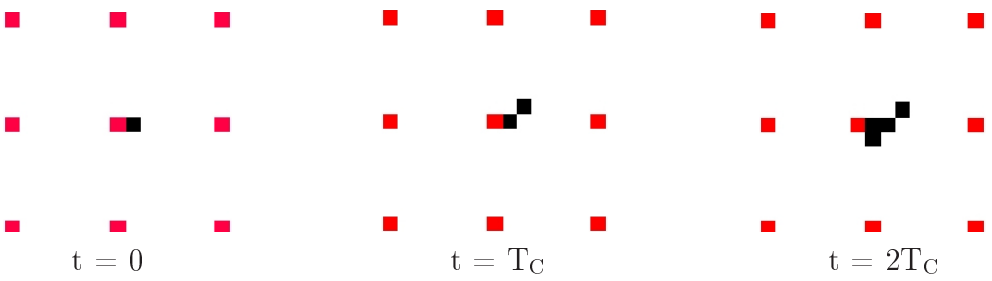


Figure 2.5: *Two-dimensional simulation of the very beginning of tumor growth starting from one single cell and a homogeneous capillary distribution (depicted red) with an intercapillary distance of 7 cell layers. Cell division of normoxic cells (black) can force existing cells to be displaced as indicated in the right.*

that all cells are treated as having equal size. Every single tumor cell is assigned its individual biological variables, such as age and current cycle phase or oxygenation status. Computer simulation of tumor growth starts out from one single well oxygenated tumor cell which divides after one cell cycle time $T_C$ as can be seen from figure 2.5. Random processes such as cell displacement after cell division are simulated by Monte-Carlo methods. In Monte-Carlo methods processes that occur according to probabilistic laws are simulated by comparing random numbers to probability distributions governing the processes.

To speed up the simulation process, only a lattice of size $64 \times 64 \times 64$ is allocated at the beginning of tumor growth. With ongoing proliferation, the lattice is enlarged.

The cell cycle phases and checkpoints are simplified to account for quiescence ($G_0$ phase), apoptosis and cell division. This is illustrated in figure 2.6. Cell proliferation is modeled by Monte-Carlo methods. Each individual cell's age is incremented by a step $\Delta t$ which varies with $T_C$. At the $G_1$-S transition it is determined whether the cell is active or whether it stays in $G_0$. The decision is made according to a uniform probability distribution reflecting the tumor growth fraction. Apoptosis is induced at the checkpoints by the same probabilistic procedure. Cells divide at the end of mitosis.

The daughter cell is randomly assigned one of the mother's 26 neighboring lattice sites. Cell division can force cells to be displaced if the lattice site chosen for the daughter is already occupied. The occupying cell itself is placed in one of its 26 adjacent sites and so on. Cell division in the inside of the tumor can hence trigger a whole cascade of displacements. Displacement can happen randomly or along straight lines. Random displacement

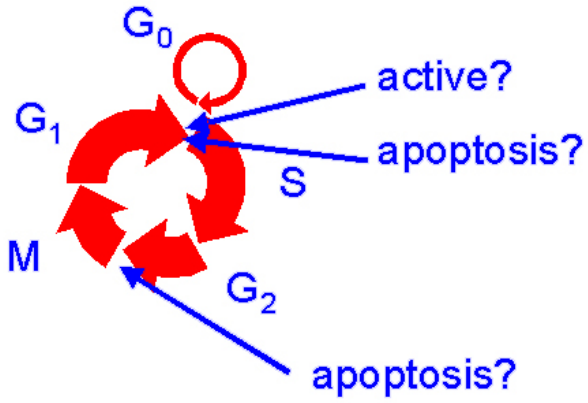


Figure 2.6: *Model of cell cycle phases and checkpoints. Apoptosis can be induced at the $G_1$-$S$ and $G_2$-$M$ checkpoints. Quiescent cells are in $G_0$ which is taken to preceed synthesis and is assumed to last as long as $G_1$.*

requires generating a new random number for each displacement, rendering this process less efficient computationally. However, random displacement yields tumors with a more realistic shape, as illustrated in figure 2.7.

For large tumor sizes the difference in the proliferation characteristics of the two displacement processes becomes negligible. Cell displacement can alter the oxygenation status of a cell by pushing it towards a capillary or away from it. Hypoxic cells can thus be reoxygenated, a process that influences tumor response to fractionated radiotherapy.

Individual tumor cells are assigned their own cycle times $T_C$ according to a normal distribution. The cycle time of each cell can change after division; the daughter cell is assigned its own cycle time. This results in a constant redistribution of cell cycles and in an asynchronous cell population.

Simulating tumor growth can be sped up by further simplifying the cell cycle. Figure 2.8 shows the cell cycle without distinguishing phases and checkpoints. The mechanisms checking for apoptosis and inactivity are located at the end of the cell cycle. If the cell passes both mechanisms, it will divide.

The oxygenation level of each cell is checked at intervalls $\Delta t$. Hypoxia and necrosis are induced independently of the cycle phase. Determining each cell's oxygenation status is done by scanning its environment for capillaries. To reduce run time, a spherical scan with a radius of 8 cell layers is performed instead of scanning row by row. Distances are euclidian distances with respect to lattice sites (see figure 2.9). Hypoxic cells are quiescent. They do not proceed in their cycle unless they are reoxygenated.

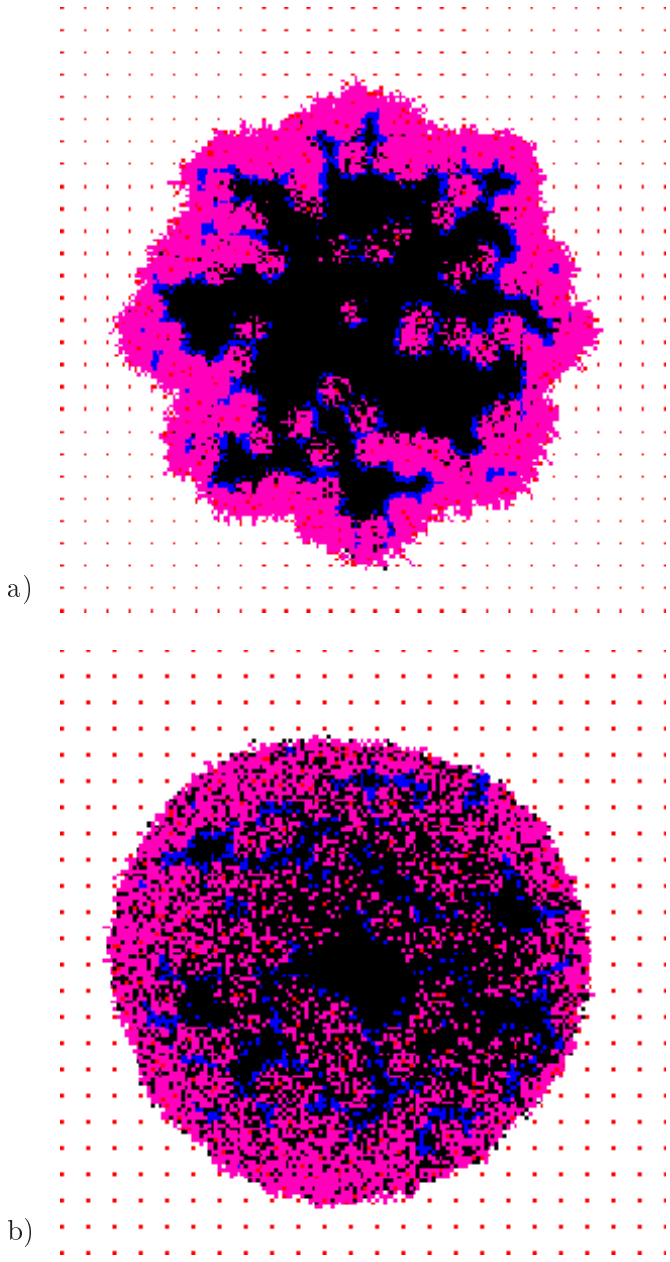


Figure 2.7: *Two-dimensional computer simulations of two tumors with $T_C = 2$ d. Both tumors are 36 d old. a) Cell displacement along straight lines. b) Random cell displacement, resulting in a less regular morphology and a more spherical shape than displacement along straight lines. Simulations were performed without apoptosis and without lysis of dead cells. Normoxic cells are depicted pink, hypoxic cells are blue and necrotic cells are black. Normal tissue is depicted white, capillaries are red.*

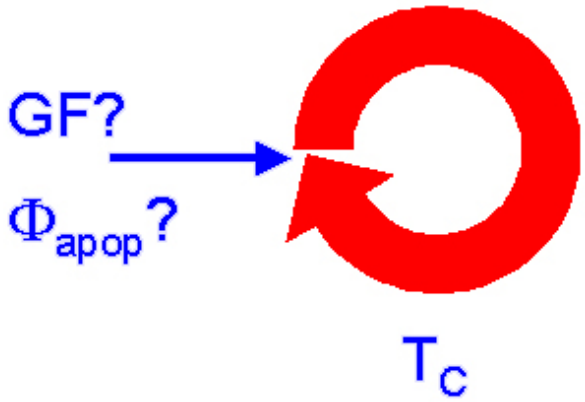


Figure 2.8: *Simulation of tumor growth can be done without distinguishing individual cell cycle phases. Mechanisms checking for activity (growth fraction GF) and apoptosis (apoptotic fraction $\Phi_{apop}$) are triggered at the end of the cell cycle.*

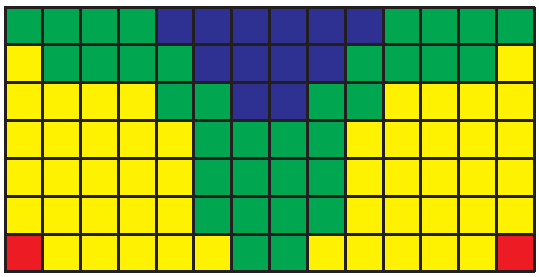

Figure 2.9: *Two-dimensional illustration of oxygenation status around capillaries (red). For capillary distances of 5 cell layers (lattice sites) or less, cells are normoxic (yellow). At capillary distances of 8 or more cells turn necrotic (blue). Hypoxic areas (green) are 6 or 7 cell layers from the nearest capillary.*

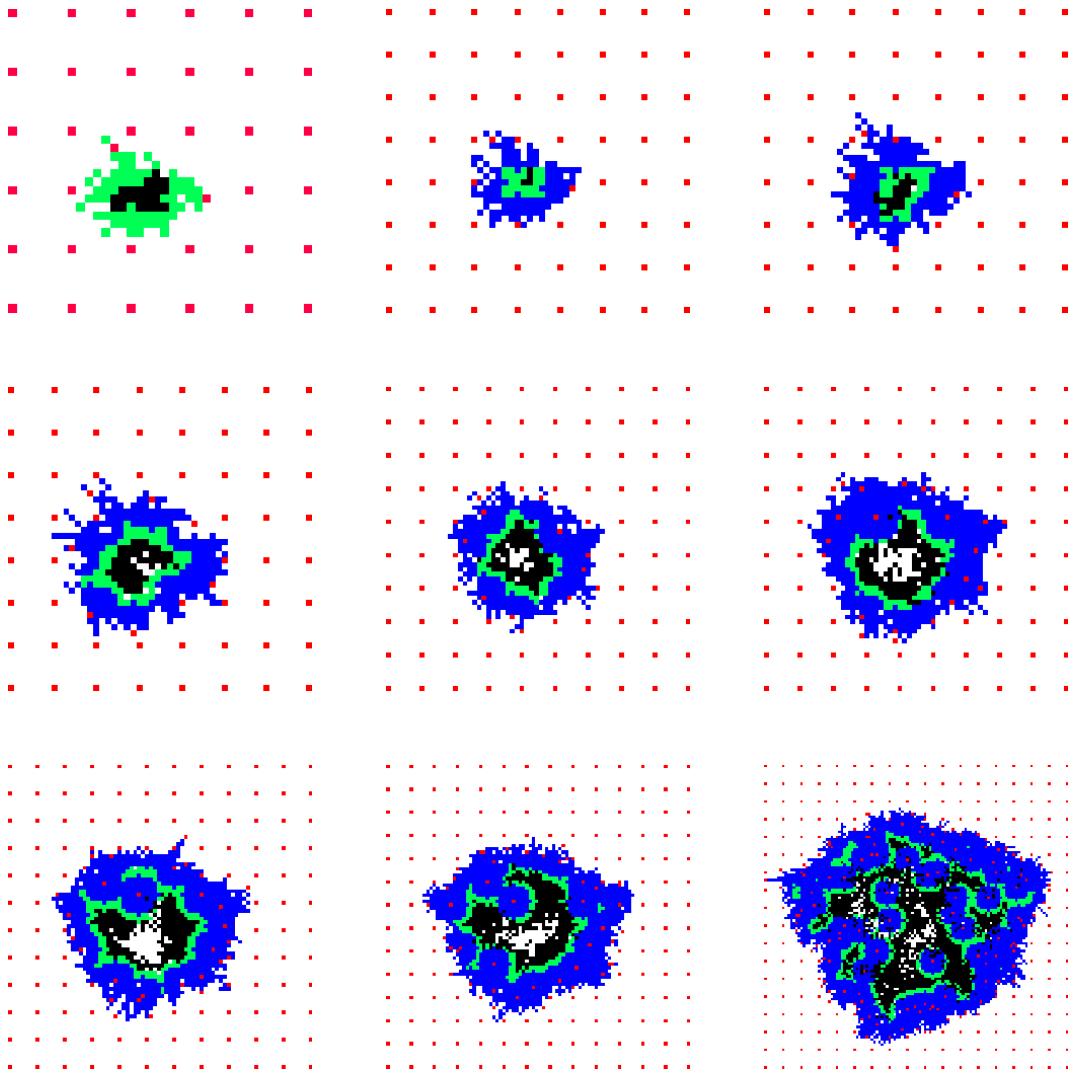

Figure 2.10: *Two-dimensional simulation of a tumor with a cycle time of 2 days and* $\Delta t = 6$ *h. From top left to bottom right: Tumor at age 14, 16, ..., 28 d. The tumor's age at the bottom right is 34 d. At age 14 d, there are normoxic and hypoxic cells. At age 16 d the first cells turn necrotic. They are resorbed within 3 d, as can be seen from the tumor at age 20 d in the left of the middle row.*

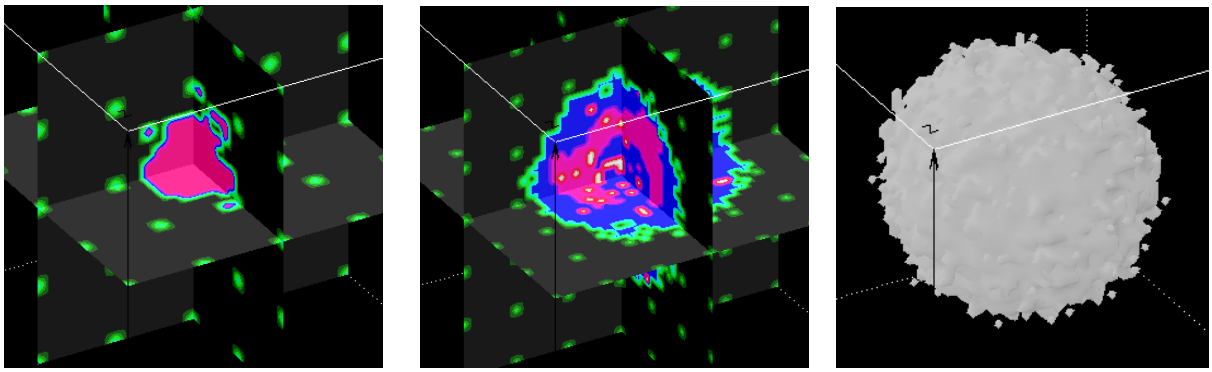

Figure 2.11: *Three-dimensional computer simulations of the beginning of tumor growth with $T_C = 2\ d$ and $\Delta t = 6\ h$. Simulation was performed using random displacement. Growth starts out from one tumor cell and a homogeneous capillary distribution (green). The tumor on the left is 21 d old, the tumor in the middle is 30 d old. The three-dimensional surface of the tumor with age 30 d is shown on the right. At 21 d there are only normoxic cells (pink). After 30 d of growth there are hypoxic areas (pink) and some necrotic cells (white) in the core. In this illustration, normoxic cells are depicted in blue.*

A computer simulation of a tumor with $T_C = 2$ d is illustrated in figure 2.10. In the top left, the tumor is 14 days old. At the bottom right its age is 34 days. For reasons of efficiency the lattice which holds the tumor cell variables increases with tumor size from $43 \times 43 \times 43$ at 14 d to $127 \times 127 \times 127$ at 34 d. It can be seen that there is an initial phase with exponential growth. Tumor growth forces capillaries to be displaced which in turn causes hypoxia and necrosis. Necrotic cells are resorbed within three days. The simulations were performed with displacement along straight lines for clarity. Usually, random displacement is chosen for computer simulations. In three dimensions, displacement of capillaries does not occur as early as it does in two dimensions. Figure 2.11 shows a tumor simulated in three dimensions with the same proliferation characteristics as the two-dimensional tumor in figure 2.10. After 21 d of growth there are still no hypoxic cells.

Simulations of two three-dimensional tumors, tumors A and B, are shown in figure 2.12 a and b, respectively. Tumor A was simulated with lysis of dead cells whereas there was no resorption in tumor B. For both tumors, the growth fraction was taken to decrease logarithmically with tumor size while apoptotic capacity increased logarithmically with size. $T_C$ was 2 d. Tumor A has a size of 21 million tumor cells and a diameter of 7 mm. Tumor B has a size of 15 million tumor cells and a diameter of 6.2 mm. Normal tissue is depicted white, capillaries are red. There are four different types of tumor

cells: Normoxic cells (pink), hypoxic cells (blue), apoptotic cells (green) and necrotic cells (black). In the very core of tumor A, necrotic centers have already been resorbed (white). The center of tumor B is largely necrotic.

Handling large three-dimensional lattices has to be done carefully to avoid long computer run times and to minimize memory requirements. Memory is allocated in one dimension to minimize access times. The three-dimensional structure of the lattice is preserved by three-way pointer referencing. Each lattice site is assigned a cell type. Normal tissue cells, capillaries and tumor cells (normoxic, hypoxic, apoptotic, necrotic) are distinguished. To save memory space, cell types are stored as characters. The variables representing the age of viable cells and the time to lysis of dead cells are transformed to be (short) integer values. Thus, memory for a structure of 5 bytes containing three variables is needed for each cell. Simulating tumors of clinically relevant sizes with a diameter of 10 mm (corresponding to a lattice of size $500 \times 500 \times 500$) requires 625 MB of RAM. If cell cycle phases are not distinguished and tumor cell cycle times are 3 d or more, time increments of $\Delta t = 12\,h$ are sufficiently long. In the case of $T_C = 80$ h, a run time of approximately 20 h is needed on a PC with a 1 GHz Pentium III processor for simulation of tumor growth up to a size of 10.5 mm in diameter.
The memory requirements can be further reduced by two procedures. Firstly, the lattice can be divided into subcubes which are treated separately. Secondly, a list can be introduced containing tumor cell structures. The three-dimensional lattice contains cell types only instead of structures. A structure containing all biological variables will be added to the list only for lattice sites occupied by tumor cells. Both procedures have the same drawback: The subcubes and the list are saved on hard disk and are not stored in the working memory. Due to the large number of cell-cell interactions many accesses to the hard disk are necessary resulting in prohibitively long computer run times.

### 2.2.3 Simulation runs

Table 2.4 shows typical parameter values of the tumor growth model used in the simulations presented in chapter 5. $T_C = 2$ d is at the lower end of cycle times of fast proliferating tumors (see table 2.1). $T_C = 7.1$ d is the cycle time of the moderately well differentiated HI subline of the Dunning R3327 tumor system chosen to compare simulations of tumor growth with corresponding experimental data. The $T_C$ values given are assumed to be the mean values of normal distributions with (an assumed) variance of $\sigma_{T_C} = \frac{T_C}{8}$. In tumor systems the growth fraction increases with ongoing loss of differentiation while the apoptotic capacity decreases. Within the same tumor, growth

| Model parameters | |
|---|---|
| Cycle time $T_C$ | 2 -7 days |
| $\sigma_{T_C}$ | $\frac{T_C}{8}$ |
| Apoptotic capacity $\Phi_{apop}$ | no apoptosis or increasing to 15%, 20% or 25% |
| Growth fraction GF | 100 % or decreasing to 85%, 80% or 75% |
| Oxygenation status | normoxic, hypoxic, necrotic cells |
| Capillary density | 1 capillary per 343 cells (mostly), 1 capillary per 216 cells |
| Lysis times for apoptotic cells | increasing from 24 h to 60, 72, 96 h |
| Lysis times for necrotic cells | increasing from 72 h to 96, 120, 144 h |

Table 2.4: *Typical values used in the simulations of tumor growth. Apoptosis, growth fraction and lysis are assumed to be size dependent.*

fraction GF and apoptotic capacitiy $\Phi_{apop}$ are taken to be logarithmically size dependent in the following way (example given for a decrease in GF from 100% to 80%):

$$\mathrm{GF}(\#\text{viable cells}) = \begin{cases} 100\% & : \quad \#\text{viable cells} \leq 5 \times 10^4 \\ 97\% & : \quad 5 \times 10^4 < \#\text{viable cells} \leq 10^5 \\ 94\% & : \quad 10^5 < \#\text{viable cells} \leq 5 \times 10^5 \\ 91\% & : \quad 5 \times 10^5 < \#\text{viable cells} \leq 10^6 \\ 88\% & : \quad 10^6 < \#\text{viable cells} \leq 5 \times 10^6 \\ 84\% & : \quad 5 \times 10^6 < \#\text{viable cells} \leq 10^7 \\ 80\% & : \quad 10^7 < \#\text{viable cells} \end{cases} \tag{2.2}$$

Apoptotic cells are taken to be resorbed more rapidly than necrotic cells are. Lysis mechanisms saturate logarithmically with increasing number of dead cells analogous to equation 2.2. Lysis times for small numbers of apoptotic cells were chosen according to D'Amico et al [31] while the choice of 72 h for resorption of (small numbers of) necrotic cells was based on Kocher et al [63, 64]. Lysis times for apoptotic and necrotic cells are not a dominant factor, however. Lysis times given are the mean values of normal distributions. Unless noted otherwise, the simulations presented in chapter 5 will start out from a homogeneous capillary distribution with an intercapillary distance of 7 cell layers in all directions. This distance was chosen because it is the lowest capillary density still resulting in a tissue with no hypoxic areas.

Simulations of tumor proliferation intended for comparison with experimental data were performed with the growth parameters of the AT1 and HI

sublines of the Dunning R3327 tumor system. The growth parameters $T_C$, $\Phi_{apop}$ and GF for these two sublines are listed in table 2.2.

a)

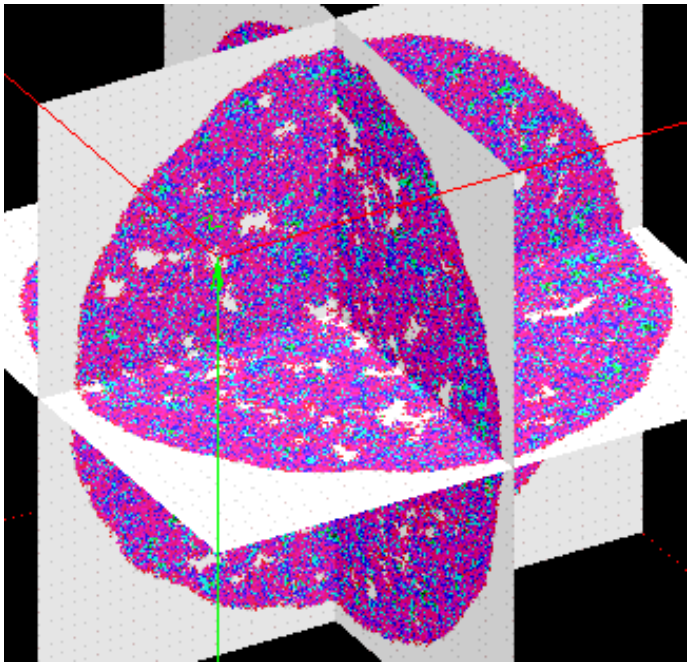

b)

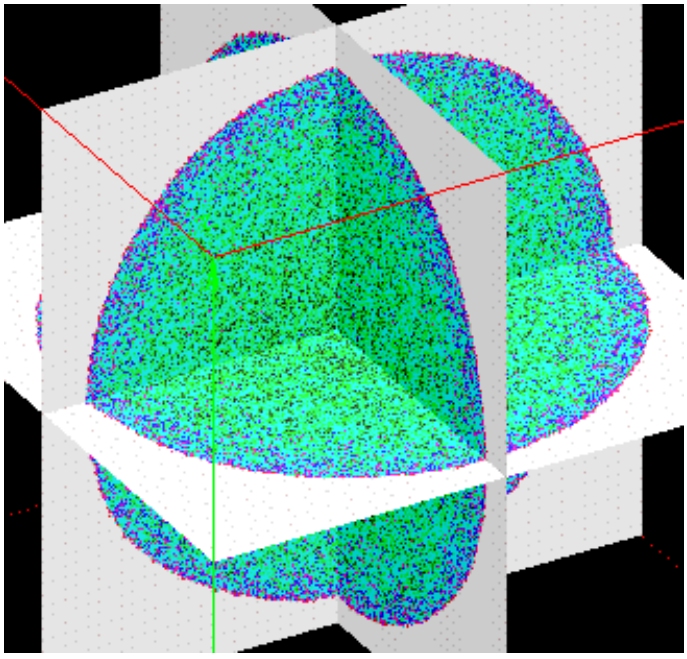

Figure 2.12: *Three-dimensional computer simulations of tumor growth with* $T_C = 2d$. *a) Tumor with lysis of dead cells, b) tumor without lysis mechanisms. Without resorption, there are large necrotic centers in the core of the tumor. Normoxic cells are depicted pink. Hypoxic cells are blue, apoptotic cells are green and necrotic cells are black. Normal tissue is depicted white, capillaries are gray.*

# Chapter 3

# Modeling tumor angiogenesis

Tumors cannot reach diameters of more than a few mm without securing their own blood supply by angiogenesis. Tumor angiogenesis, the mechanism by which tumors manage to generate new capillaries, is a central process in the growing of tumors. Without angiogenesis, the tumor's core is deprived of nutrients and oxygen. Large parts of the core are hypoxic or necrotic. Only the rim of the tumor contains viable cells. The normoxic fraction decreases to about 50%, as can be seen from figure 3.1. This can be deduced from the two-dimensional simulation of the beginning of tumor growth shown in figure 2.10. Tumor cell proliferation results in displacement of capillaries which causes cells to turn hypoxic and necrotic.
In this chapter, a model for tumor angiogenesis will be devised.

## 3.1 The biological basis of tumor angiogenesis

Angiogenesis, the formation of blood vessels, is a complex process involving endothelial cells and growth factors. Fibroblast growth factors (bFGF and aFGF) stimulate quiescent endothelial cells to undergo mitosis. Vascular endothelial growth factors (VEGF) enhance vascular permeability. The steps undergone in blood vessel formation are degredation of the vessel tube membrane, invasion of endothelial cells into the stroma, migration of a sprout of endothelial cells, proliferation of endothelial cells at the leading edge of the sprout and differentiation and adhesion at its tail [56]. The cells adhering to each other in the tail form a new capillary tube. Tumor vasculature is irregular, forming branches, loops and shunts [71, 23]. The tumor growth model presented here does not include vasculary structures, so no attempt is made to model the sprouting, migration and branching process in detail. In this model, angiogenesis effects endothelial cells, not blood vessels. Also, all

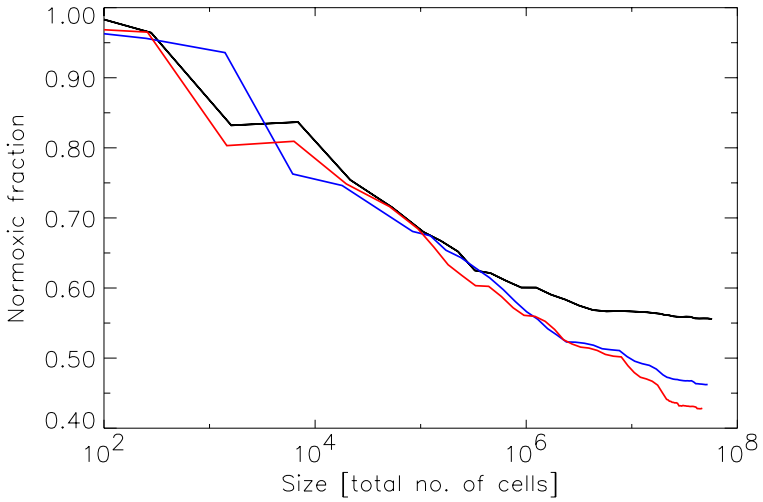


Figure 3.1: *Without angiogenesis, the normoxic fraction decreases with increasing tumor size. Simulated normoxic fractions are shown for three tumors with* $T_C = 80\ h$*, but different growth fractions GF and apoptotic capacities* $\Phi_{apop}$*. For the black curve, GF was taken to be 100% and* $\Phi_{apop}$ *was 0%. The colored curves resulted from simulations in which GF decreased and* $\Phi_{apop}$ *increased with growing tumor size. GF was taken to decrease to 85% (blue) and 80% (red).* $\Phi_{apop}$ *was taken to increase to 15% (blue) and 20% (red). The rate with which a tumor grows depends on the fraction of normoxic cells.*

growth factors involved in angiogenesis will be treated as one single entity called tumor angiogenesis factors (TAF).

## 3.2 A cellular model for tumor angiogenesis

### 3.2.1 Biological parameters

The angiogenesis model devised here is based on three assumptions.

1. It is hypoxic cells that secrete angiogenesis factors (TAF) [23]. The amount of angiogenesis factors produced in hypoxic areas is directly proportional to the number of hypoxic cells (and is given in arbitrary units, a.u.).

2. The factors diffuse around hypoxic areas and are consumed by capillaries.

3. Quiescent capillaries are stimulated by the factors to divide [84, 56, 85]. This implies that angiogenesis is only possible if capillary cells are

reached by the TAF. A certain amount of TAF is needed to stimulate capillary cells to divide. If TAF levels are below a certain threshold, no capillary division takes place. Angiogenesis does not occur instantly; the quiescent capillaries need time to respond to the stimulus. Capillaries that have already been induced to divide are not stimulated again until the end of mitosis.

Diffusion is governed by a steady state equation including consumption of TAF [54]

$$D^2 \Delta c - Mc = 0\,, \tag{3.1}$$

which reduces to $\frac{d^2 c}{d r^2} + \frac{2\frac{d c}{d r}}{r} - \frac{Mc}{D^2} = 0$ for radial symmetry. $c$ is the TAF concentration and $M$ its consumption rate. The diffusion radius is larger than that for oxygen diffusion mainly because the factors are not consumed by hypoxic or normoxic cells. In analogy to the modeling of oxygen concentration around capillaries, the distribution of TAF around hypoxic areas is simplyfied by a step function.

The three parameters employed in the angiogenesis model are the threshold value of TAF needed to induce capillary division, the distribution of TAF around hypoxic areas and the capillary response time. Since the concentration of angiogenesis factors around hypoxic areas is assumed to behave according to steady state diffusion (see equation 3.1), it is not time dependent.

### 3.2.2 Implementation

Calculating the number of new capillaries generated in the vicinity of a hypoxic area is based on introducing a subgrid with subcubes of size $(140\ \mu\text{m})^3$. Thus diffusion of TAF around hypoxic areas is treated on a coarser scale than diffusion of oxygen around capillaries. The subcube size chosen is motivated by the intercapillary distance at the onset of tumor growth. Counting of hypoxic cells, determining the amount of angiogenic factors produced, calculating the subsequent stimulus that reaches capillaries and generation of new capillaries is performed within these subcubes. The definition of the subgrid is illustrated in figure 3.2.

The step function that simplifies the distribution of TAF is defined with respect to the subcubes. The values of the step function represent the fraction of TAF that stays within the subcube of a hypoxic area itself as well as the fraction reaching the adjacent subcubes (140 $\mu$m away) and the diagonally neighboring subcubes (200 $\mu$m away). No angiogenesis factors are considered to diffuse farther than into the diagonally adjacent subcubes. The step

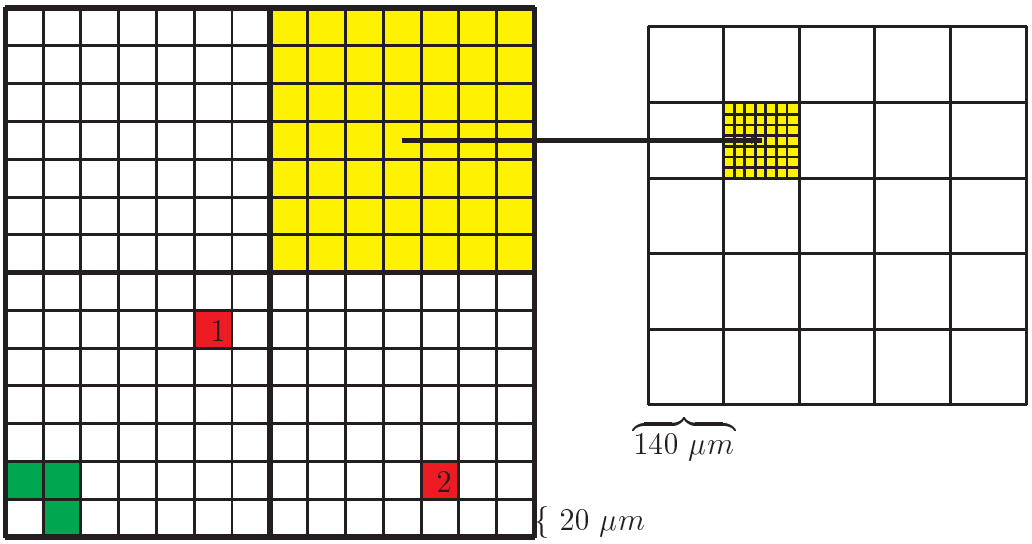


Figure 3.2: *The angiogenesis model is defined on a subgrid of subcubes with a volume of (140 $\mu m$)$^3$. Hypoxic cells (green) produce tumor angiogenesis factors (TAF) which diffuse and reach capillaries (red). More TAF reaches capillary 1 than capillary 2.*

function modeling the concentration $c(R)$ of angiogenesis factors reaching a subcube a distance $R$ away is defined as:

$$c(R) = \begin{cases} \frac{4}{7} \text{ of TAF} & : \text{ consumed in hypoxic area's subcube} \\ \frac{4}{7} \times \frac{1}{2} \text{ of TAF} & : \text{ reaches subcubes } R = 140\ \mu m \text{ away} \\ \frac{4}{7} \times \frac{1}{4} \text{ of TAF} & : \text{ reaches subcubes } R = 200\ \mu m \text{ away} \end{cases} \tag{3.2}$$

$c(R)$ is defined to be the amount of TAF diffusing into all subcubes distance $R$ away. In three dimensions, each subcube has 6 adjacent subcubes 140 $\mu$m away and 12 diagonally adjacent subcubes 200 $\mu$m away. Considering this, equation 3.2 yields the amount of TAF $c\prime(\vec{R})$ reaching a single adjacent subcube:

$$c\prime(\vec{R}) = \begin{cases} \frac{4}{14} \times \frac{1}{6} \text{ of TAF} & : \text{ reaches a subcube } \mid \vec{R} \mid = 140\ \mu m \text{ away} \\ \frac{4}{28} \times \frac{1}{12} \text{ of TAF} & : \text{ reaches a subcube } \mid \vec{R} \mid = 200\ \mu m \text{ away} \end{cases} \tag{3.3}$$

To obtain the number of new capillaries generated in a subcube, the amount of TAF reaching it must be calculated. This is done by weighing the amount of TAF produced within the subcube itself and its neighbours with the functions defined in equations 3.2 and 3.3. If this amount exceeds

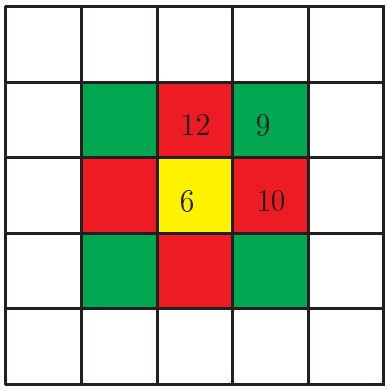


Figure 3.3: *Capillary division only happens for tumor angiogenesis factors (TAF) levels above a certain threshold. For the number of hypoxic cells shown in the four subcubes, capillary division in the yellow subcube will be induced for a threshold of 5 a.u. Adjacent subcubes are red, diagonally neighboring subcubes green. The amount of TAF in the yellow subcube is determined by equations 3.2 and 3.3.*

a certain threshold, the number of induced capillaries equals the number of quiescent capillaries. This is illustrated in figure 3.3.

Consider the yellow subcube in figure 3.3 which has six hypoxic cells. The two red subcubes one lattice point (corresponding to 140 $\mu$m) away have ten and twelve hypoxic cells and the green subcube with a subgrid distance of $\sqrt{2}$ (corresponding to 200 $\mu$m) has another nine hypoxic cells. The amount of angiogenesis factor reaching the yellow subcube is

$$\begin{aligned} \text{amount of TAF} &= 6 \times \frac{4}{7} \\ &\quad +10 \times \frac{4}{14} \times \frac{1}{4} + 12 \times \frac{4}{14} \times \frac{1}{4} \\ &\quad +9 \times \frac{4}{28} \times \frac{1}{4} \\ &= 5.32 \text{ a.u.} \end{aligned}$$

The factor $\frac{1}{4}$ stems from the number of adjacent subcubes 140 $\mu$m and 200 $\mu$m away. If the threshold is 5 a.u. for induction of capillary division and the yellow subcube has three quiescient cells, three capillaries will be generated. If there are no quiescent capillaries in the yellow subcube, no new capillaries will be generated there. New capillaries are placed randomly within the subcube, triggering a cascade of cell displacements analogous to the displacement following cell division described in section 2.2.

a)

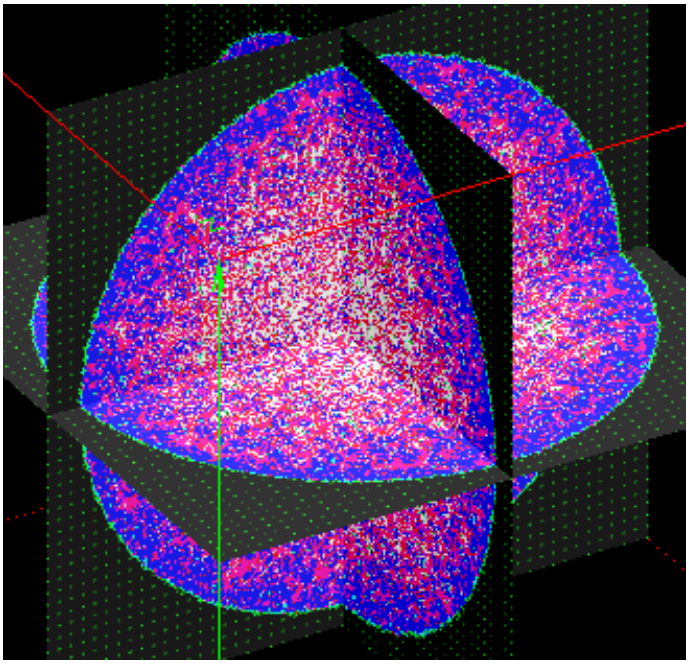

b)

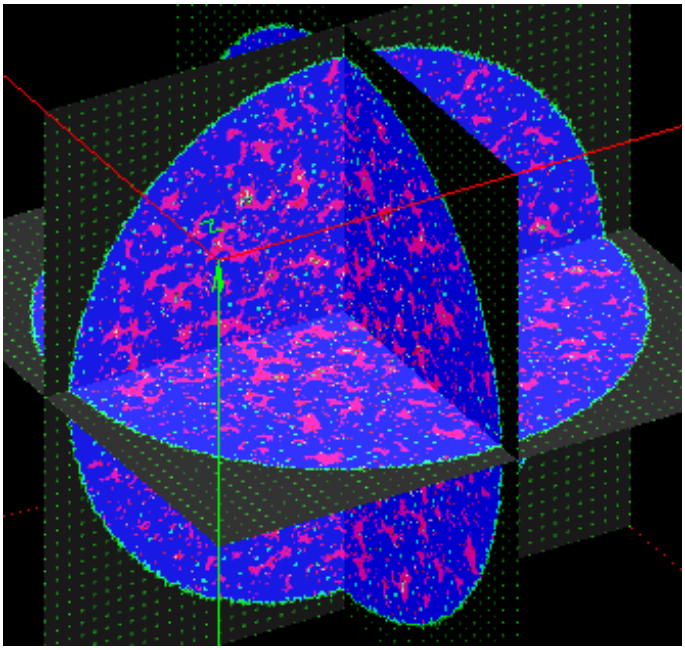

Figure 3.4: *Tumor growth simulated with (b) and without (a) angiogenesis. Both simulations of tumor proliferation were run with a relatively long tumor cell cycle time of* $T_C = 115\ h$. *Simulation of angiogenesis for the bottom tumor was performed with a low threshold of 80 a.u. of tumor angiogenesis factors (TAF) for capillary stimulation. Angiogenesis increases the normoxic fraction and thus enhances tumor growth. Normoxic cells are depicted blue. Hypoxic cells are red, necrotic cells white and capillaries green.*

The importance of angiogenesis for normoxic fraction and necrotic areas within the tumor is demonstrated in figure 3.4, which shows three-dimensional simulations of a slowly proliferating tumor cell line. The tumor cell cycle times were $T_C = 115$ h. The simulations shown are for tumor growth with and without angiogenesis. Both tumors pictured have about 15 million viable cells. The tumor proliferating without angiogenesis took 170 d to grow to that size whereas the tumor simulated with angiogenesis reached a size of 15 million viable cells within 130 d.

### 3.2.3 Simulation runs

| Model parameters | |
|---|---|
| TAF concentration with diffusion radius $R$ | step function simplifying exp. decrease $R = 200\ \mu$m |
| Threshold for cap. stimulation | 80, 100, 120 a.u. of TAF |
| Capillary response time | $T_C = 48$ h, 72 h or 120 h |

Table 3.1: *Parameter values used for the simulation of tumor angiogenesis.*

The value $R = 200\,\mu$m for the diffusion radius was motivated by the fact that TAF is not consumed by normoxic cells and thus diffuse farther than oxygen ($R = 150\,\mu$m) does. Simulation runs not discussed here showed that increasing the diffusion radius to $R = 240\,\mu$m had no pronounced effect on tumor angiogenesis, so $R = 200\,\mu$m was chosen for computational reasons. The threshold for capillary stimulation in arbitrary units of TAF was motivated by the observation that as little as 50 to 60 hypoxic cells can induce angiogenesis. Values for capillary cell cycle times were chosen because division of endothelial cells is observed no earlier than 48 h of stimulation [44].

# Chapter 4

# Modeling tumor response to radiotherapy

Radiotherapy aims at maximizing (local) tumor control while minimizing the probability for normal tissue complications. Three-dimensional conformal radiotherapy techniques have been developed to administer high doses to the tumor volume while sparing organs at risk as much as possible. To further increase the therapeutic window the radiobiological properties of tumors and normal tissues have to be considered. One strategy that takes advantage of a different response to radiation is fractionated therapy. By delivering the total dose in a number of small fractions, the higher repair capacity of many normal tissues can be exploited. Simulating the tumor control achieved with a certain total dose and time pattern would aid radiation oncologists in the treatment planning process. A cellular radiobiological model allowing simulations of tumor response to radiotherapy is devised in this chapter.

The interactions of radiation with tissues and the processes killing cells are described in sections 4.1.1 to 4.1.3. The influence of the microenvironment on tumor response is discussed in section 4.1.4. Section 4.1.5 gives the rationale for fractionated radiotherapy and introduces time-dose patterns applied in clinical practice. The time factor in radiotherapy is described in section 4.1.6. These concepts will be simplified in section 4.2 to formulate a cellular radiobiological model that allows simulation of tumor response to radiotherapy.

Time dependent effects have been incorporated into the linear-quadratic model (LQM) to estimate tumor response to fractionated radiotherapy. Terms added to the LQM to account for repopulation, repair and redistribution will be discussed in section 4.1.6.

## 4.1 The radiobiological basis of radiotherapy

### 4.1.1 Interaction of photons and particles with cells

Electromagnetic radiation is indirectly ionizing. Damage is not caused by the photons themselves but by the charged particles they produce during their interaction with matter. The process of photon absorption depends on the photon energy and on the material the photon interacts with.

At low photon energies the dominant process of absorption is the photoelectric effect. The photon interacts with a bound electron of an atom transferring its energy $h\nu$ and releasing the electron with a kinetic energy $E_{kin} = h\nu - E_{binding}$. $E_{binding}$ is the binding energy of the electron. As a consequence of electron emission in an inner shell, another electron from an outer shell will take its place emitting a photon with energy $h\nu = E_{inner} - E_{outer}$. For soft tissues this radiation has a low energy and is of no importance. Instead of a photon an Auger electron from an outer shell might be emitted. At the lower end of the energy range used in radiation diagnostics it is the photoelectric effect that is dominant. At the higher end of this range ($\approx$100 keV) and especially for energies used in radiation treatment (1 MeV $\leq E \leq$10 MeV) it is the Compton effect that is important for photon absorption. In the Compton process a photon with energy $h\nu$ interacts with a free electron (an electron in a shell with low binding energy). It transferes some of its energy, is scattered by an angle $\theta$, and continues with energy

$$E'_\gamma = h\nu \frac{1}{1+\alpha(1-\cos\theta)} \, , \alpha = \frac{h\nu}{m_e c^2} \, .$$

For a scattering angle of $\theta = \pi$ the energy transfer is maximum. For low photon energies there is a lot of scattering and little energy transfer. For high photon energies there is a lot of energy transfer and little scattering.

Photon absorption also depends on the absorbing material. For soft tissues with a low atomic number $Z$, the coefficient for photoelectric absorption is proportional to $Z^3$. For matter with high $Z$, such as metals, it is proportional to $Z^4$. In contrast, the Compton process does not depend on $Z$. For energies above 10 MeV generation of electron-positron pairs is important. Its absorption coefficient is proportional to $Z$.

In radiotherapy, the photoelectric effect and, more importantly, the Compton effect produce electrons that cause cell damage. This is called direct radiation action. Its time scale is in the order of $10^{-15}$ seconds.

The electrons can continue to generate free radicals, atoms or molecules with unpaired electrons. In biological tissues it is mostly oxygen radicals $O\cdot$ or hydroxil radicals $OH\cdot$ that are produced. They are highly reactive. It

is believed that radicals within a distance of ± 1 nm of the DNA helix can cause DNA damage. DNA damage by free radicals is referred to as indirect radiation action. The time scale of indirect radiation action is in the order of $10^{-5}$ seconds. For radiation with a high linear energy transfer (LET), the energy transferred to the absorbing matter per unit length of radiation track, direct action is the dominant process. This is the case for protons or heavy ions, but radiotherapy with charged particles is not considered in this work. In photon therapy with energies of 1 MeV$\leq E \leq$10 MeV and an LET of about $\approx$1 keV/$\mu$m approximately one third of the radiation action is indirect. Within the radiation track approximately 5 radicals are produced per 100 eV of absorbed energy.

Radiation dose is defined as absorbed energy per mass, $D(x) = \frac{dE_{abs}}{dx}$, its unit is Gray (Gy). A dose of 1 Gray is defined as 1 Joule of absorbed energy per 1 kg mass.

### 4.1.2 Cell damage and the linear-quadratic model (LQM)

Modeling cell killing by radiation is based on the assumption that the critical target is the DNA. Damage done outside of the cell's nucleus is taken to be of minor importance.

Radiation causes three types of DNA damage. The most common is damage to one of the DNA bases adenine, cytosine, guanine and thymine, with a rate of 2000 to 4000 per cell and Gy. Single-strand breaks of the sugar desoxyribose that form the DNA backbone are produced at a rate of 1000 per cell and Gy. Both are repaired efficiently. The damage that is considered to be crucial is double-strand breaks which occur at a rate of 40 per cell and Gy [33]. Non-repairable DNA double-strand breaks are thought to be responsible for cell killing [92]. In general, cells with lethal lesions are assumed to die at the next attempt of mitosis, but with a certain probability lethally hit cells will undergo a small number of mitoses before dying.

Cell survival after radiation depends on dose in a linear-quadratic manner when plotted as the logarithm of survival fraction versus dose [34]. The linear-quadratic model explains this relationship in a mechanistic manner by proposing two components for cell killing [70, 27]. The linear component corresponds to lethal events that are proportional to dose. Lethal events are assumed to be caused by one single particle (intra-track interaction). The component quadratic in dose corresponds to two sublethal lesions interacting to form a lethal event. The quadratic component is also referred to as the dual radiation concept: The two sublethal lesions are assumed to stem from

two independent particle hits (inter-track interaction), hence a quadratic relationship between number of lethal lesions and dose. The mean number of lethal events is

$$\alpha D + \beta D^2 \ , \tag{4.1}$$

$D$ being the radiation dose. The fraction of cells surviving radiation with dose $D$ is

$$SF(D) = \exp(-\alpha D - \beta D^2) \ , \tag{4.2}$$

which follows from Poisson statistics. The parameters $\alpha$ and $\beta$ are in units of $\mathrm{Gy}^{-1}$ and $\mathrm{Gy}^{-2}$, respectively. For $D = \frac{\alpha}{\beta}$ both mechanisms yield the same amount of cell killing as can be seen from equation 4.2 and figure 4.1. Surviving cells need to survive both mechanisms of cell kill. This is why the linear-quadratic model is also referred to as the single-hit, multi-hit model.

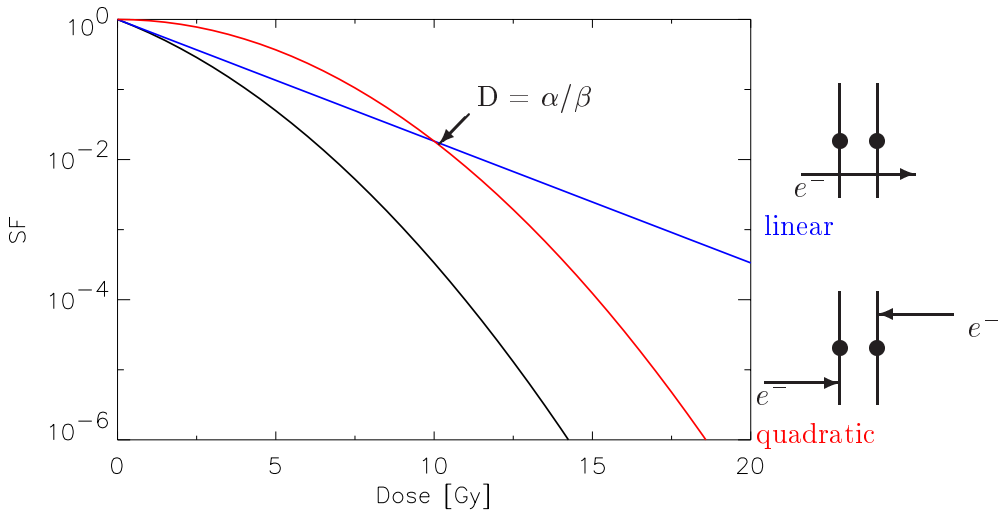


Figure 4.1: *Cell survival fraction (SF) is the product of the survival fractions of two mechanisms. The linear component (blue) stems from lethal lesions caused by a single particle and results in* $SF = \exp(-\alpha D)$. *The quadratic component (red) is the consequence of the interaction of two sublethal lesions yielding* $SF = \exp(-\beta D^2)$. *A dose of* $D = \frac{\alpha}{\beta}$ *yields the same amount of cell killing for both mechanisms.*

Evidence supporting the biological mechanisms of the LQM is obtained by measuring fragmented DNA after irradiation. Measurements can be performed with constant field gel electrophoresis [37] or with the alkaline unwinding technique [32]. The fraction of DNA released depends on dose in a linear-quadratic manner [32, 37]. The assumption that cell killing stems from the interaction of radiation with the DNA is supported by experiments

where radioactive tritiated thymidine ($^3$HTdR) was incorporated into DNA. The cells were killed by the radiation dose due to the $\beta$-particles released by $^3$HTdR. Since these $\beta$-particles are of very short range, cell killing must be caused by events within the DNA.

Intrinsic radiosensitivities of different cell lines show a great variability [34]. Cell survival curves are studied in vitro. Measuring cell survival is done by counting the colonies formed from surviving cells upon irradiation with various single doses [32, 68]. This procedure implies that the survival curves and $\alpha$- and $\beta$-values represent survival with complete repair of sublethal DNA damage. For most human cell lines the survival fraction at 2 Gy ($SF_2$) varies between 0.1 and 0.9. At this dose cell killing is mainly by $\alpha$-inactivation kinetics [27], so $\alpha$-values may be derived from the $SF_2$-values. The $\alpha$- and $\beta$-values for selected human cancer cell lines in table 4.1 are taken from Chapman et al [11, 29].

| Tumor cell line | $\alpha\,[\mathrm{Gy}^{-1}]$, $\beta\,[\mathrm{Gy}^{-2}]$ |
|---|---|
| HT-29 (colon) | 0.03, 0.06 |
| OVCAR10 (ovary) | 0.16, 0.06 |
| A2780 (ovary) | 0.47, 0.07 |
| DU-145 (prostate) | 0.31, 0.05 |
| PC-3 (prostate) | 0.24, 0.07 |
| TSU (prostate) | 0.06, 0.05 |

Table 4.1: *Parameters $\alpha$ and $\beta$ of the LQM for selected human tumor cells taken from Chapman et al [11, 29].*

Most normal tissues are less radiosensitive than tumor cells are. The following two figures, figures 4.2 and 4.3, show survival curves according to the LQM for various parameters $\alpha$ and $\beta$. For high radiation doses the quadratic component for cell killing becomes dominant.

Radiosensitivity is highest for mitotic cells. In $G_1$, cells are relatively radioresistant. Maximum radioresistance is observed during synthesis. Cell populations are usually asynchronous with a certain fraction of cells being in each of the four cycle phases. The variability in radiosensitivites during different cycle phases can be explained by different chromatid structures throughout the cell cycle. Energy deposition happens along the radiation tracks. During mitosis the chromosomes are highly condensed [29] and the probability for double-strand breaks is largest. Studying the radiosensitivities of cycle phases requires synchronizing the cell population.

Radiation can also induce apoptosis which adds to the fraction of cells killed. Radiation induced apoptosis has been discussed in the literature [36,

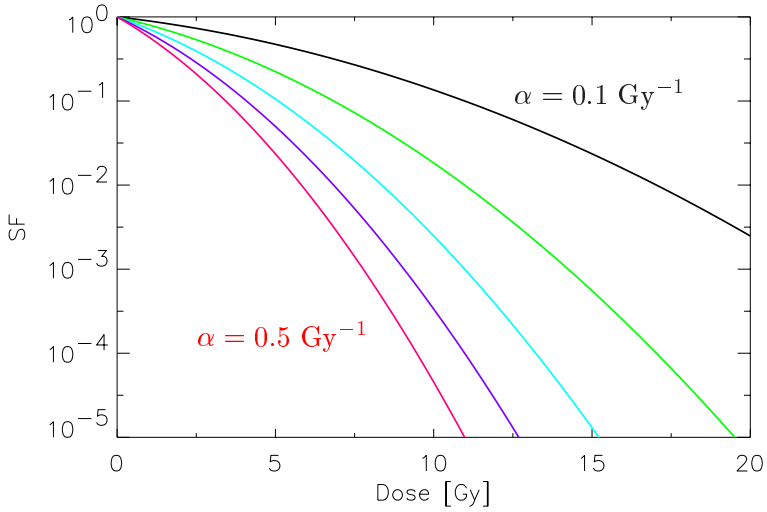


Figure 4.2: *Survival fractions (SF) calculated with the LQM for parameters* $\alpha = 0.1$ $Gy^{-1}$ *(black),* $\alpha = 0.2$ $Gy^{-1}$ *(green),* $\alpha = 0.3$ $Gy^{-1}$ *(cyan),* $\alpha = 0.4$ $Gy^{-1}$ *(blue), and* $\alpha = 0.5$ $Gy^{-1}$ *(red).* $\frac{\alpha}{\beta} = 10$ *Gy was taken for all SF.*

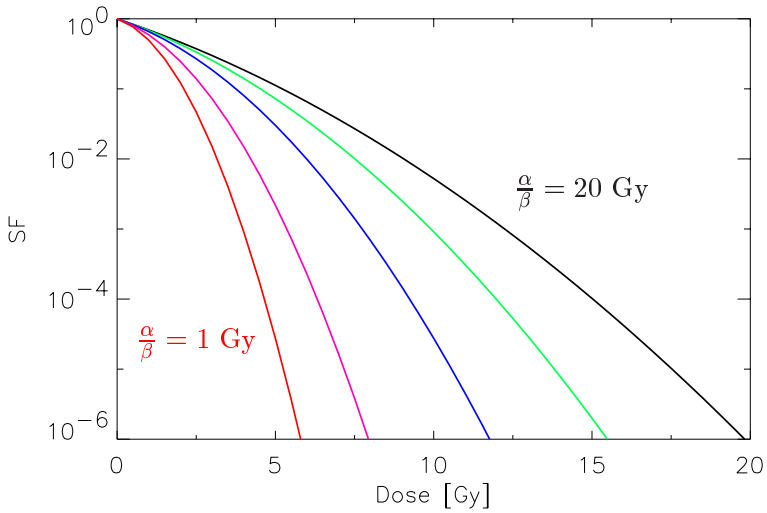


Figure 4.3: *Survival curves according to the LQM for different* $\frac{\alpha}{\beta}$*-ratios.* $\frac{\alpha}{\beta} = 1$ *Gy (red),* $\frac{\alpha}{\beta} = 2$ *Gy (pink),* $\frac{\alpha}{\beta} = 5$ *Gy (blue),* $\frac{\alpha}{\beta} = 10$ *Gy (green), and* $\frac{\alpha}{\beta} = 20$ *Gy (black).* $\alpha = 0.3$ $Gy^{-1}$ *for all survival fractions.*

2, 31, 79], but is not considered here. So far, no consensus could be achieved on how relevant radiation induced apoptosis is for treatment outcome [36].

### 4.1.3 Repair of sublethal damage

Three repair mechanisms for double-strand breaks are known. Homologous recombination is basically error-free since it uses an exactly homologous DNA-stretch. Non-homologous recombination can result in large deletions in the DNA. Non-homologous end-joining is very efficient and presumably the most common repair pathway in mammals. The excision repair pathway for base damage is also highly effective [86], but base damage is not considered here.

Repair of double-strand breaks can fail and cause aberrations due to misrepair. Early in the cycle phase misrepair of double-strand breaks will result in chromosome aberrations. Radiation interaction after DNA duplication in the synthesis phase will cause chromatid aberrations. The most common aberrations are rings and dicentrics, which are chromosome aberrations, and the anaphase bridge, which is a chromatid aberration [55]. Dicentric fragments have two centromeres and result from incorrect joining of two separate chromosome ends with double-strand breaks. An acentric with no centromere is formed from the remaining DNA fragments of the two chromosomes. A ring results from incorrect end-joining of two arms of the same chromatid with double-strand breaks. Resulting from the interaction of two chromosomes with double-strand breaks, the formation of aberrations serves as an explanation for the quadratic component of the linear-quadratic model [70, 27]. Nonlethal aberrations like deletion of DNA fragments can cause mutagenesis but are not covered in this context.

The number of double-strand breaks immediately after radiation and the fraction of remaining unrepaired double-strand breaks at several repair times can be studied by gel electrophoresis [33, 37]. It can be shown that the number of non-repaired double-strand breaks correlates with cell survival fraction [37, 38].

Repair mechanisms are often associated with cell cycle checkpoints at the $G_1$-S and the $G_2$-M transitions [111, 112] (see section 2.1.1). DNA damage causes a cell cycle delay during which repair is attempted [10]. Cells with non-repaired DNA damage will not pass. The $G_1$-S checkpoint will induce $G_1$ arrest or apoptosis whereas the $G_2$-M checkpoint will usually cause mitotic death.

The molecular basis for cell cycle delay and repair mechanisms is not discussed here. However, it is a target for new strategies in radiation oncology. It has been shown that inhibiting $G_2$ delay can radiosensitize cells whereas

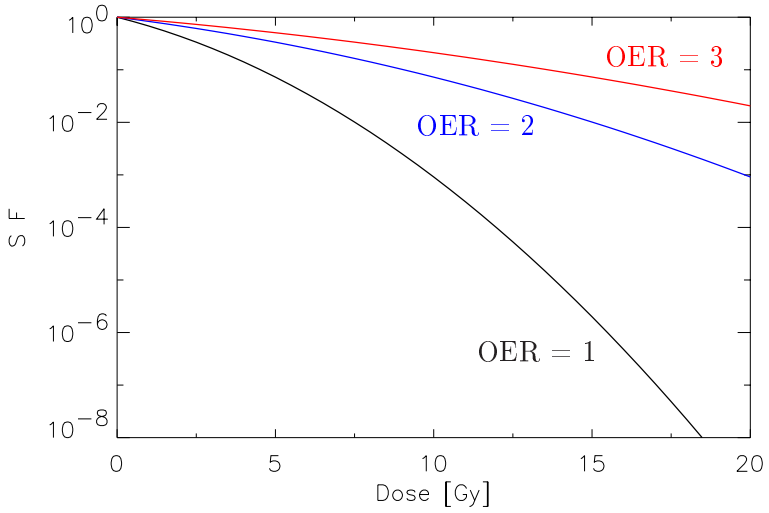


Figure 4.4: *Survival fraction (SF) depends on oxygen supply. In the LQM the oxygen effect is quantified by the OER. Survival fractions are shown for* $\alpha = 0.35$ $Gy^{-1}$ *and* $\frac{\alpha}{\beta} = 10$ *Gy. At a dose of 10 Gy, survival for OER = 2 (blue survival curve) is 80 times higher than it is for OER = 1 (black). For OER = 3 (red) the difference is even more pronounced.*

cells with prolonged $G_2$ delay have enhanced radioresistance [77]. Inhibiting repair of tumor cells while stimulating repair mechanisms within normal tissues would greatly enhance the therapeutic window in radiotherapy.

### 4.1.4 Oxygen effect

In section 4.1.1 two types of radiation action on the DNA have been introduced: direct interaction and indirect interaction which involves the creation of free radicals, mainly $O\cdot$ radicals. Tumor growth forces displacement of capillaries which in turn results in lack of oxygen within the tumor. The lack of oxygen in hypoxic areas translates into a reduced indirect action of radiation on the DNA. The reduction in radiosensitivity of hypoxic cells is called the oxygen effect. In the LQM it is quantified by the oxygen enhancement ratio (OER), a factor which reduces the dose entering the expression calculating cell survival (see figure 4.4). For hypoxic cells the survival fraction is

$$SF(D) = \exp\left(-\alpha\frac{D}{\mathrm{OER}} - \beta\left(\frac{D}{\mathrm{OER}}\right)^2\right). \tag{4.3}$$

For photons, OER values are between 2.5 and 3 for doses of 2 Gy and more [55, 94]. The oxygen effect is slightly reduced at doses of 1.5 Gy and less. For high-LET radiation there is hardly any indirect radiation action,

so the oxygen effect is negligible and the OER is one. Controlling hypoxic tumor cells, an important aspect in photon radiotherapy, is not an issue in radiotherapy with protons or heavy ions.

It was argued in section 2.1.2 that oxygen diffuses around capillaries and is subsequently consumed resulting in an oxygen concentration around capillaries that decreases exponentially with distance to the capillaries (see figure 2.2). However, experiments on radiosensitivity have shown that radiosensitivity remains almost constant until oxygen tension drops to very low levels. Figure 4.5, taken from Hall [55], shows relative radiosensitivity versus oxygen tension $pO_2$ in mm Hg.

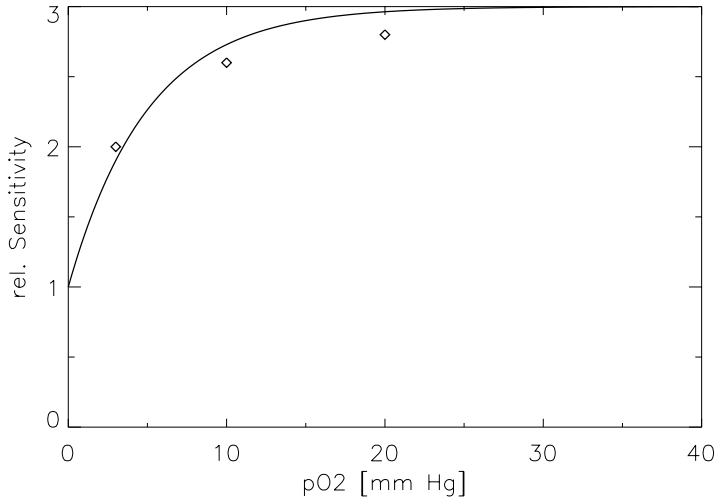


Figure 4.5: *Fully oxygenated cells (oxygen tension $pO_2 \simeq 40$ mm Hg for venous blood flow) are three times more sensitive to irradiation than anoxic cells are. Even at $pO_2$ levels as low as 3 mm Hg cells are still twice as radiosensitive as anoxic cells are. The oxygen effect only becomes pronounced at very low levels of $pO_2$. Sensitivities are given in arbitrary units.*

The tumor growth model introduced in section 2.2 simplifies oxygen diffusion around capillaries by a step function, distinguishing only well oxygenated (normoxic), unproliferating (hypoxic) and starved (necrotic) cells. Figure 4.5 illustrates why the relationship between oxygen tension and reduction of radiosensitivity can be simplified by the same step function. From the perspective of radiation response, merely distinguishing normoxic and hypoxic cells is a reasonable simplification.

### 4.1.5 Fractionation

Higher total doses are tolerated by normal tissues if the dose is applied in fractions. At the same time, dose per fraction hardly effects tumor control. This can be explained by the parameters of the linear-quadratic formalism. In the linear-quadratic model, fractionating the total dose, i.e., delivering $N$ doses of size $\frac{D}{N}$, increases the survival fraction significantly due to the quadratic term. This is easily understood by calculating the survival fraction for $N$ doses of $d = \frac{D}{N}$, where $D$ is the total dose. This yields

$$SF(D) = \Big( \exp\big( -\alpha\frac{D}{N} - \beta(\frac{D}{N})^2\big)\Big)^N = \exp\big( -\alpha D - \beta\frac{D^2}{N}\big) \qquad (4.4)$$

compared to

$$SF(D) = \exp(-\alpha D - \beta D^2)$$

for a single (unfractionated) total dose of size D. The gain in cell survival is $\exp(\beta D^2 \frac{N-1}{N})$.

Late responding tissues have a lower $\frac{\alpha}{\beta}$-ratio than acutely responding tissues, such as tumors, do. For lower $\frac{\alpha}{\beta}$-ratio the shoulder of the survival curve is more pronounced. Consequently, the sparing of cells achieved by the reduction of dose per fraction is more pronounced (see figure 4.6). For 5 fractions of 2 Gy and $\alpha = 0.3$ Gy$^{-1}$ the gain in survival fraction is around $1.6 \times 10^5$ for $\frac{\alpha}{\beta} = 2$ Gy (late responding tissues) versus a gain of 11 for $\frac{\alpha}{\beta} = 10$ Gy (acutely responding tissues). This motivates the interpretaion of $\frac{\alpha}{\beta}$ as repair capacity.

Experimental data on the influence of dose per fraction on radiation tolerance were compiled by Thames et al. [104]. From these data, Fowler derived $\frac{\alpha}{\beta}$-ratios for various tissues [48]. For breast treatments $\frac{\alpha}{\beta}$ seems to be in the range of 7 to 11 Gy for early reactions, and 2 to 4 Gy for late effects [108]. The following tables, tables 4.2 and 4.3, taken from Thames and Hendry [106], list $\frac{\alpha}{\beta}$-values for a number of early and late responding normal tissues as well as for selected tumors. The higher $\frac{\alpha}{\beta}$-ratios for most tumors compared to late responding normal tissues was the main rationale for introducing fractionated radiotherapy.

Administration of 1.8 to 2 Gy per fraction once a day with weekends off is regarded as standard practice [4]. Hyperfractionation is defined as a treatment in which doses per fraction are 1.6 Gy at the most, whereas accelerated fractionation refers to dose delivery patterns that reduce the overall treatment time or increase the dose per week [4]. Recently fractionation schemes

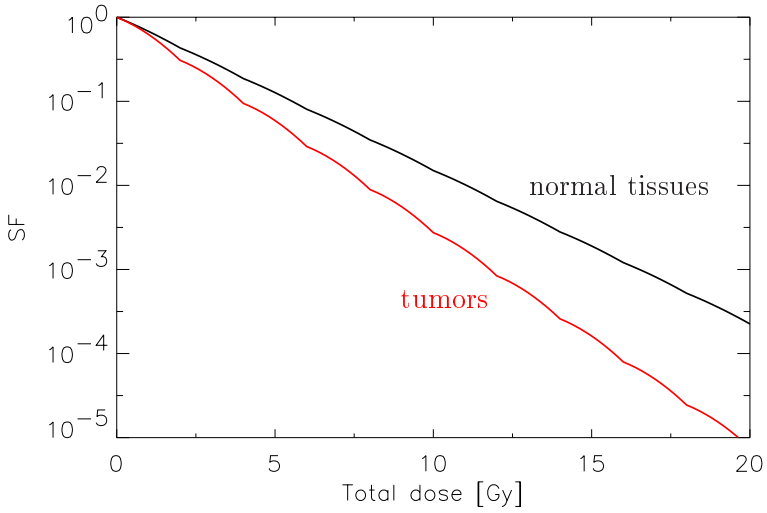


Figure 4.6: *Cell survival fraction (SF) of fractionated radiotherapy for typical $\frac{\alpha}{\beta}$-ratios for tumors ($\frac{\alpha}{\beta} = 10$ Gy, black) and for normal tissues ($\frac{\alpha}{\beta} = 3$ Gy, red). Fractionated delivery of total dose yields a higher sparing of cells for normal tissues than for tumors. Cell survival was calculated for $\alpha = 0.35$ $Gy^{-1}$.*

have been devised that escalate dose per fraction during the course of therapy of rapidly proliferating tumors such as non-small-cell lung cancer (NSCLC) [78]. In most time-dose patterns there is no treatment on weekends. Different ways to compensate for gaps and missed treatment days have been studied by Hendry et al [57].

Fractionation of the total dose delivered also reduces the oxygen effect in hypoxic cells. At doses below 2 Gy the oxygen enhancement ratio drops to about 2 for most tissues. In accelerated and hyperfractionated radiotherapy doses of 1.6 Gy and less are given per fraction.

### 4.1.6 The "4 Rs" of radiotherapy

In fractionated radiotherapy total dose is administered in doses of 1.5 Gy to 2 Gy per fraction over a time course of weeks. Calculating survival fractions according to equation 4.2 of the LQM does not take into account time dependent effects that are due to the dynamic behavior of tumors and normal tissues. The most important time factors have been identified by Withers as the "4 Rs" of radiotherapy [115]: Repopulation, repair, redistribution and reoxygenation.

Repopulation is due to proliferation of undamaged cells which might happen at an accelerated rate because growth fraction and apoptotic capacity can be size dependent [97, 98]. Little changes in $T_S$ and in $T_C$ have been

| Response | $\frac{\alpha}{\beta}$ in Gy |
|---|---|
| Early | |
| skin | 9.5-12 |
| colon | 8.5-10 |
| testis | 13-14 |
| Late | |
| spinal cord | 2-5 |
| kidney | 1-2.4 |
| lung | 2-4.5 |

Table 4.2: *$\frac{\alpha}{\beta}$-ratios for acute and late effects taken from Thames and Hendry [106].*

| Tumor | $\frac{\alpha}{\beta}$ in Gy |
|---|---|
| Mam. Ca. N.T. | 7.5-17.5 |
| CH3 Mam. Ca | 12.5-18.5 |
| Squamous Ca. | 12 |
| Fibrosarcoma | 4 |
| Slow sarcoma | 20-30 |

Table 4.3: *$\frac{\alpha}{\beta}$-ratios for selected tumor cells taken from Thames and Hendry [106].*

observed throughout treatments, however [13, 97, 98]. Attempts have been made to incorporate repopulation into the linear-quadratic model by introducing a term $\gamma$ linear in time $t$ [109, 107]:

$$SF(D) = \exp(-\alpha D - \beta D^2 + \gamma t) \; .$$

The dose equivalent of regeneration per day $D_{prolif}$ is used to quantify repopulation: $D_{prolif} = \frac{\gamma}{\alpha+\beta d}$ with $d = \frac{D}{N}$. Values for $\gamma$ are obtained by maximum likelihood estimation from clinical data [108].

Repair of sublethal damage happens between fractions. For conventional fractionation inter-fraction intervals seem to be long enough to complete repair. For accelerated treatments and especially for hyperfractionation this might not be true [39, 3, 9]. In the linear-quadratic formalism it is the quadratic multi-hit component that is sublethal and can be repaired [105, 30, 29]. Several models have tried to account for repair of DNA damage by adding terms to the LQM. In the incomplete repair model the fraction $\theta$ of unrepaired sublethal damage decreases exponentially with time

$$\theta = \exp(-\mu t) \; ,$$

$\mu$ being the repair rate [105]. Taking into account repair mechanisms is important for predicting treatment outcome in brachytherapy, where dose is delivered continuously at a low dose rate [20]. There is no time for repair between the deposition of the doses so incomplete repair must be considered. For doses below 0.6 Gy hypersensitivity of cells is observed [68, 75]. Cell survival is less than according to the linear-quadratic model. This might be due to a failure to induce repair mechanisms at low doses. Late responding tissues tend to have a higher repair capacity than acutely responding tissues and tumors do, so considering repair mechanisms is more important for many normal tissues than it is for tumors.

Redistribution refers to asynchronous cycle phases of surviving tumor cells. Cell cycles vary in their radiosensitivity. Upon irradiation, a higher fraction of cells will be in S phase, the least radiosensitive phase. Between fractions the cell population will again become asynchronous resulting in a resensitization of tumor cells. Redistribution has been incorporated into the LQM by Brenner et al [18] and Smith et al [100]. Redistribution results in asynchronous sensitivities. Fluctuations in $\beta$ are considered to be small; the probability distribution of $\alpha$ is taken to be gaussian with variance $\sigma^2$. Averaging over asynchronous subpopulations yields

$$SF(D) = \exp(-\alpha D - \beta D^2 + \frac{\sigma^2}{2} D^2) \; .$$

It is assumed that extra resistance outweighs extra sensitivity, which results in an extra term that increases the survival fraction by $\exp(\frac{\sigma^2}{2} D^2)$.

Due to ongoing cell division and tumor angiogenesis, hypoxic cells may be reoxygenated between fractions. This results in higher radiosensitivity.

## 4.2 A cellular model for tumor response to radiotherapy

Modeling tumor response to radiation is based on the stem cell principle and on the linear-quadratic formalism for DNA damage. Using the stem cell principle is founded on the observation that tumor cells are proliferating and not functional cells [72]. Much of the time factor in fractionated radiotherapy introduced in section 4.1.6 is already accounted for by the dynamic behavior of the tumor growth model. Of the "4 Rs" of radiotherapy only repair needs to be modeled separately. Treatment pattern dependent effects like reoxygenation, repopulation and redistribution are consequences of the cellular approach to tumor modeling. Repopulation happens through ongoing proliferation of undamaged cells which can be enhanced by a growth fraction that

is assumed to increase with decreasing cell number. In addition, apoptotic fraction is taken to decrease with decreasing tumor size. Redistribution of cell cycles happens due to the reassignment of cycle times of surviving proliferating cells. Cell cycle delay caused by repair also contributes to redistribution. Reoxygenation of hypoxic cells occurs because of cell displacement throughout the tumor as a consequence of ongoing proliferation. Angiogenesis also results in reoxygenation of hypoxic cells.

### 4.2.1 Biological parameters

Based on the interaction of radiation with tissues, the mechanisms of cell killing, cell response to damage and the time factor in fractionated radiotherapy, a model can be devised that allows computer simulation of tumor response. The following parameters are included in the model for tumor response to radiotherapy.

1. Cell survival.
   Survival fraction is calculated according to the linear-quadratic model (LQM). Every single tumor cell is considered a potential target. Only if all viable tumor cells have been killed is the tumor considered to be controlled.

2. Radiosensitivity.
   The dominant factor in modeling fractionated radiotherapy is the intrinsic radiosensitivity of tumor cells which is given by the parameters $\alpha$ and $\beta$ of the LQM. Cell cycle phases can differ in their sensitivities [88, 29]. Since cells are individually taken into consideration, a heterogeneous cell population can easily be modeled by assigning every cell its own parameters $\alpha$ and $\beta$ according to a normal distribution.
   Hypoxic cells are considered to be quiescent. Their radiosensitivity is assumed to be that of the $G_1$ phase.

3. Oxygen effect.
   Oxygen levels influence radiosensitivity [102, 72]. The number of free $O\cdot$ radicals is reduced in hypoxic areas, limiting indirect radiation action. In the LQM the oxygen effect is considered by dividing the dose by a factor OER (oxygen enhancement ratio) as indicated in equation 4.3. The oxygen effect is slightly lower for doses of 1.5 Gy than for doses of 2 Gy or more.

4. Cell death and postmitotic survival.
   Lethally hit normoxic cells are taken to die upon entering mitosis. With

a certain probability $P_{pms}$, however, postmitotic survival for a small number of cell cycles is allowed. Not moving through cycle phases, hit hypoxic cells are considered to die after one cycle time [64].

5. Repair of sublethal damage.
   The quadratic component of the LQM stems from sublethal damage [105, 30] which can potentially be repaired with a certain probability [37]. In this model of tumor response, repair mechanisms can either be triggered instantly or repair can take place at the $G_1$-S and $G_2$-M checkpoints [10]. No repair is possible for hypoxic cells.
   Most tumors show less repair capacity than normal tissues do. Typical $\frac{\alpha}{\beta}$-ratios are about 10 Gy for tumors, versus ratios of about 2-5 Gy for most late responding tissues. For tumors, repair of sublethal damage between fractions is not a dominant effect. Complete repair between fractions is assumed in simulations unless stated otherwise.

6. Cell cycle delay.
   The cell cycle delay due to (successful or unsuccessful) repair is taken to be 6 h. In this setting, taking into account repair only has a significant influence on tumor control for short intervals between fractions.
   The cell cycle delay caused by repair contributes to the redistribution of cell cycles between fractions.

### 4.2.2 Implementation

Tumor response to radiotherapy is simulated by a Monte-Carlo technique. Three more cell types are added to the ones defined in the implementation of the tumor growth model in section 2.2.2: Lethally und sublethally hit normoxic cells and lethally hit hypoxic cells. Since hypoxic cells do not cycle, there is no repair mechanisms in hypoxic cells and all hits are taken to be lethal. Cell survival is simulated for each tumor cell individually according to the linear-quadratic formalism and the sensitivity of the cell. A normoxic cell survives if a random number drawn from a uniform probability distribution is less than its individual survival probability

$$SF_{\text{cell}}(D) = \exp(-\alpha_{\text{cell}} D - \beta_{\text{cell}} D^2) \ .$$

A hypoxic cell is taken to survive if the same probabilistic procedure yields a number less than

$$SF_{\text{cell}}(D) = \exp\left( - \alpha_{\text{cell}} \frac{D}{OER} - \beta_{\text{cell}} (\frac{D}{OER})^2 \right) \ .$$

If repair mechanisms of sublethally hit normoxic cells are taken into account, the probability for a lethal hit is

$$SF_{\text{cell}}(D) = \exp(-\alpha_{\text{cell}} D)$$

and the probability for a sublethal hit is

$$SF_{\text{cell}}(D) = \exp(-\beta_{\text{cell}} D^2) \ .$$

To reduce memory requirements, the parameters $\alpha$ and $\beta$ are determined (randomly) at each radiation event. The dose is taken to be administered instantaneously. No dose-rate is considered. Radiosensitivities that vary within the cell cycle can be accounted for by determining $\alpha$ and $\beta$ values according to four different normal distributions, depending on the cell age.

Repair of sublethally hit cells and postmitotic survival of lethally hit cells is determined by the same probabilistic technique. For each lethally hit cell a random number is drawn from a uniform probability distribution upon entering mitosis to determine whether the cell survives. If so (i.e. if the number drawn is less than $\mathrm{P}_{\text{pms}}$), the daughter inherits the cell's damage. Cells killed by radiation are treated the same way necrotic cells are. They are resorbed within the same lysis times. Two repair mechanisms can be modeled. Repair is either triggered instantaneously or at the $\mathrm{G}_2$-M checkpoint. Repair is attempted for all hit cells causing a delay in the cell cycle. A cell is successfully repaired if a random number drawn from a uniform probability distribution is less than $\mathrm{P}_{\text{rep}}$.

The mechanisms for cell killing and possible repair are incorporated in the cell cycle model of tumor growth introduced in section 2.2.2. As indicated, repair mechanisms are checked once the cell passes the $\mathrm{G}_1$ phase or the $\mathrm{G}_2$ phase. The mechanism deciding whether the cell dies of mitotic death is activated at the transition from $\mathrm{G}_2$ to M. The resulting cell cycle model is illustrated in figure 4.7. The importance of further simplifying the cell cycle model to speed up simulations has been pointed out in section 2.2.2. If cell cycle phase dependent radiosensititvities are not considered and complete repair between fractions is assumed, simulations are performed according to a cell cycle model that checks for activity, apoptosis and mitotic death at the end of the cell cycle (see figure 4.8).

Figure 4.9 shows a tumor before (a) and after (b) six weeks of conventional radiotherapy corresponding to a total dose of 60 Gy. At the onset of radiotherapy the tumor had 50 million cells and a diameter of 10.5 mm. Almost all normoxic cells (blue) have already been killed and absorbed at the end of therapy. A significant fraction of viable hypoxic cells (red) has survived. Reduced sensitivity of hypoxic cells was due to a large OER value which was taken to be OER = 3. The tumor cycle time was $\mathrm{T}_{\mathrm{C}} = 65$ h.

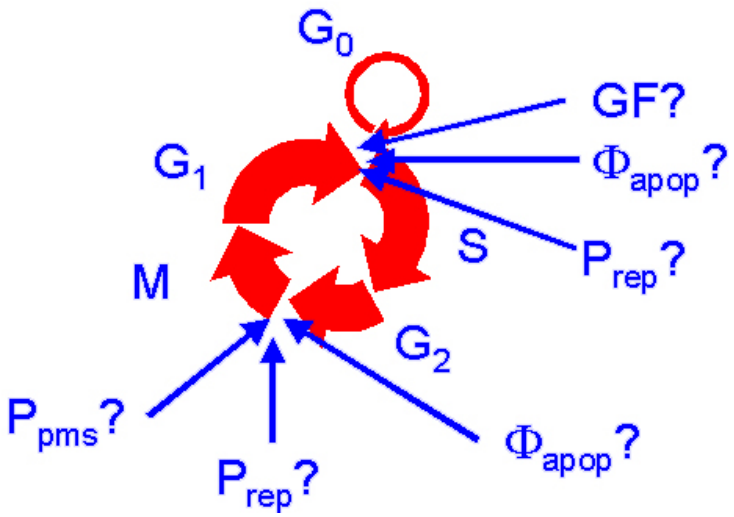


Figure 4.7: *Model of the cell cycle including mechanisms for repair of sublethal damage and mitotic death. Activity of unhit normoxic cells (determined by GF) is decided on after $T_{G_1}$. At this point (and again after $T_{G_1}$), apoptosis might also occur with a probability $\Phi_{apop}$. For hit cells two mechanisms are activated: Repair of sublethal damage with probability $P_{rep}$ at the $G_1$-$S$ and $G_1$-$M$ checkpoints or mitotic death at the $G_1$-$M$ transition.*

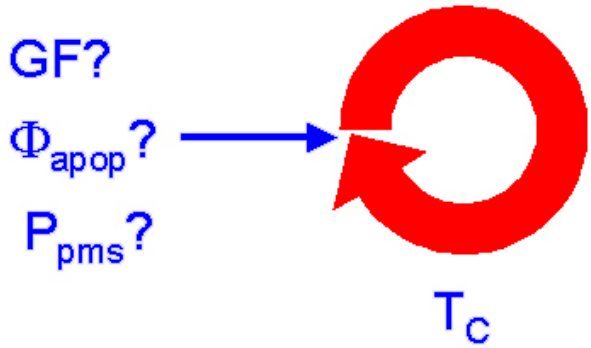


Figure 4.8: *Simplification of the cell cycle model pictured in 4.7. Mechanisms for activity, apoptosis and mitotic death are located at the end of the cell cycle and are checked once every $T_C$.*

### 4.2.3 Simulation runs

| Model parameters | |
|---|---|
| Radiosensitivity | $\alpha = 0.3 - 0.4\,\mathrm{Gy}^{-1}$, $\frac{\alpha}{\beta} = 10\,\mathrm{Gy}$ |
| $\sigma_\alpha$ | $\frac{\alpha}{8}$ |
| $\frac{\alpha}{\beta}$ | 10 Gy |
| Oxygen effect | OER = 3 for D =2 Gy<br>OER = 2.5 for D = 1.5 Gy |
| Cell cycle delay due to repair | 6 h |
| Probability for postmitotic survival | $P_{pms} = \frac{1}{3}$ |
| Repair mechanism | complete repair between fractions or<br>$P_{rep} = 0$, $\frac{1}{3}$ at checkpoints |
| Dose fractionation pattern | standard: 2 Gy once daily<br>accelerated: 1.5 Gy every 12 h |

Table 4.4: *Typical parameter values used in the simulations of tumor response to fractionated radiotherapy.*

The radiosensitivities considered in the simulations presented are considered to be typical for many human tumors (see table 4.4 for typical $\alpha$ and table 4.3 for typical $\frac{\alpha}{\beta}$-ratios). The OER values were chosen according to experiments published by Hall [55]. The cell cycle delay was assumed to be 6 h due to short repair halftimes published by Dahm-Daphi et al [33] and Smith et al [100]. However, analysis of clinical data on continuous hyperfractionated accelerated radiotherapy suggests that repair is not complete within 6 h [39, 3]. The probability for postmitotic survival is assumed to be $\frac{1}{3}$ because some cells are observed to survive mitosis in spite lethal DNA-damage, but few cells undergo more than three or four mitoses after being lethally hit. For $P_{pms} = \frac{1}{3}$ only $(\frac{1}{3})^3 = 3.7\%$ of lethally hit normoxic cells will undergo three more mitoses and only $(\frac{1}{3})^4 = 1.2\%$ of lethally hit normoxic cells will undergo four more mitoses. Repair mechanisms have been studied extensively for normal tissues but no repair halftimes have been published for tumor cell lines. No probability for repair $P_{rep}$ of sublethal damage can be given. A repair probablity $P_{rep} = \frac{1}{3}$ was assumed, but this is only relevant for one simulation presented, in which no complete repair was assumed between fractions.

In the case of phase dependent radiosensitivities and incomplete repair due to low inter-fraction intervalls the parameter values listed in table 4.5 were used for simulation of tumor response to radiotherapy. The phase dependent radiosensitivities chosen reflect experiments showing that mitosis is

a)

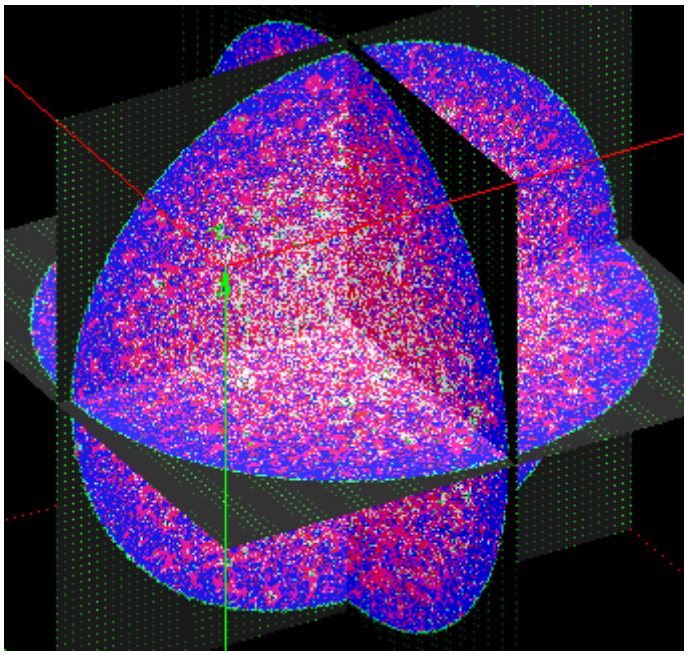

b)

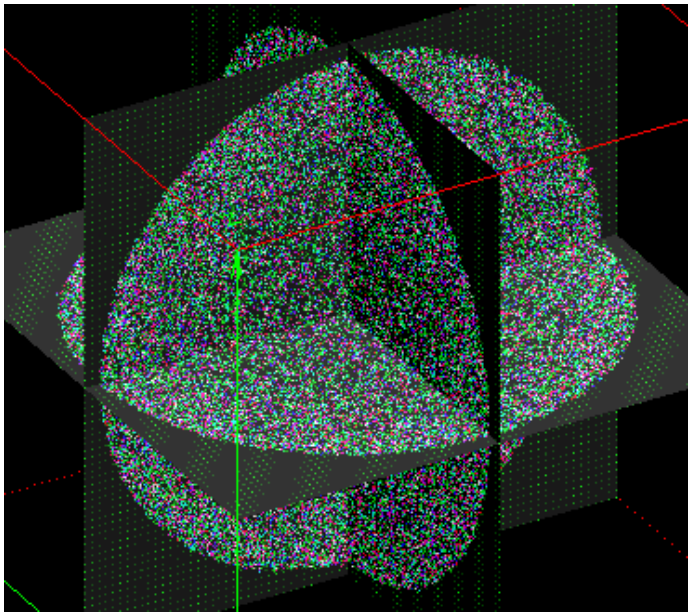

Figure 4.9: *Tumor with* $\alpha = 0.4\ Gy^{-1}$ *and* $\frac{\alpha}{\beta} = 10\ Gy$ *before (a) and after (b) six weeks of conventional therapy (2 Gy given once a day with weekends off).* $T_C = 65$ h, $GF = 100\%$ *and* $\Phi_{apop} = 0$ % *was chosen. Normoxic tumor cells are blue, hypoxic tumor cells red and necrotic tumor cells white. Capillaries are depicted green. At the end of the simulated therapy there are almost no normoxic cells left while a significant number of hypoxic cells have survived because of a pronounced oxygen effect with OER = 3.*

| Model parameters | |
|---|---|
| $T_C$ | 115 h |
| $T_{G_1}$, $\alpha_{G_1}$ | 83 h, $\alpha = 0.4$ Gy$^{-1}$ |
| $T_S$, $\alpha_S$ | 14 h, $\alpha = 0.1$ Gy$^{-1}$ |
| $T_{G_2}$, $\alpha_{G_2}$ | 12 h, $\alpha = 0.5$ Gy$^{-1}$ |
| $T_M$, $\alpha_M$ | 6 h, $\alpha = 0.5$ Gy$^{-1}$ |
| $\sigma_\alpha$ | $\frac{\alpha}{8}$ |
| $\frac{\alpha}{\beta}$ | 5 Gy |
| Oxygen effect | OER = 3 |
| Cell cycle delay due to repair | 6 h |
| Repair mechanism | $P_{rep} = 0 - \frac{1}{3}$ at checkpoints |
| Dose fractionation pattern | accelerated: 1.5 Gy every 12 h |

Table 4.5: *Model parameters for the simulation of tumor response including cycle phase dependent sensitivities and repair mechanisms. These values were only used in the simulation of the effect of incomplete repair on tumor response shown in figure 5.16.*

the most and synthesis the least sensitive cycle phase. Literature on phase dependent radiosensitivities is scarce. Phase dependent radiosensitivities have only been measured for a few human cell lines in vitro [88, 11].

# Chapter 5

# Results

In this chapter simulation results based on the radiobiological model developed in the three previous chapters will be presented. In section 5.1 it will be shown how the model parameters effect tumor growth. The influence of angiogenesis on tumor growth is demonstrated in 5.2. A central aspect of this work was the desire to compare simulation results with experimental data in vivo. The Dunning R3327 tumor system in Copenhagen rats was chosen as a reference point for simulations of tumor growth. This tumor system has been introduced briefly in section 2.1.4. Comparing simulated growth curves with corresponding experimental data stresses the need to include angiogenesis in simulations of tumor proliferation. Section 5.4 deals with the influence of the model parameters on tumor response.

It will be demonstrated that tumor response does not only depend on the intrinsic radiosensitivities of tumors but on their growth characteristics, too. Comparing simulations of tumor growth for the cell kinetics parameters of the AT1 and the HI sublines of the Dunning R3327 tumor system emphasizes the role angiogenesis plays in tumor proliferation. The way angiogenesis influences tumor response to fractionated radiotherapy is discussed.

All simulations presented in this chapter were performed with the parameter values given in tables 2.4, 3.1 and 4.4 for tumor growth, tumor angiogenesis and tumor response to irradiation, respectively. The ranges chosen for the parameter values are either motivated by experimental data or considered to be typical in the literature. A major objective of this work was to verify that simulations according to the cellular model are in qualitative agreement with experimental data. Another goal was to identify the dominant parameters influencing tumor behavior. Parameter values entering the simulations presented in the next four sections were chosen with these two objectives in mind.

## 5.1 Tumor growth

Simulations of unperturbed tumor growth were performed with the parameter values given in table 2.4. Simulations of tumor growth were performed for $T_C$-values as low as 2.7 d (65 h) and as high as 7.1 d (170 h). Growth fraction and $\Phi_{apop}$ were taken to be size dependent. Within a tumor GF was taken to decrease logarithmically with tumor size while $\Phi_{apop}$ was considered to increase logarithmically with tumor size (see equation 2.2). Lysis mechanisms were assumed to saturate logarithmically with increasing number of dead cells in an analogous manner. Within the range of lysis times given in table 2.4, lysis times do not have a dominant effect on tumor behavior. Therefore, all simulations will be performed with maximum lysis times of 96 h and 144 h for apoptotic and necrotic cells, respectively. The oxygenation status of tumor cells was determined by their distance to the nearest capillary. Normoxic, hypoxic and necrotic cells were distinguished. The capillary system was modeled by a capillary distribution that was homogeneous at the beginning of tumor growth with an intercapillary distance of 7 cell layers (see figure 2.5). Only to demonstrate the effect the microenvironment has on tumor proliferation were simulations performed with different capillary systems.

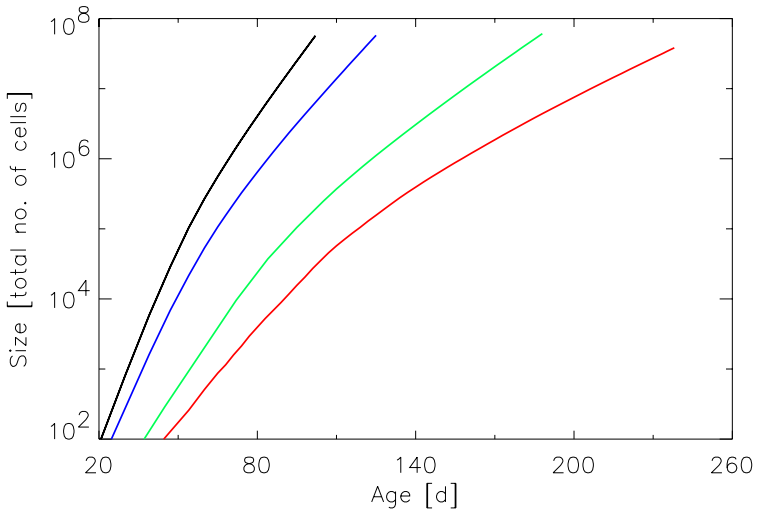


Figure 5.1: *Tumor growth depends on the cell cycle time $T_C$. Growth curves are shown for various $T_C$: $T_C = 55$ h (black curve), $T_C = 80$ h (blue), $T_C = 115$ h (green), $T_C = 150$ h (red). All simulations represent tumors with apoptotic capacity $\Phi_{apop} = 0$ and growth fraction GF = 100%.*

In normal tissues there is an equilibrium between cell cycle time ($T_C$),

actively proliferating cells (growth fraction GF) and programmed cell suicide (determined by the apoptotic capacity $\Phi_{\mathrm{apop}}$). In tumors this equilibrium is lost and there is uncontrolled growth. Simulations of tumor growth for various cell cycle times $T_C$ show an increase in proliferation rate with decreasing $T_C$ (figure 5.1). Tumor proliferation also depends on growth fraction and apoptosis. Increasing cell cycle times and apoptotic capacity while lowering growth fraction slows down the rate of proliferation and ultimately results in equilibrium. This is illustrated in figure 5.2, which shows simulated growth curves for the same cell cycle time $T_C = 80$ h but different fractions of apoptotic and quiescent cells. The logarithmic increase in apoptotic fraction was from 0% to 15% for the blue curve and from 0% to 20% for the red curve. The growth fraction decreased logarithmically from 100% to 85% for the blue curve and from 100% to 80% for the red curve.

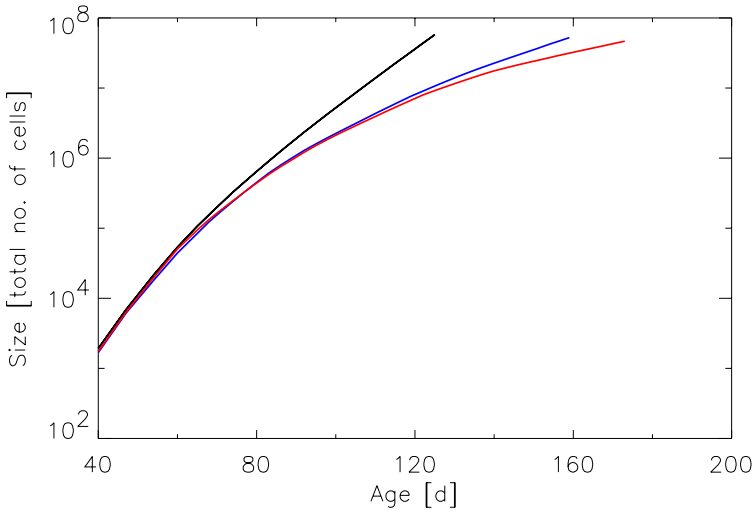


Figure 5.2: *Tumor growth curves for different apoptotic capacity $\Phi_{apop}$ and growth fraction GF. Tumors with $\Phi_{apop} = 0\%$ and GF = 100% (black curve) proliferate faster than tumors where there is still some (size dependent) apoptosis and some (size dependent) fraction of quiescent cells (colored curves). Growth was simulated with $T_C = 80$ h. $\Phi_{apop}$ increased logarithmically from 0% to 15% (blue) and from 0% to 20% (red) while the growth fraction decreased on the same logarithmic scale from 100% to 85% (blue) and from 100% to 80% (red).*

throughout the simulations presented here. The diffusion radius remained constant at 200 $\mu$m, corresponding to 10 cell layers. A capillary cycle time of 120 h was applied in one simulation to demonstrate that capillary cycle time does not have a pronounced effect on tumor proliferation (see figure 5.5). All other simulations of tumor growth with angiogenesis were performed with capillary cycle times $T_C = 72$ h.

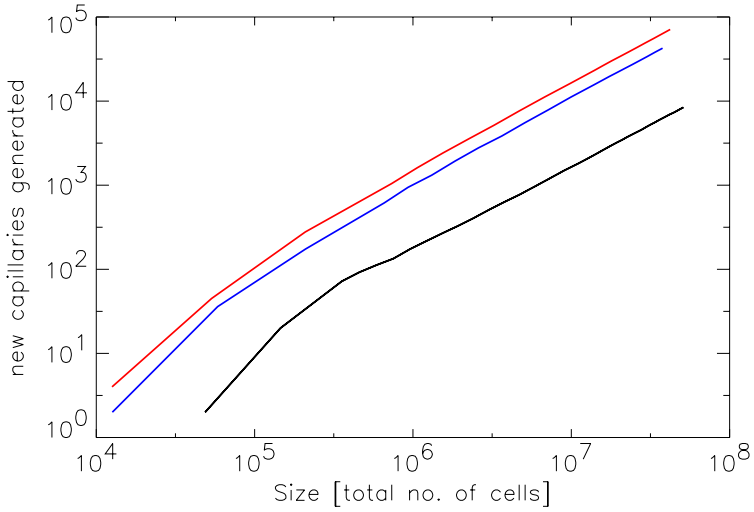


Figure 5.4: *Number of newly produced capillaries due to tumor angiogenesis vs. tumor size. Different thresholds for capillary stimulation are shown: 120 a.u. (black), 100 a.u. (blue) or 80 a.u. (red) of tumor angiogenesis factors (TAF) are needed for capillary stimulation. $T_C = 72$ h was chosen for capillaries, the tumor cell cycle time was $T_C = 115$ h. The number of new capillaries produced depends on the amount of TAF needed to stimulate capillary division.*

Figure 5.4 shows the number of induced capillaries for various thresholds. Tumor angiogenesis increases the number of normoxic cells which is the fraction of cells that proliferate (figure 5.5). Thus, angiogenesis enhances tumor growth (figure 5.6). There is a competition between proliferation of tumor cells and generation of new capillaries. Angiogenesis has a more pronounced effect on normoxic fraction for slowly proliferating tumors. If $T_C$ is too low, angiogenesis cannot keep up (figure 5.7). Simulations were performed with the same parameters of the angiogenesis model, but with three different tumor cell cycle times. Whereas the normoxic fraction recovers to values above 85% for low thresholds in the slowly proliferating tumor ($T_C = 115$ h) resulting in the red curve, it remains below 80% for the fast proliferating tumors ($T_C = 65$ h and $T_C = 80$ h for the black and blue curves, respectively).
Within the range studied, the capillary response time is not a dominant

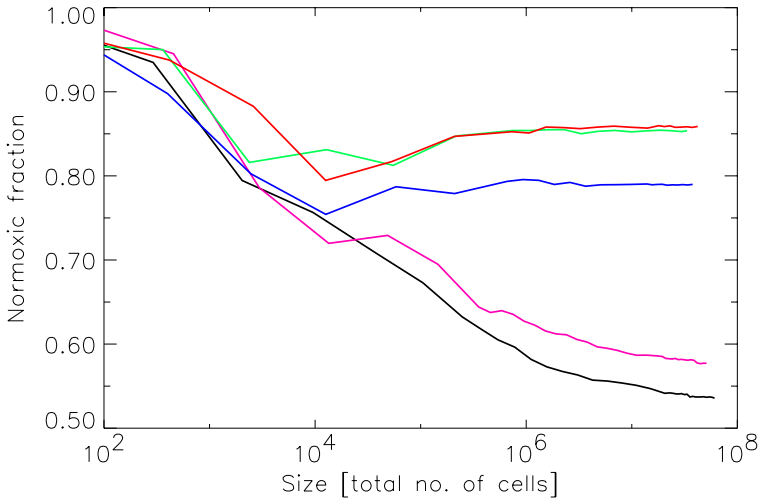


Figure 5.5: *Normoxic fraction vs. tumor size. Stimulus thresholds in a.u. of tumor angiogenesis factors (TAF) used for the simulations were 120 (pink), 100 (blue) and 80 (green and red). Simulations of tumor angiogenesis were performed with tumor cycle times of* $T_C = 115$ *h. Capillary cycle times were* $T_C = 120$ *h for the green curve and* $T_C = 72$ *h for all other tumor simulations. Without angiogenesis the normoxic fraction decreases with tumor size (black curve), reducing the tumor growth rate. Angiogenesis increases the normoxic fraction.*

parameter as can be seen from figure 5.5. For a tumor cell cycle time of $T_C = 115$ h, increasing the capillary cycle time $T_C$ from 72 to 120 h delays tumor angiogenesis but does not influence the normoxic fraction. The reason for this is that most capillaries are in $G_0$, waiting to be stimulated. Only if a significant fraction of capillaries were actively moving through their cell cycle would their cycle time influence angiogenesis.

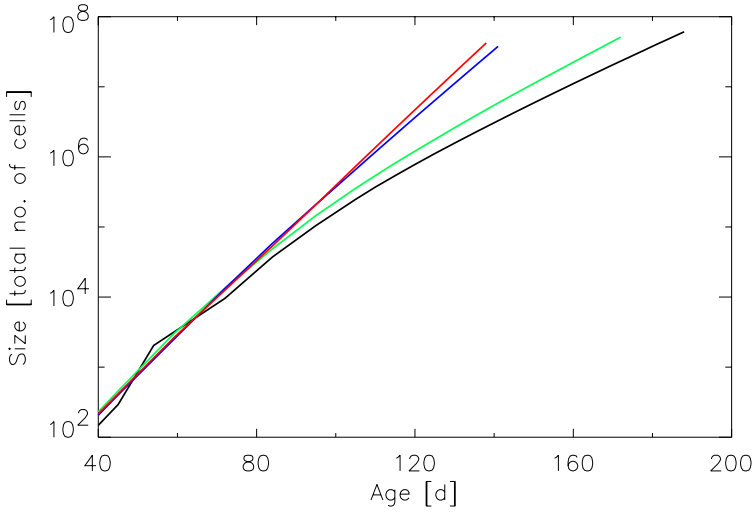


Figure 5.6: *Tumor proliferation with and without angiogenesis. The black growth curve shows tumor proliferation without angiogenesis. Tumor angiogenesis enhances tumor growth. Capillary stimulation thresholds chosen were 120 a.u. of tumor angiogenesis factors (green), 100 a.u. (blue) and 80 a.u. (red). $T_C$ was 115 h for tumor cells and 72 h for capillaries. The tumor growth rate increases with decreasing stimulation threshold.*

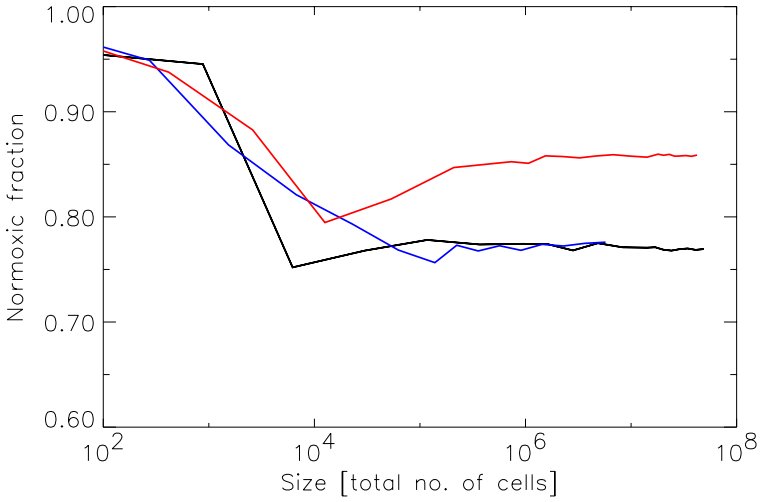


Figure 5.7: *Normoxic fractions versus tumor size for the same stimulus threshold (80 a.u. tumor angiogenesis factors) but for different cell cycle times $T_C$. The red curve represents tumor proliferation with $T_C = 115$ h. $T_C$ was 80 h for the blue curve and 65 h for the black curve. The effect of angiogenesis on the tumor depends on the tumor cell proliferation. For fast growing tumors, new capillaries are not induced fast enough to keep tumor cells from turning hypoxic or even necrotic.*

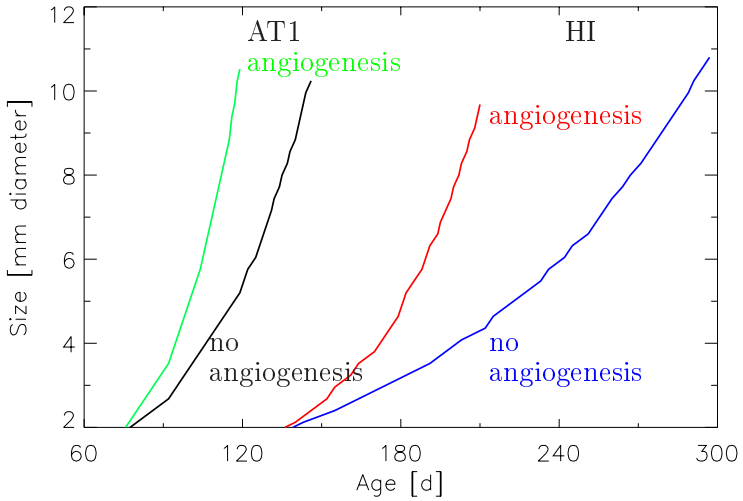


Figure 5.8: *Simulated growth curves for the cell kinetics parameters of the AT1 and HI sublines of the R3327 Dunning tumor system with and without tumor angiogenesis. Angiogenesis was simulated using a threshold of 80 a.u. of tumor angiogenesis factors. Tumor angiogenesis reduces the tumor volume doubling time. The effect of angiogenesis is more pronounced for the moderately well differentiated HI subline than for the anaplastic AT1 subline.*

## 5.3 Comparing simulated tumor growth with experimental growth curves in vivo

Simulations were performed with the growth parameters of two of the sublines of the Dunning R3327 tumor system, the AT1 and HI sublines. The cell kinetics parameters for these two sublines were measured with flow cytometry methods [72, 93] and are given in table 2.2. Observed tumor volume doubling times were calculated using equation 2.1 and are presented in table 2.3. Figure 5.8 shows simulated tumor growth with and without angiogenesis for the AT1 and HI sublines. Simulations were performed with no apoptosis and a growth fraction of 100% for both sublines. The threshold considered for angiogenesis was 80 a.u. of TAF and the capillary cycle time was $T_C = 72$ h.

It can be derived from figure 5.8 that simulations of tumor growth not considering tumor angiogenesis result in volume doubling times much lower than observed experimentally. Volume doubling times were calculated from the growth curves according to

$$V(t) = V_0 \exp(\frac{\ln 2}{\mathrm{T_D}} t) \ .$$

From two volumes $V_1$ and $V_2$ at times $t_1$ and $t_2$ the volume doubling time $\mathrm{T_D}$ can be extracted by

$$\ln V_2 - \ln V_1 = \frac{\ln 2}{\mathrm{T_D}} (t_2 - t_1) \ .$$

For the AT1 subline, $\mathrm{T_D}$ was 9 d without angiogenesis. $\mathrm{T_D}$ decreased to 6.1 d when angiogenesis was accounted for in the simulations. The observed mean volume doubling time was 5.6±0.4 d. For the HI subline, the effect was even more pronounced. $\mathrm{T_D}$ decreased from 21.1 d without angiogenesis to 10.3 d when angiogenesis was considered. The HI tumors have an observed mean volume doubling time of 10±1.1 d [72]. This can be explained by the cell kinetics and the proliferation rates of the two sublines. The HI tumor grows much slower, allowing angiogenesis to keep up with its growth. In table 5.1 experimental volume doubling times are compared to those obtained by the simulations shown in figure 5.8. Simulations of angiogenesis were performed with thresholds of 80 a.u. of TAF for both the AT1 and the HI tumors.

| Dunning R3327 Subline | observed $\mathrm{T_D}$ [d] | simulated $\mathrm{T_D}$ [d] | |
|---|---|---|---|
| | | no angiogenesis | angiogenesis |
| AT1 | 5.6±0.4 | 9 | 6.1 |
| HI | 10±1.1 | 21.1 | 10.3 |

Table 5.1: *Volume doubling times $T_D$ for two Dunning R3327 sublines obtained experimentally from male Copenhagen rats and from the simulations illustrated in figure 5.8. Experimental doubling times were taken from Lohr et al [72].*

## 5.4 Tumor response to irradiation

The tumor response model includes parameters to describe intrinsic (cycle phase dependent) radiosensitivities, repair of sublethal cell damage, cell cycle delay, postmitotic survival and the oxygen effect. Simulation results are presented for typical parameter sets (see table 4.4). For most simulations,

complete repair between fractions is assumed and sensitivities do not vary throughout the cell cycle. An $\frac{\alpha}{\beta}$-ratio of 10 Gy was chosen, a value considered to be typical for tumors (see table 4.3). Repair and phase dependent sensitivities are only considered in one example to demonstrate that repair effects are not dominant in tumor control, but must be considered for moderately acute responding tissues (which are assumed to have $\frac{\alpha}{\beta}$-ratios of approximately 5 Gy). Both fractionation schemes studied here, conventional and accelerated fractionation, were assumed to have weekends off. In all simulation results presented, tumor response will be given as the number of normoxic cells surviving each day of the treatment. In conventional fractionation 10 Gy are delivered per week, whereas one week of accelerated treatment corresponds to a total dose of 15 Gy.

Tumor response is first and foremost determined by the intrinsic radiosensitivity. In the LQM, radiosensitivity is quantified in terms of the parameters $\alpha$ and $\beta$. Figure 5.9 presents simulated tumor response for a conventional fractionation pattern. The growth parameters for all three tumor cell lines were $T_C = 80$ h, GF = 100% and $\Phi_{apop} = 0\%$. The radiosensitivities were $\alpha = 0.3$ $Gy^{-1}$ for the cell line corresponding to the black curve and $\alpha = 0.35$ $Gy^{-1}$, $\alpha = 0.4$ $Gy^{-1}$ for the blue and red curves respectively. As can be seen from table 4.4, $\frac{\alpha}{\beta} = 10$ Gy was assumed for all cell lines. The OER was taken to be 3, a value which drastically reduces the sensitivity of hypoxic cells. Complete repair between fractions was assumed. The relatively radioresistant cell line with $\alpha = 0.3$ $Gy^{-1}$ (black survival curve) could not be controlled for a total dose as high as 70 Gy. The effect of two of the "4 Rs", repopulation and reoxygenation, on tumor response can clearly be seen from figure 5.9. There is significant repopulation during weekends where there is no treatment. Repopulation between fractions during the first week of treatment is illustrated for the red curve representing the most sensitive cell line. Figure 5.9 also stresses the importance of reoxygenation. At the end of the treatment it can be seen that killing of all normoxic cells might not correspond to tumor control because of reoxygenation of hypoxic cells.

Treatment outcome also depends on the time-dose pattern applied. Figure 5.10 shows how the time-dose pattern influences tumor control. Two cell lines with different radiosensitivities but with the same cell proliferation differ in tumor response. The black curve represents cell survival for a relatively radioresistant cell line ($\alpha = 0.3$ $Gy^{-1}$) that could not be controlled with a conventional treatment of seven weeks, corresponding to a total dose of 70 Gy. Simulated accelerated fractionation yielded tumor control at a total dose of 69 Gy, corresponding to 31 days of treatment (red cell survival curve). The blue survival curve resulted from simulation of a conventional radiotherapy

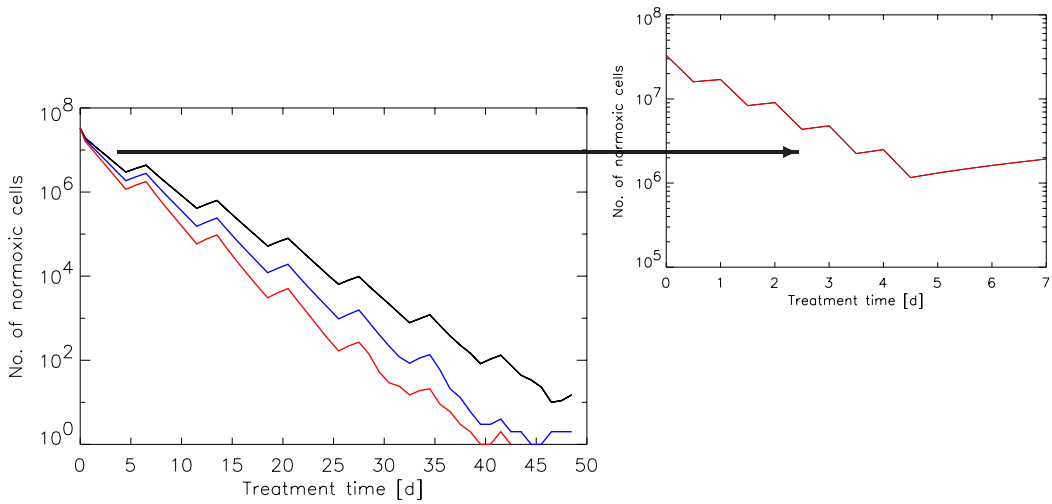


Figure 5.9: *Simulated cell survival (represented by the number of surviving normoxic cells) depends on the intrinsic radiosensitivity.* $\alpha = 0.3\ Gy^{-1}$ *for the black survival curve and* $\alpha = 0.35\ Gy^{-1}$, $\alpha = 0.4\ Gy^{-1}$ *for the blue and red curves, respectively. The growth characteristics were* $T_C = 80\ h$, *GF=100% and* $\Phi_{apop} = 0$. *A conventional dose-fractionation scheme of 2 Gy once per day with weekends off was simulated.*

of a tumor with the same cell kinetics, but a higher radiosensitivity. Tumor control was possible for a total dose of 70 Gy.

Among the time dependent factors in radiotherapy, repopulation is the dominant effect. The influence of the growth parameters $T_C$, GF and $\Phi_{apop}$ on tumor control is demonstrated in figures 5.11 and 5.12. Both figures show cell survival for the standard time-dose pattern in which 2 Gy are administered once daily with the weekends off. A pronounced oxygen effect with OER = 3 was considered.

Tumor control was not achieved for relatively radioresistant cell lines ($\alpha = 0.3\ Gy^{-1}$) if the cell cycle time was too short and tumor proliferation subsequently too high. Figure 5.11 shows survival for cell lines with no ability for apoptosis and a growth fraction of 100%. Tumor control for total doses of 70 Gy is possible only for $T_C = 115$ h. Figure 5.12 shows cell lines with varying degrees of differentiation, corresponding to varying growth fractions and apoptotic capacities. The least differentiated cell line is not controlled even at total doses as high as 70 Gy (black cell survival curve), whereas the two cell lines that still show apoptotic and quiescent cells (colored curves) are controlled with conventional fractionation and a total dose of less than 60 Gy. Growth fraction varied size dependently from 85% to 100% for the

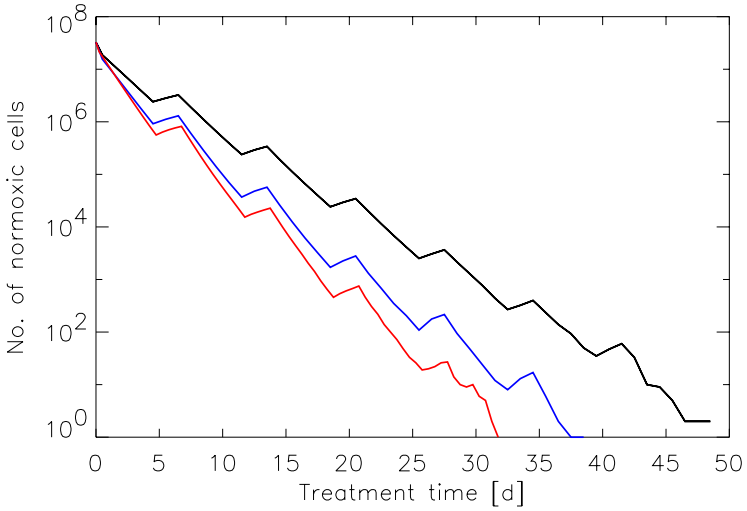


Figure 5.10: *Tumor response for different time-dose patterns. Cell survival is shown for two cell lines differing only in radiosensitivity. Control was possible with conventional fractionation at a total dose of less than 60 Gy (corresponding to 6 weeks of treatment) for* $\alpha = 0.4\ Gy^{-1}$ *(blue). The cell line corresponding to the black and red curves (*$\alpha = 0.3\ Gy^{-1}$*) could only be controlled with accelerated fractionation and a total dose of 69 Gy (corresponding to 31 days of treatment).* $T_C = 115\ h$ *was chosen for both cell lines.*

blue curve and from 80% to 100% for the red curve. Apoptotic fraction $\Phi_{\text{apop}}$ varied between 0% and 15% and 0 % and 20%, respectively.

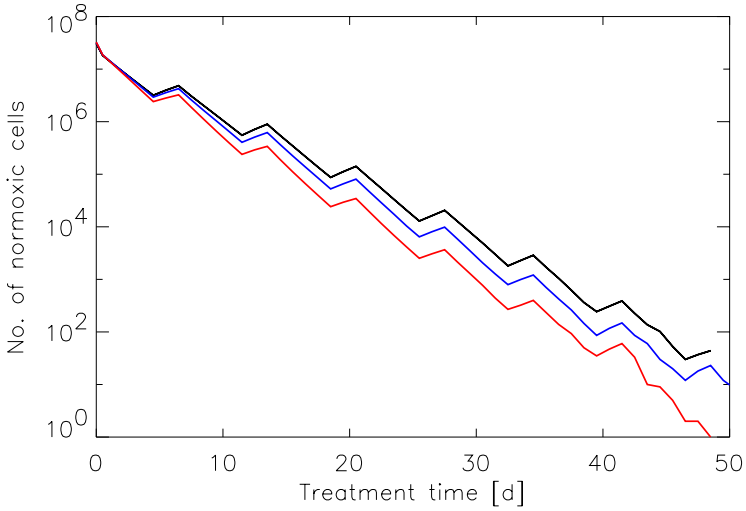


Figure 5.11: *Cell survival for tumors with different cell cycle times.* $T_C = 65\ h$ *for the black survival curve and* $T_C = 80\ h$ *and* $T_C = 115\ h$ *for the blue and red curves, respectively. Conventionally fractionated therapy of the three tumors was simulated with* $\alpha = 0.3\ Gy^{-1}$*. Only the slowly proliferating tumor (*$T_C = 115\ h$*) was controlled at a total dose of 70 Gy, corresponding to 49 treatment days.*

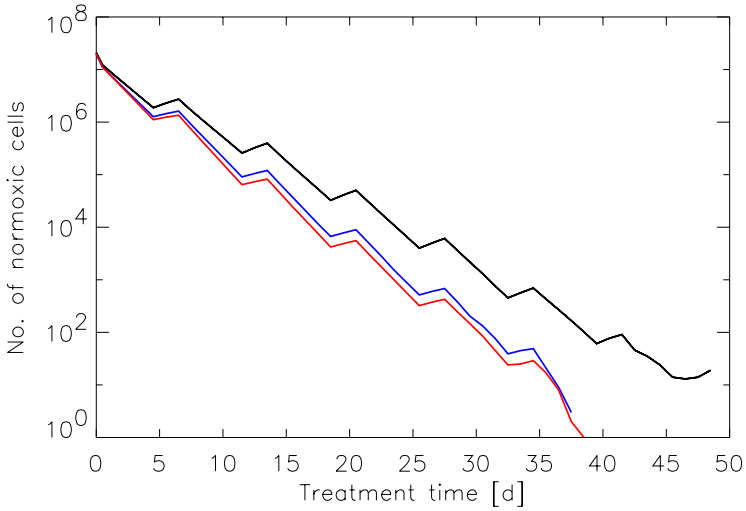


Figure 5.12: *GF and* $\Phi_{apop}$ *influence tumor response. Higher growth fraction and lower apoptotic capacity mean more ongoing tumor proliferation throughout the treatment. Simulation of tumor response for* $GF = 100\%$ *and* $\Phi_{apop} = 0$ *yielded the black survival curve. The colored curves represent well differentiated cell lines. With ongoing proliferation GF decreased from 100% to 85% and 80% for the blue and red curves, respectively, while* $\Phi_{apop}$ *increased form 0% to 15% and 20% for the blue and red curves, respectively.*

Several authors have pointed out that hypoxia adversely effects treatment outcome in radiotherapy [58, 59, 22, 120, 23, 51, 94]. The role of hypoxia and the oxygen effect in tumor control is demonstrated by simulating radiotherapy for various oxygen enhancement ratios. For doses of 2 Gy and more, OER values are typically between 2.5 and 3. At doses of 1.5 Gy and below, there is a reduced oxygen effect with OER $\simeq 2$. Figure 5.13 shows the decrease in the number of surviving normoxic cells for two levels of oxygen effect. For high-LET radiation there is no oxygen effect and OER = 1.

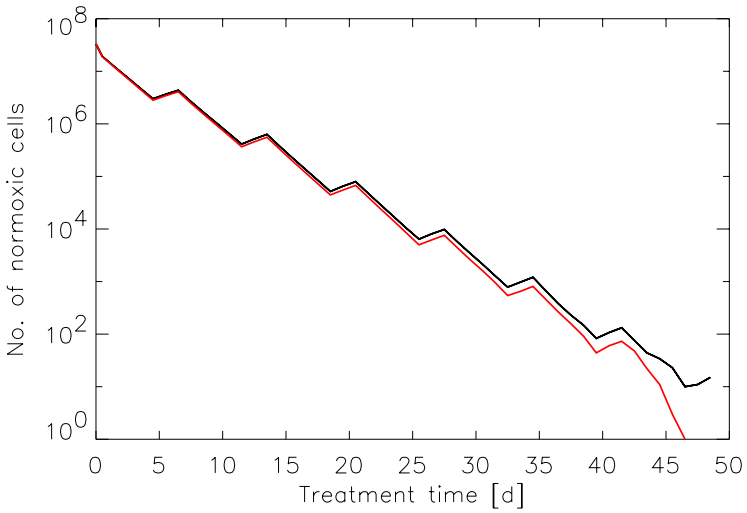


Figure 5.13: *The oxygen effect adversely effects tumor control. Conventional radiotherapy was simulated for OER = 3 (black curve) and OER = 2.5 (red curve).*

Tumor angiogenesis increases the normoxic fraction, enhancing repopulation between fractions. Tumor control should hence require additional dose for tumors with angiogenesis. On the other hand, tumor angiogenesis decreases the hypoxic fraction. Since hypoxic cells are less radiosensitive than normoxic cells are, this effect should facilitate tumor control. Including tumor angiogenesis in the simulation of tumor response to irradiation allows to predict which of the two effects, increased repopulation or increased radiosensitivity, is dominant. For fast proliferating tumors, the effect of repopulation prevails over the resensitization of hypoxic cells. Control of tumors with angiogenesis requires higher total doses than control of tumors without angiogenesis as can be seen in figure 5.14. For slowly proliferating tumors, angiogenesis greatly reduces the hypoxic fraction, facilitating tumor control (figure 5.15).

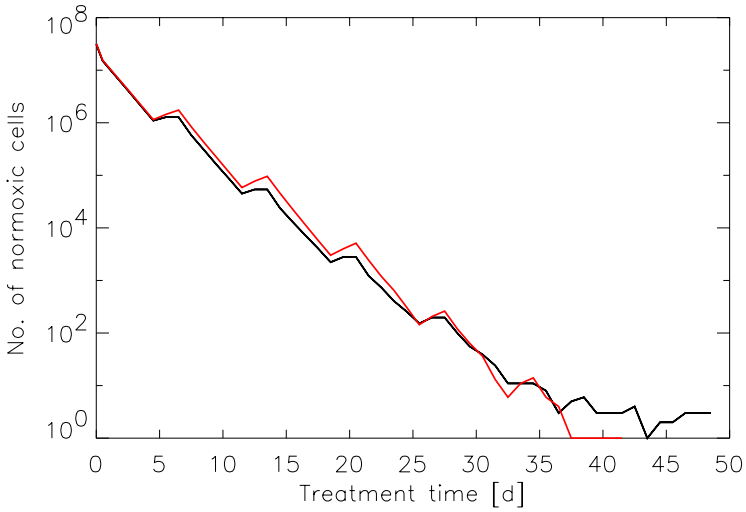


Figure 5.14: *Tumor response with (black) and without angiogenesis (red). Simulations of conventional fractionation were performed for a short cell cycle time $T_C = 80\ h$ and a high radiosensitivity $\alpha = 0.4\ Gy^{-1}$. For fast proliferating tumors, angiogenesis enhances repopulation which adversely effects tumor control even for very high capillary stimulation thresholds.*

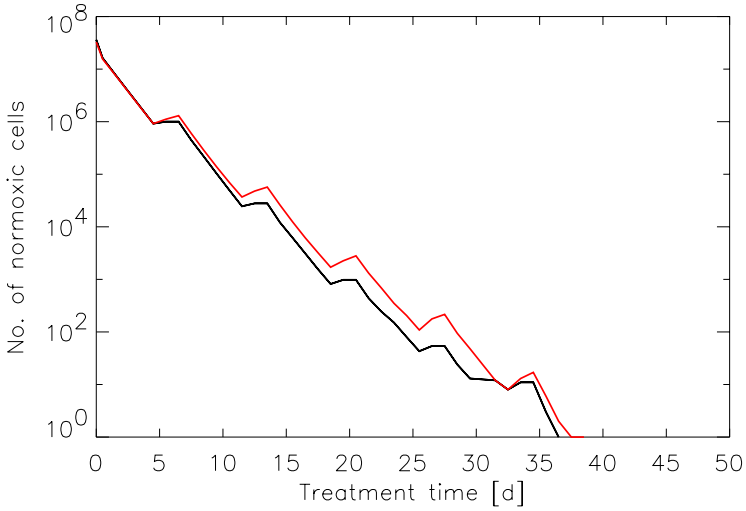


Figure 5.15: *Tumor response to conventionally fractionated radiotherapy for a radiosensitivity of $\alpha = 0.4\ Gy^{-1}$with (black) and without angiogenesis (red). Both survival curves were simulated with a relatively long cell cycle time $T_C = 115\ h$. In slowly proliferating tumors such as these, the reduction of the hypoxic fraction due to angiogenesis outweighs the effect of repopulation.*

Repair of sublethal damage has been assumed to be completed between fractions in the simulations presented so far. For accelerated fractionation and repair within 6 h at the $G_1$- and $G_2$-checkpoints this is no longer true. Tumors are assumed to have high $\frac{\alpha}{\beta}$-ratios, so incomplete repair is not an important effect because only a small fraction of DNA-damage is sublethal. For doses of 1.5 Gy and $\alpha = 0.4$ Gy$^{-1}$ and $\frac{\alpha}{\beta} = 10$ Gy only $1 - \exp(-0.04 \times 2.25) = 9\%$ of the normoxic cells aquire a sublethal DNA-damage compared to $1 - \exp(-0.4 \times 1.5) = 45\%$ of normoxic cells that get a lethal hit. Late responding (normal) tissues have lower $\frac{\alpha}{\beta}$-ratios. For $\alpha = 0.4$ Gy$^{-1}$ and $\frac{\alpha}{\beta} = 3$ Gy, the fraction of normoxic cells aquiring a sublethal DNA-damage is $1 - \exp(-0.133 \times 2.25) = 26\%$.

Simulations were performed with phase dependent sensitivities, mitosis being the most sensitive and synthesis being the least sensitive cycle phase. The sensitivities and repair parameters chosen are given in table 4.5.

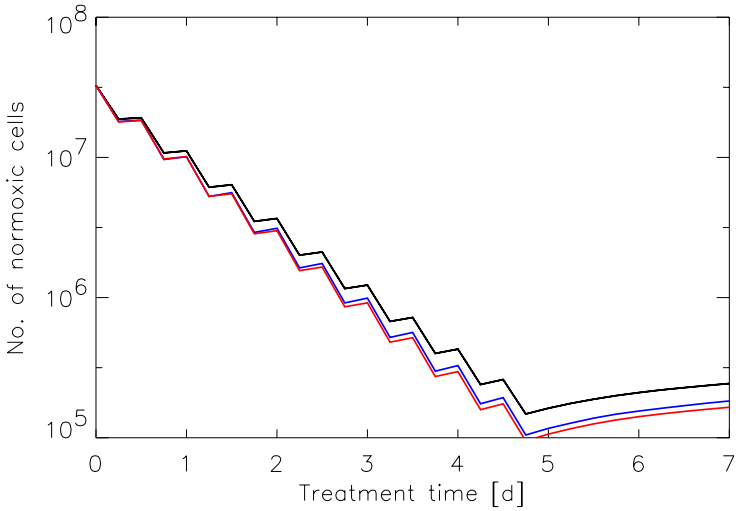


Figure 5.16: *Simulated survival fractions for accelerated radiotherapy with three different scenarios for repair mechanisms. The $\frac{\alpha}{\beta}$-ratio was chosen to be 5 Gy for all three survival curves. There was either complete repair between fractions (resulting in the black curve), no repair at all (red) or repair at the $G_1$- and $G_2$-checkpoints with a probability of $P_{rep} = \frac{1}{3}$. The survival fraction for incomplete repair between fractions is lower than that for complete repair but higher than that for no repair at all.*

For an $\frac{\alpha}{\beta}$-ratio of 5 Gy, corresponding to moderately acutely responding tissues, the survival fraction throughout accelerated fractionation with repair at the $G_1$- and $G_2$-checkpoints is lower than the survival fraction with complete repair and higher than that with no repair at all between fractions (see

figure 5.16). Allowing for repair of sublethal damage at the $G_1$-S and $G_2$-M checkpoints with a certain repair probability $P_{rep}$ results in an exponential decrease in time of cells with sublethal damage analogous to the incomplete repair model by Thames [105].

# Chapter 6

# Discussion

### The cellular radiobiological model

The objective of this work was to devise and implement a radiobiological model that allows a more realistic description of tumor growth and tumor response to radiotherapy than current models do. By considering each tumor cell individually, the cellular radiobiological model that has been introduced in this work includes the main processes influencing tumor behavior.

The tumor growth model (section 2.2) takes into account three growth parameters determining the tumor cell kinetics ($T_C$, $\Phi_{apop}$ and GF), the microenvironment and the diffusion of oxygen around capillaries, as well as lysis times for apoptotic and necrotic cells. Modeling tumor proliferation including tumor angiogenesis (section 3.2) is performed along the following principle: Hypoxic areas produce tumor angiogenesis factors (TAF) which diffuse into the environment, inducing capillaries to divide if TAF concentrations exceed a certain threshold. Tumor response to irradiation (section 4.2) is determined by the radiosensitivities $\alpha$, $\beta$ of the linear-quadratic model, the oxygen effect, a probability $P_{pms}$ for postmitotic survival, a cell cycle delay due to repair and repair mechanisms for sublethal DNA-damage.

A principal advantage of the cellular model presented in this work is taking into account the time factor in fractionated radiotherapy. Repopulation due to division of undamaged tumor cells, redistribution of cell cycles and reoxygenation of hypoxic cells due to cell displacement are all consequences of the ongoing tumor proliferation and are dealt with by the tumor growth model. Of the "4Rs" in radiotherapy only repair of sublethal damage between fractions must be accounted for separately. Previously no unified model existed in the literature dealing with all four time dependent effects at the same time. It is the ease with which the time factor in radiotherapy is accounted for that makes the cellular approach to modeling tumor response so

appealing.

The methods presented allow three-dimensional computer simulation of tumors with diameters of 12 mm containing 100 million tumor cells. This is achieved by simplifying processes such as blood supply and interaction of radiation with tissues. Also, allocation of three-dimensional data structures is implemented in a way that minimizes computer run times. Previous three-dimensional computer simulations of tumors were restricted to sizes of less than one million cells.

**Simulation results based on the cellular model**

The simulation results presented in chapter 5 illustrate how tumor proliferation depends on the three growth parameters, cell cycle time, growth fraction and apoptotic capacity (figure 5.2), and not on the cell cycle time alone (figure 5.1). A low growth fraction and the ability of tumor cells to undergo apoptosis can slow down tumor proliferation to an equilibrium between cell proliferation and cell death. Within the range studied, lysis times for dead cells have no pronounced effect on tumor behavior. The influence exerted on tumors by their microenvironment is demonstrated by the relationship between tumor proliferation rate and the capillary density of the host tissue (figure 5.3).

Tumor angiogenesis increases the normoxic fraction, thus enhancing tumor proliferation (figures 5.6 and 5.7). The dominant factor of the tumor angiogenesis model is the amount of TAF needed to stimulate capillaries to divide.

The need to compare simulated growth curves and survival fractions with experimental data in vivo was crucial throughout the process of developing the simulation methods presented here. The Dunning R3327 prostate tumor system was chosen for comparing simulated tumor growth curves with tumor proliferation observed in male Copenhagen rats. The cell kinetics of this tumor system are well known for several sublines with varying degrees of differentiation (table 2.2). Experimentally observed tumor volume doubling times are given in table 2.3.

The results presented on unperturbed proliferation of Dunning R3327 AT1 and HI prostate tumors show that simulated tumor growth curves are in qualitative agreement with corresponding tumor proliferation in animals. Simulated tumor volume doubling times are in remarkable quantitative agreement with observed tumor volume doubling times (table 5.1). However, parameters entering the simulations of angiogenesis are known with large uncertainties only, so further studies are necessary to validate the simulation tools developed. The results also emphasize the role angiogenesis has

in tumor proliferation. A realistic tumor model that bears comparison with experimental and clinical data must account for angiogenesis (figure 5.8 and table 5.1).

Tumor control is not only determined by the intrinsic radiosensitivities of tumors (figure 5.11) but also by their proliferation characteristics (figure 5.12). The results presented on tumor control by radiotherapy stress the importance of the time factor in fractionated radiotherapy. Repopulation between fractions is a major factor in tumor control. Possible reoxygenation of hypoxic cells means that elimination of all normoxic cells might not suffice for tumor control. The adverse effect of hypoxia on tumor control reported by many authors is demonstrated by simulations of tumor response to irradiation for different OER-values (figure 5.13). Tumor angiogenesis enhances tumor proliferation (possibly rendering tumor control more difficult) while decreasing the hypoxic fraction (possibly rendering tumor control easier). From the simulation results no general conclusion can be drawn on how angiogenesis effects tumor control. The influence of angiogenesis on tumor control depends on the cell kinetics of the tumor. In fast proliferating tumors angiogenesis enhances repopulation and increases the cell survival fraction after irradiation (figure 5.14). In slowly proliferating tumors the decrease in hypoxic fraction due to angiogenesis outweighs the effect of increased repopulation resulting in tumor control for lower total doses (figure 5.15). For moderately acute responding tissues (with an assumed $\frac{\alpha}{\beta}$-ratio of 5 Gy), incomplete repair between fractions is a relevant time dependent effect (figure 5.16) in accelerated dose fractionation.

From the results presented it can be seen that simulation of tumor response cannot be done adequately without taking into account the dynamic characteristics of tumor growth. The most important time dependent effect of the "4 Rs" is repopulation, followed by reoxygenation. Redistribution does not seem to influence treatment outcome significantly. Incomplete repair is of importance for accelerated fractionation only. The way angiogenesis influences tumor response to fractionated radiotherapy depends on whether angiogenesis can keep up with tumor proliferation or not.

The cellular model and the simulation tools developed allow the estimation of tumor control for different radiobiological parameters and time-dose patterns. Tumor entities can be distinguished by their growth parameters, their intrinsic radiosensitivities, and their oxygen supply which in turn is determined by the capillary density of the host tissue and its angiogenic response. Tumors with different degrees of differentiation differ in their growth parameters and radiosensitivities. Comparing different time-dose patterns in terms of their tumor control is of special interest in radiotherapy. The simula-

tion methods introduced here can be used to study tumor control for different fractionation schemes. An estimation can be made whether a new (and possibly more time-consuming) fractionation scheme does indeed enhance tumor control. Simulations like the ones presented could help to identify patients who might profit from accelerated fractionation schemes.

### Critical discussion of the cellular model

Tumor growth and tumor response to irradiation involve complex biological processes on a molecular scale. Deriving a tumor model requires simplifying these complex processes by including only the most important aspects and formulating mechanisms describing tumor behavior on a cellular level. Restrictions on computer run times impose further simplifications in the mechanisms and parameters included.

In the tumor growth model devised here simplifications were made concerning tumor morphology. The current model results in hypoxic areas, necrotic centers and resorbed cells which is consistent with observed tumor growth. However, tumors in vivo are more diffuse and heterogeneous than the simulated tumors presented in this work. The potential of accounting for tumor heterogeneity and including tumor shrinkage will be discussed in the following Outlook chapter.

Tumor angiogenesis has previously been modeled using systems of partial differential equations. The simulations of blood vessel creation presented by Chaplain et al [25, 28] include the formation of vessel branches and loops. Highly irregular structures including loops, shunts and blind ends are typical of tumor vasculature. Markus et al presented cellular automata that simulate blood vessel creation [74].
The tumor angiogenesis model presented here does not consider any vascular structure since literature allowing a quantitative analysis of microvasculature is scarce. Less et al have quantified branching patterns of the microvasculature in a mammary carcinoma [71] but usually oxygen distributions within tumors are studied [51, 43, 76, 94]. Comparing simulated microvasculature to corresponding experimental data would not be possible. Therefore, the model that has been devised in section 3.2 focuses on the subsequent effect of increased blood supply on tumor cells. In previous angiogenesis models based on differential equations this was not attempted.

The linear-quadratic model has drawn much criticism [19]. It is argued that it is a data fit that lacks biological basis. Survival curves are generally obtained for cells in culture and extrapolation of cell behavior to situations in vivo have to be done with care. Cell response to radiation might be

different in tissues than in culture. In addition, radiation energy is absorbed differently in tissues and in culture. Survival curves show linear-quadratic form only for doses between 1 Gy and 10 Gy.
Since single doses in fractionated radiotherapy are in that range, the LQM is used throughout this work to calculate cell killing.

### Critical discussion of the radiobiological parameters of the cellular model

Input parameters entering the computer simulations are motivated by biological experiments (as indicated in sections 2.2.3, 3.2.3 and 4.2.3) rather than by fitting clinical data. Predicting tumor behavior with the cellular model is founded on the assumption that the radiobiological model parameters are known with sufficient certainty.

For the Dunning R3327 tumor system chosen to compare simulated tumor proliferation with corresponding experimental data, parameter values obtained by two different laboratories vary. The cell cycle time $T_C$ of the AT1 subline for example is 18% lower according to Overgaard et al [93] ($T_C = 3.1 \pm 0.2$ d) than according to Lohr et al [72] ($T_C = 3.8 \pm 0.25$ d). Nevertheless, for this particular tumor system, the cell kinetics parameters are known to a sufficient degree to justify simulations of tumor behavior based on the cellular approach presented here. Another growth parameter, the apoptotic capacity, is known to be zero with little margin of error for instance. A detailed study of how the inter-laboratary variability in biological parameters effects tumor doubling times and tumor responses to irradiation predicted by simulations still needs to be done.

Presently, cell kinetics parameters for human tumor cell lines are usually known with a large variability only. Predicting treatment outcome based on cell kinetics parameters has been difficult. Efforts have been made to correlate labeling indices LI and durations $T_S$ of the S phase to tumor size, tumor stage, DNA content and patient age. Few statistically significant relationships for $T_S$ have emerged, however. Zätterström et al report that $T_S$ depends significantly on tumor age, but this is for a model system, xenografted human squamous cell carcinoma in the head and neck (HNSCC) in mice [121]. The parameter most likely to vary with cell differentiation and tumor age is LI, whereas $T_C$ seems to remain relatively constant. Bennett et al conclude that for HNSCC no important differences in cell kinetics can be found between primary, recurrent or metastatic tumors [7]. Terry et al find no correlation between tumor stage and cell kinetics [103].

Compiling median (or mean) data on cell proliferation as given in Table 2.1 is misleading. Inter-patient variability is so large that one could argue

knowing median (or mean) tumor proliferation parameters is of little use. In addition to the inter-patient variability there is a great variability in the results obtained by different laboratories [6]. Wilson reviewed a list of publications on median LI and $T_S$ for HNSCC. Median LI ranged from 6.3% to 12.7% and median $T_S$ from 8.1 to 14 h. Wilson concludes that the results on studies on cell proliferation have not been consistent and that no consensus has emerged on whether $T_{pot}$ can serve as a clinical predictor for treatment outcome in radiotherapy [114]. Begg et al conclude from a multi-center analysis for head and neck cancer that only LI (corresponding to growth fraction) offers some evidence of being correlated to tumor control [6]. According to their study, $T_{pot}$ provides only a weak predictor of radiotherapy outcome.

Establishing cellular simulation tools of tumor growth requires sophisticated measurements of tumor cell kinetics. Prior to predicting tumor behavior in clinical practice based on the cellular radiobiological model, it has to be assessed how the variability in the input parameters effects simulated tumor control.

The parameters entering the angiogenesis model have also not been established to a satisfying extent. The choice of 80 arbitrary units of tumor angiogenesis factors for the capillary stimulation threshold was motivated by the observation that as little as 50 to 60 hypoxic cells can trigger angiogenesis. Choosing a diffusion radius of 200 $\mu$m was motivated by computational efficiency rather than by biological experiments. Simulations presented on tumor angiogenesis are intended to qualitatively demonstrate the effect angiogenesis has on tumor behavior. A thorough validation of the tumor growth model including angiogenesis requires a more detailed knowledge on the diffusion characteristics of TAF than is currently available in the literature.

Phase dependent radiosensitivities have only been measured for a few human cell lines in vitro [88, 11], so comparing simulations including phase dependent sensitivities with experimental data is difficult at present.

Studies on continuous hyperfractionated accelerated radiotherapy have shown an increase in normal tissue complications due to incomplete repair between fractions [39, 3]. Bentzen et al estimated repair halftimes in the order of 4 h to 5 h for selected late responding tissues in the head and neck [9]. In recent studies, biphasic repair models with a fast repair process (repair halftime in the order of minutes) and a slow repair process (repair halftime in the order of hours) have been successfully fitted to experimental data of late responding normal tissues [100, 33]. For human fibroblasts, repair was complete within about 12 h [37, 38]. Only about 2.5% of all induced double-strand breaks remained non-repaired. It is not clear, however, how the fraction of non-repaired double-strand breaks translates into cell killing.

Also, no repair halftimes for tumors have been studied so far.
Simulations of tumor response to accelerated radiotherapy that bear comparison with experimental data require repair probabilities for tumor cell lines as input parameter. Data on the probabilitites $P_{rep}$ with which sublethal damage is repaired are currently not available in the literature. To date, simulations of tumor response to fractionated radiotherapy distinguishing complete and incomplete repair cannot be compared to experimental data.

The tumor model and the simulation tools that have been developed in this work are not limited to a single tumor entity. Predictions of tumor response to irradiation can be made based on the cellular radiobiological model for any tumor for which the radiobiological parameters are sufficiently well known.

# Chapter 7

# Outlook

### Comparing computer simulations to experimental data

The simulation methods devised in this work intend to provide the foundation for integrating a simulation tool that calculates tumor control probabilities into the treatment planning process in radiotherapy. This can only be done after a thorough comparison of simulated tumor growth and tumor response to experimental as well as to clinical data.

Comparing simulated and observed tumor growth could help to quantify parameters of the angiogenesis model that are not sufficiently well known at present. Simulated tumor growth and experimental growth curves of Dunning R3327 prostate tumors can be compared for two different settings. Tumor growth in vivo can be observed either after transplanting fresh pieces of tumors subcutaneously or after injecting tumor cells. It has been shown that there is little angiogenesis in the case of injected tumor cells, so these two experiments allow validating the tumor growth model with and without angiogenesis.

All current radiobiological models dealing with the time factor in radiotherapy define global parameters that are fitted to clinical data. Evaluating fractionated radiotherapy performed on Copenhagen rats with AT1 tumors by the Dept. of Radiobiology at DKFZ allows comparing observed tumor response of AT1 prostate tumors with simulated tumor response. Tumor response to radiotherapy has been quantified by the growth delay of recurrent tumors [87]. The parameters $\alpha$ and $\beta$ of the LQM can be extracted from experiments that have been performed on cell cultures of the AT1 subline by the same group [95].

### Obtaining dose-response curves

To be of clinical relevance, the model devised must predict the probability of (local) tumor control for different tumor entities and time-dose patterns. The stochastic element in simulating treatment outcome for tumor patients is twofold. Firstly, tumor control is defined as sterilization of every single clonogenic tumor cell. Simulation of response to radiotherapy for two tumors with equal radiobiological parameters and equal dose-fractionation could yield zero surviving tumor cells in one case and one single (or a few) surviving tumor cells in the other. Only the first of the two tumors would be considered as controlled. The tumor control probability (TCP) would be $\frac{1}{2}$. The second stochastic aspect in simulating tumor control is the inter-patient variability in intrinsic biological parameters. Different tumors of the same cell line (or subline) show some variance in their radiobiological parameters. Whereas a tumor with a (mean) cell cycle time of 3 days might be controlled with a certain fractionation pattern, a tumor with a (mean) cell cycle time of 3 days and 3 hours might not be. Probabilities for tumor control for different tumor entities can be obtained by accounting for the variability in biological parameters in the patient population when simulating tumor response. Monte-Carlo simulation for a number of simulations of tumor control for identical radiobiological parameters demonstrates the stochastic aspect in radiotherapy due to the requirement that all clonogenic tumor cells must be killed (figure 7.1). No population averaging has been done. Performing large-scale Monte-Carlo simulations to obtain tumor control probabilities for a heterogenous patient population still needs to be done. Dose-response curves obtained in this manner can be compared to those obtained from existing phenomenological [52] and mechanistic [80, 82, 110] TCP models.

### Improving the cellular radiobiological model

The requirement of realistic computer run times leads to simplifications of biological processes in the implementation of the tumor model. Elaborating on four aspects that have been simplified should yield an even more detailed tumor model:

1. In the radiobiological model presented here, only three levels of oxygenation are distinguished resulting in normoxic, hypoxic and necrotic cells. The oxygen effect is included by introducing a parameter OER for hypoxic cells. For normoxic cells the OER is one. Recently it has been pointed out by Wouters et al [120] and Brown et al [23] that cells with intermediate levels of oxygen can be as important as the hypoxic fraction for tumor response to fractionated radiotherapy. A function

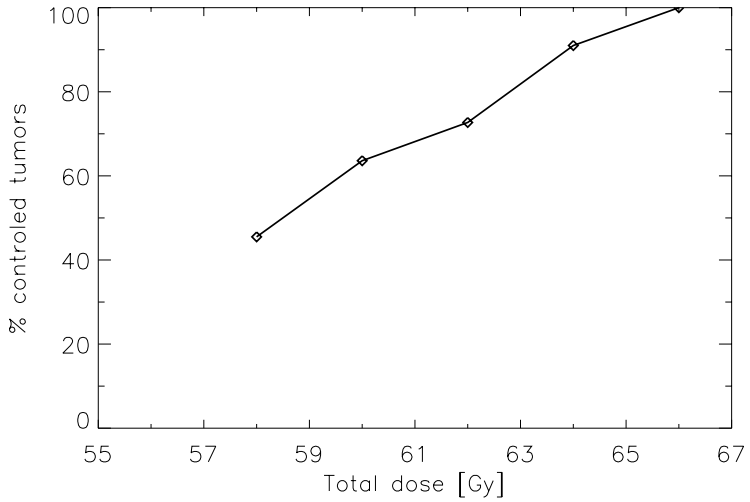


Figure 7.1: *Dose-response curve (fraction of controlled tumors vs total dose) obtained by Monte-Carlo simulations. A total of 11 simulations of tumor growth and tumor irradiation with conventional dose fractionation were performed.* $T_C = 80\,h$, $\Phi_{apop} = 0\%$ *and GF=100%. Radiosensitivities were* $\alpha = 0.4\ Gy^{-1}$ *and* $\frac{\alpha}{\beta} = 10$ *Gy. Values given for* $T_C$ *and* $\alpha$ *are mean values of normal distributions to allow for heterogeneity within the tumors.*

relating oxygenation status and OER to capillary distance according to experiments (see figure 4.5) should improve the tumor response model.

2. Apoptotic and necrotic cells are resorbed by phagocytosis. The implemented lysis mechanisms correspond to resorption of dead cells by adjacent cells. The lattice site of a resorbed cell is assumed to stay empty until it is reoccupied due to cell division or cell displacement. In tumors in vivo a large fraction of necrotic cells is phagocytized by macrophages and immune cells penetrating the tumor [12]. This causes a heterogeneous tumor morphology not accounted for in the current model.

3. Tumor cells infiltrate normal tissues resulting in a diffuse tumor rim and in a heterogeneous tumor. Introducing regions along which tumor cells proliferate preferentially should yield more realistic tumor morphologies.

4. Certain tumors, such as carcinoma of the cervix uteri, shrink as a consequence of cell killing by irradiation while others, such as sarcomas, do not. The influence of tumor shrinkage on tumor response and on

recurrence has been studied by Kocher et al [63, 64], but has not been included in the model presented here.

5. In the simulations on tumor response to irradiation, no effect of radiation on capillary cells has been considered. The consequences of capillary cell killing by irradiation on tumor response need to be studied in detail. According to Kocher et al [65] killing of endothelelial cells should result in less tumor cell survival.

The oxygen distribution within the tumor resulting from a more sophisticated model can be compared with experimentally obtained oxygen distributions. Corresponding data are available from the Dept. of Radiobiology at DKFZ, where oxygen tension was measured by polariographic methods [94] and by NMR [76].

### A closer look at radiobiological parameters

Knowing the radiosensitivities of tumors is absolutely crucial in estimating tumor control based on the linear-quadratic formalism. Tumors are assumed to have high $\frac{\alpha}{\beta}$-ratios and low repair capacity. In all simulation results presented, $\frac{\alpha}{\beta} = 10$ Gy was assumed for tumors. For high $\frac{\alpha}{\beta}$-ratios, including repair mechanisms in the computer simulation methods drastically increases run time without resulting in significantly different cell survival curves. However, data have recently been published indicating $\frac{\alpha}{\beta}$-values as low as $\frac{\alpha}{\beta} \simeq 2$ Gy for human prostate tumors [21, 50], implying that repair mechanisms between accelerated fractions must be accounted for. Quantifying the effect low $\frac{\alpha}{\beta}$-ratios have on the tumor control achieved by different time-dose patterns applied in clinical practice is an important application of the simulation tools developed in this work.

All simulations of tumor response to irradiation were performed with a cell cycle delay of 6 h based on the observation of low repair halftimes [33, 100, 37]. However, repair might not be completed within 6 h. Quantifying the effect different repair times and cell cycle delays have on tumor response for accelerated fractionation might be important in clinical practice.

### Dose inhomogeneities and organ movement

The trade-off between tumor control and sparing of organs at risk can result in inhomogeneous dose distributions in the target volume. The cellular approach to radiobiological modeling allows to study the influence of dose inhomogeneities, such as cold spots, on tumor control. Time-dose patterns in which an additional radiation boost is applied to part of the tumor volume

can also be simulated. The position and the size of cold spots are easily varied.

Inaccuracies in patient positioning and organ movement during or between fractions can adversely effect treatment outcome. The effect of these two aspects on tumor control can be studied by the simulation methods developed. Organ movement can be modeled by translating and rotating the tumor.

### Tumor recurrence

Sparing organs at risk can require radiation doses to the tumor that are not sufficiently high to eliminate all tumor cells. Surgical resection of tumors can also result in a small number of surviving tumor cells due to diffuse tumor boundaries or anatomical complexity. A recurrence caused by repopulation of surviving tumor cells can be simulated using the simulation methods presented here. Factors such as necrotic areas of the original tumor and a microvasculature that has been displaced by the original tumor can be included in the simulations of tumor recurrence.

### Comparing simulated tumor response to irradiation to clinical data

More than 300 patients with prostate carcinoma have been treated by three-dimensional conformal radiotherapy tecuniques at the Radiological University Hospital, Heidelberg. These data are availiable for a retrospective analysis, in which tumor control based on levels of PSA (prostate specific antigen) is compared with tumor control predicted by the cellular model. For all patients the three-dimensional physical dose distributions as well as the tumor specific prognostic factors are known. These are tumor stage, Gleason score (quantifying the degree of differentiation of the tumor) and PSA-levels prior to treatment. An important parameter of the study is the tumor volume, which can be quantified empirically from the prostate volume, the Gleason score and the PSA-level prior to treatment [1, 83]. The degree of differentiation of the tumor can be used to identify patients with tumor cells that proliferate faster and are more radiosensitive. Patient data can be classified into groups according to the parameters tumor size, physical dose and degree of differentiation. Tumor control that has been achieved can be compared to tumor control predicted by the simulation methods. Varying the parameters within the inter-patient variabilities allows to assign tumor control probabilities to each of the patient groups.
The work done to compare simulated tumor behavior with experimental data on Copenhagen rats with Dunning R3327 prostate tumors can serve as a

foundation to such a retrospective clinical study.

### New treatment modalities

Strategies to improve the outcome of radiation treatments aim at enlarging the therapeutic window, which is defined as the difference in tumor response and normal tissue complications.

An example for a biological strategy to improve treatment outcome is to increase the tumor radiosensitivity. Radiosensitivity can be influenced by hyperthermia (heat is believed to increase blood perfusion and to inhibit repair mechanisms, resulting in an increased radiosensitivity), by chemotherapeutic agents, which delay cell cycle progression and repair (such as Pentoxyphiline) or by radiosensitizers such as Misonidazole and Etanidazole, which deliver free radicals to hypoxic areas, reducing the OER.

A combination of chemotherapy and radiotherapy can be modeled by turning off the repair mechanisms that are allowed for at the $G_1$-S and $G_2$-M checkpoints and by reducing the cell cycle delay. Radiosensitization by agents supplying free radicals can be modeled by diffusion processes similar to the diffusion of tumor angiogenesis factors. Hypoxic cells reached by radiosensitizers have a reduced OER.

Physical concepts aim to further conform the high dose region to the planning target volume. One strategy to achieve this is by delivering charged particles. Today, mostly photons with a mean energy between 2 MeV and 10 MeV are applied in radiotherapy. Radiotherapy with charged particles requires energies of about 200 MeV to 400 MeV per nucleon and is restricted to very few facilities worldwide. Charged particles have more favorable physical and biological properties. Whereas dose deposition for photons decreases exponentially with depth, dose deposition for charged particles increases towards the Bragg-Peak and then drops to almost zero. Also, charged particles have a large linear energy transfer (LET), a quantity describing the energy deposited in tissues per unit length of the radiation track. High-LET radiation is characterized by a higher fraction of irrepairable lethal cell damage, a reduced oxygen effect [55] and less variability of radiosensitivity of cells throughout their cell cycle [116]. Radiation with different LET can be modeled by LET dependent radiosensitivities. For high-LET radiation such as heavy ions, there is no sublethal damage and $\beta = 0$. Also, there is no indirect action for high-LET radiation and the OER is one.

# Chapter 8

# Conclusion

The cellular radiobiological model and the simulation methods developed in this work were motivated by the need to quantify tumor control by radiotherapy for different tumor entities, grades of differentiation and time-dose patterns. Three-dimensional computer simulation of tumors with diameters of 12 mm and more is feasible with the methods developed.

Comparing simulated tumor growth with corresponding experimental data was an important aspect of this work. The Dunning R3327 prostate tumor system in Copenhagen rats was chosen for comparison because prostate cancer is the most common cancer among men in Germany and because cell kinetics parameters of the Dunning tumor system are well known for different degrees of differentiation. The results presented illustrate the important role tumor angiogenesis has in tumor proliferation. The comparison of simulated and experimental data demonstrate that simulated tumor growth curves are in qualitative agreement with tumor proliferation observed in animals.

The simulation methods presented allow to identify the most important radiobiological factors influencing tumor response to radiotherapy. Different fractionation schemes can be compared in terms of their tumor control. The cellular approach to radiobiological modeling allows estimations on how the time factor in radiotherapy effects tumor control for different time-dose patterns.

The work presented serves as a foundation to integrate the tool developed in this work to predict tumor control into the treatment planning process. The promising results presented in chapter 5 encourage further studies to compare predictions of tumor proliferation and tumor response to irradiation to experimental and clinical data.

# Bibliography


[1] M. Aihara, R.M. Lebovitz, T.M. Wheeler, Prostate specific antigen and Gleason grade: An immunohistochemical study of prostate cancer. *J Urol* **151** 1558-1564 (1994).

[2] Algan Ö, Stobbe CC, Helt AM, Hanks GE, Chapman JD, Radiation inactivation of human prostate cancer cells: The role of apoptosis. *Radiat Res* **146** 267-275 (1996).

[3] Ang KK, Jiang J, Thames HD, Stephens LC, Smith CD, Feng Y, Impact of spinal cord repair kinetics on the practice of altered fractionation schedules. *Radiother Oncol* **25** 287-294 (1992).

[4] Beck-Bornholdt HP, Dubben HH, Liertz-Petersen C, Willers H, Hyperfractionation: Where do we stand? *Radiother Oncol* **43** 1-21 (1997).

[5] Begg AC, Hofland I, Kummermehr J, Tumor cell repopulation during fractionated radiotherapy: Correlation between flow cytometric and radiobiological data in three murine tumors. *Eur J Cancer* **27** 537-543 (1991).

[6] Begg AC, The value of pretreatment cell kinetic parameters as predictors for radiotherapy outcome in head and neck cancer: A multi-center analysis. *Radiother Oncol* **50** 13-23 (1999).

[7] Bennett MH, Wilson GD, Dische S, Saunders MI, Martindale CA, Robinson BM, O'Halloran AE, Leslie MD, Liang JH, Tumour proliferation assessed by combined histological and flow cytometric analysis: Implications for therapy in squamous carcinoma of the head and neck. *Br J Cancer* **65** 870-878 (1992).

[8] Bentzen SM, Thames HD, Clinical evidence for tumor clonogen regeneration: Interpretations of the data. *Radiother Oncol* **22** 161-166 (1991).

[9] Bentzen SM, Saunders MI, Dische S, Repair halftimes estimated from observations of treatment-related morbidity after CHART or conventional radiotherapy in head and neck cancer. *Radiother Oncol* **53** 219-226 (1999).

[10] Bernhard EJ, McKenna WG, Muschel RJ, Radiosensitivity and the cell cycle. *The Cancer J Sci Am* **Jul-Aug 5** 194-204 (1999).

[11] Biade S, Stobbe CC, Chapman JD, The intrinsic radiosensitivity of some human tumor cells throughout their cell cycles. *Rad Res* **147** 416-421 (1997).

[12] Blank KR, Rudoltz MS, Kao GD, Muschel RJ, McKenna WG, The molecular regulation of apoptosis and implications for radiation oncology. *Int J Radiat Biol* **71** 455-466 (1997).

[13] Bolger BS, Cooke TG, Symonds RP, McLean AB, Stanton PD, Measurement of cell kinetics in cervical tumours using BrdUrd. *Br J Cancer* **68** 166-171 (1993).

[14] Bortfeld T, Bürkelbach J, Boesecke R, Schlegel W, Methods of image reconstruction from projections applied to conformal radiotherapy. *Phys Med Biol* **35** 1423-1434 (1990).

[15] Bortfeld T, Boyer AL, Schlegel W, Kahler DL, Waldron TJ, Realization and verification of three-dimensional conformal radiotherapy with modulated fields. *Int J Radiat Oncol Biol Phys* **30** 899-908 (1994).

[16] Brenner DJ, Huang Y, Hall EJ, Fractionated high dose-rate vs. low dose-rate regimens for intracavitary brachytherapy of the cervix: Equivalent regimens for combined brachytherapy and external irradiation. *Int J Radiat Oncol Biol Phys* **21** 1415-1423 (1991).

[17] Brenner DJ, Dose, volume, and tumour-control predictions in radiotherapy. *Int J Radiat Oncol Biol Phys* **26** 171-179 (1993).

[18] Brenner DJ, Hlatky LR, Hahnfeldt PJ, Hall EJ, A convenient extension of the linear-quadratic model to include redistribution and reoxygenation. *Int J Radiat Oncol Biol Phys* **32** 379-390 (1995).

[19] Brenner DJ, Herbert DE, The use of the linear-quadratic model in clinical radiation oncology can be defended on the basis of empirical evidence and theoretical argument. *Med Phys* **24** 1245-1248 (1997).

[20] Brenner DJ, Armour E, Corry P, Hall E, Sublethal damage repair times for a late-responding tissue relevant to brachytherapy (and external-beam radiotherapy): Implications for new brachytherapy protocols. *Int J Radiat Oncol Biol Phys* **41** 135-138 (1998).

[21] Brenner DJ, Hall EJ, Fractionation and protraction for radiotherapy of prostate carcinoma. *Int J Radiat Oncol Biol Phys* **43** 1095-1101 (1999).

[22] Brizel DM, Sibley GS, Prosnitz LR, Scher RL, Dewhirst MW, Tumor hypoxia adversely affects the prognosis of carcinoma of the head and neck. *Int J Radiat Oncol Biol Phys* **38** 285-289 (1997).

[23] Brown JM, Gaccia J, The unique physiology of solid tumors: Opportunities (and problems) for cancer therapy. *Cancer Res* **58** 1408-1416 (1998).

[24] Burman C, Kutcher GJ, Emami B, Goitein M, Fitting of normal tissue tolerance data to an analytic function. *Int J Radiat Oncol Biol Phys* **21** 123-135 (1991).

[25] Byrne HM, Chaplain M, Mathematical models for tumor angiogenesis: Numerical simulations and nonlinear wave solutions. *Bulletin of Mathematical Biology* **57** pp. 461-486 (1995).

[26] Carlton JC, Terry NH, White RA, Measuring potential doubling times of murine tumors using flow cytometry. *Cytometry* **12** 645-650 (1991).

[27] Chadwick KM, Leenhouts HP, A molecular theory of cell survival. *Phys Med Biol* **18** 78-87 (1973).

[28] Chaplain M, Anderson A, Mathematical modeling, simulation and prediction of tumour-induced angiogenesis. *Invasion Metastasis* **16** 222-234 (1996).

[29] Chapman JD, Stobbe CC, Gales T, Das IJ, Zellmer DL, Biade S, Matsumoto Y, Condensed chromatin and cell inactivation by single-hit kinetics. *Radiat Res* **151** 433-441 (1999).

[30] Curtis SB, Lethal and potentially lethal lesions induced by radiation- A unified repair model. *Radiat Res* **106** 252-270 (1986).

[31] D'Amico AV, McKenna WG, Apoptosis and a re-investigation of the biologic basis for cancer therapy *Radiother Oncol* **33** 3-10 (1994).

[32] Dahm-Daphi J, Dikomey E, Non-repairable DNA strand breaks and cell killing studied in CHO cells after X-irradiation at different passage numbers. *Int J Radiat Biol* **66** 553-555 (1994).

[33] Dahm-Daphi J, Dikomey E, Brammer I, DNA-Repair, cell killing and normal tissue. *Strahlenther Onkol* **174: SIII** 8-11 (1998).

[34] Deacon J, Peckham MJ, Steel GG, The radioresponsiveness of human tumours and the initial slope of the cell survival curve. *Radiother Oncol* **2** 317-323 (1984).

[35] Denekamp J, Cell kinetics and cancer therapy. C.C. Thomas, Springfield, IL (1982).

[36] Dewey WC, Ling CC, Meyn RE, Radiation-induced apoptosis: Relevance to radiotherapy. Int J Radiat Oncol Biol Phys **33** 781-796 (1995).

[37] Dikomey E, Brammer I, Johansen J, Bentzen SM, Overgaard J, Relationship between DNA double-strand breaks, cell killing and fibrosis in confluent skin fibroblasts derived from breast cancer patients. *Int J Radiat Oncol Biol Phys* **46** 481-90 (2000).

[38] Dikomey E, Brammer I, Relationship between cellular radiosensitivity and non-repaired double-strand breaks studied for different growth states, dose rates and plating conditions in a normal human fibroblast line. *Int J Radiat Biol* **76** 773-81 (2000).

[39] Dische S, Saunders MI, Continuous, hyperfractionated, accelerated radiotherapy (CHART): An interim report upon late morbidity. *Radiother Oncol* **16** 67-74 (1989).

[40] Donoghue JA, The response of tumors with Gompertzian growth characteristics to fractionated therapy. *Int J Radiat Oncol Biol Phys* **72** 325-339 (1997).

[41] Düchting W, Ulmer W, Lehrig R, Ginsberg T, E. Dedeleit, Computer simulation and modeling of tumor spheroid growth and their relevance for optimization of fractionated radiotherapy. *Strahlenther Onkol* **168** pp. 354-360 (1992).

[42] Düchting W, Ulmer W, Ginsberg T, Cancer: A challenge for control theory and computer modeling. *European Journal of Cancer* **32A** 1283-1292 (1996).

[43] Fenton BM, Raubertas RF, Boyce DJ, Quantification of micro-regional heterogeneities in tumor oxygenation using intravascular $HbO_2$ saturations. *Radiat Res* **141** 49-56 (1995).

[44] Folkman J, The vascularization of tumors. *Sci Am* 234 58-73 (1976).

[45] Folkman J, Angiogenesis in cancer, vascular, rheumatoid and other disease. *Nature Medicine* **1** pp. 27-31 (1995).

[46] Folkman J, Fighting cancer by attacking its blood supply. *Scientific American* **Sept. 1996** 116-119 (1996).

[47] Foster G, Cooke TG, Cooke LD, Stanton PD, Bowie G, Stell PM, Tumour growth rates in squamous carcinoma of the head and neck measured by in vivo BrdUrd incorporation and flow cytometry. *Br J Cancer* **65** pp. 698-702 (1992).

[48] Fowler JF, What next in radiotherapy? *Br J Cancer* **49 (Suppl VI)** 285-300 (1984).

[49] Fowler JF, The phantom of tumor treatment - continually rapid proliferation unmasked. *Radiother Oncol* **22** 156-158 (1991).

[50] Fowler J, Chappell R, Ritter M, Is $\frac{\alpha}{\beta}$ for prostate tumors really low? *Int J Radiat Oncol Biol Phys* **50** 1021-1031 (2001).

[51] Fyles AW, Milosevic M, Wong R, Kavanagh M-C, Pintilie M, Chapman W, Levin W, Manchul L, Keane TJ, Hill RP, Oxygenation predicts radiation response and survival in patients with cervix cancer. *Radiother Oncol* **48** 149-156 (1998).

[52] Goitein M, The probability of controlling an inhomogeneously irradiated tumor. In: *Zink S, ed, Evaluation of treatment planning for particle beam radiotherapy.* 5.8.1-5.8.17 Bethesda, MD: National Cancer Institute (1987).

[53] Hahnfeldt P, Hlatky L, Resensitization due to redistribution of cells in the phases of the cell cycle during arbitrary radiation protocols. *Radiat Res* **145** 134-143 (1996).

[54] Hahnfeldt P, Panigrahy D, Folman J, Hlatky L, Tumor development under angiogenic signaling: A dynamical theory of tumor growth, ttreatment response, and postvascular dormancy. *Cancer Res* **59** 4770-4775 (1999).

[55] Hall E, Radiobiology for the Radiobiologist, 4th edition. J.B. Lippincott Comp., Philadelphia (1994).

[56] Hanahan D, Folkman J, Patterns and emerging mechanisms of the angiogenic switch during tumorgenesis. *Cell* **86** 353-364 (1996).

[57] Hendry JH, Bentzen SM, Dale SG, Fowler JF, Wheldon TE, Jones B, Munro AJ, Slevin NJ, Robertson AG, A modelled comparison of the effects of using different ways for missed treatment days in radiotherapy. *Clinical Oncology* **8** 297-307 (1996).

[58] Höckel M, Knoop C, Schlenger K, Vorndran B, Baußmann E, Mitze M, Knapstein P, Vaupel P, Intratumoral $pO_2$ predicts survival in advanced cancer of the uterine cervix. *Radiother Oncol* **26** 45-50 (1993).

[59] Höckel M, Schlenger K, Aral B, Mitze M, Schäfer U, Vaupel P, Association between tumor hypoxia and malignant progression in advanced cancer of the uterine cervix. *Cancer Res* **56** 4509-4515 (1996).

[60] Horsman MR, Khalil AA, Nordsmark M, Grau C, Overgaard J, Relationship between radiobiological hypoxia and direct estimates of tumor oxygenation in a mouse tumor model. *Radiother Oncol* **28** 69-71 (1993).

[61] Isaacs JT, Coffey DS, Model systems for the study of prostate cancer. In: *Murphy GP ed., Clinics in oncology.* W.B. Saunders, New York 479-498 (1983).

[62] Kerr JFK, Wyllie AH, Currie AR. Apoptosis: A basic biological phenomenon with wide-ranging implications in tissue kinetics. *Br J Cancer* **26** 239-57 (1972).

[63] Kocher M, Treuer H, Reoxygenation of hypoxic cells by tumor shrinkage during irradiation. *Strahlenther Onkol* **171** 219-230 (1995).

[64] Kocher M, Treuer H, Müller R-P, Quantification of tumor reoxygenation during accelerated radiation therapy. *Radiology* **205** pp. 263-268 (1997).

[65] Kocher M, Treuer H, Voges J, Sturm V, Müller R-P, Computer simulation of cytotoxic and vascular effects of radiosurgery in solid and necrotic brain metastases. *Radiother Oncol* **54** 149-156 (2000).

[66] Kutcher GJ, Burman C, Calculation of complication probability factors for non-uniform normal tissue irradiation: The effective volume method. *Int J Radiat Oncol Phys* **16** 1623-1630 (1989).

[67] Kuttig H, Klinische Aspekte. In: *zum Winkel, ed., Wirkungssteigerung der Strahlentherapie maligner Tumoren.* Springer, Heidelberg (1987).

[68] Lambin P, Marples B, Fertil B, Malaise EP, Joiner MC, Hypersensitivity of a human cell line to very low radiation doses. *Int J Radiat Biol* **63** 639-650 (1993).

[69] Landuyt W, Fowler J, Ruifrok A, Stüben G, van der Vogel A, van der Schueren E, Kinetics of repair in the spinal cord of the rat. *Radiother Oncol* **45** 55-62 (1997).

[70] Lea DE, Catcheside DG, The mechanism of the induction by radiation of chromosome aberrations in Tradescantia. *J Genet* **44** 216-245 (1942).

[71] Less JR, Skalak TC, SevickEM, Jain RK, Microvascular architecture in a mammary carcinoma: Branching patterns and vessel dimensions. *Cancer Res* **51** 265-273 (1991).

[72] Lohr F, Wenz F, Flentje M, Peschke P, Hahn EW, Measurement of the proliferative activity of three different sublines of the Dunning rat prostate tumor R3327. *Strahlenther Onkol* **169** 438-445 (1993).

[73] Lyman JT, Complication probability as asessed from dose-volume histograms. *Radiat Res* **104** S13-S19 (1985).

[74] Markus M, Böhm D, Schmick M, Simulation of vessel morphogenesis using cellular automata. *Math Biosciences* **156** 191-206 (1999).

[75] Marples B, Joiner MC, The response of chinese hamster V79 cells to low radiation doses: Evidence of enhanced sensitivity of the whole cell population. *Radiat Res* **133** 41-51 (1993).

[76] Mason RP, Hunjan S, Le D, Constantinescu A, Barker BR, Wong PS, Peschke P, Hahn EW, Antich PP, Regional tumor oxygen tension: Fluorine echo planar imaging of hexafluorobenzene reveals heterogeneity of dynamics. *Int J Radiat Oncol Biol Phys* **42** 747-750 (1998).

[77] McKenna WG, Iliakis G, Weiss MC, Increased $G_2$ delay in radiation-resistant cells obtained by transformation of primary rat embryo cells with the oncogenes v-myc and H-ras. *Radiat Res* **125** 283-287 (1991).

[78] Mehta M, Scrimger R, Mackie R, Paliwal B, Chappell R, Fowler J, A new approach to dose escalation in non-small-cell lung cancer. *Int J Radiat Oncol Biol Phys* **49** 23-33 (2001).

[79] Muschel RJ, Soto DE, McKenna WG, Bernhard EJ, Radiosensitization and apoptosis. *Oncogene* **25** 3359-63 (1998).

[80] Nahum AE, Tait DM, Maximizing local control by customized dose prescription for pelvic tumours. In: *A. Breit (Eds.) Advanced radiation therapy tumor response monitoring and treatment planning* 425-431, Springer-Verlag, Heidelberg (1992).

[81] Niemierko A, Goitein M, Modeling of normal tissue response to radiation: The critical volume model. *Int J Radiat Oncol Biol Phys* **25** 135-145 (1993).

[82] Niemierko A, Goitein M, Implementation of a model for estimating tumor control probability for an inhomogeneously irradiated tumor. *Radiother Oncol* **29** 140-147 (1993).

[83] A.F. Olumi, J.P. Richie, D.J. Schultz, A.V. D'Amico, Calculated volume of prostate cancer identifies patients with clinical stage T1c disease at high risk of biochemical recurrence after radical prostatectomy: A preliminary study. *Urology* **56** 273-277 (2000).

[84] O'Reilly MS, Boehm T, Shing Y, Chen C, Rosenthal RA, Moses M, Lane WS, Cao Y, Sage, EH, Folkman J, Angiostatin: A novel angiogenesis inhibitor that mediates the suppression of metastases by a Lewis lung carcinoma. *Cell* **79** 315-328 (1994).

[85] O'Reilly MS, Holmgren L, Shing Y, Fukai N, Vasios G, Lane WS, Flynn WS, Birkhead JR, Olsen BR, Folkman J, Endostatin: An endogeneous inhibitor of angiogenesis and tumor growth. *Cell* **88** 277-285 (1997).

[86] Paulovich AG, Toczyski DP, Hartwell LH, When checkpoints fail. *Cell* **88** 315-321 (1997).

[87] Peschke P, Hahn EW, Wenz F, Lohr F, Braunschweig F, Wolber G, Zuna I, Wannenmacher M, Differential Sensitivity of three sublines of the rat Dunning tumor system R3327 to radiation and/or local tumor hyperthermia. *Radiat Res* **150** 423-430 (1998).

[88] Quiet CA, Weichselbaum RR, Grdina DJ, Variation in radiation sensitivity during the cell cycle of two human squamous cell carcinomas. *Int J Radiat Oncol Biol Phys* **20** 733-738 (1991).

[89] Raff M, Cell suicide for beginners. *Nature* **396**, 119-122 (1998).

[90] Rao BR, Slotman BJ, Geldof AA, Perez CA, Radiation sensitivity of Copenhagen rat prostatic carcinoma *Int J Radiat Oncol Biol Phys* **20** 981-985 (1991).

[91] Rich T, Allen L, Wyllie AH, Defying death after DNA damage. *Nature* **407** 777-788 (2000).

[92] Ritter MA, Cleaver JE, Tobias CA, High-LET radiations induce a large proportion of non-rejoining DNA breaks. *Nature* **266** 653-655 (1977).

[93] Salling LN, Hoyer M, Overgaard J, The effect of castration on tumor growth rate and cell kinetics in hormone sensitive and hormone insensitive rat prostatic adenocarcinoma. *Scand J Urol Nephrol Suppl* **172** 73-79.

[94] Sauer G, Weber K, Peschke P, Eble J, Measurement of hypoxia using the Comet Assay correlates with preirradiation microelectrode $pO_2$ histography in R3327-AT rodent tumors. *Radiat Res* **154** 439-446 (2000).

[95] Schlicker A, Enzymhemmung, Wirksamkeit und Verteilung freier und trägergebundener Radiosensibilisatoren: 3-Aminobenzamid- und 4-Amino-1,8-naphthalmid-Humanserumalbumin. PhD thesis, Universität Heidelberg (1998).

[96] Secomb TW, Hsu R, Dewhirst MW, Klitzman B, Gross JF, Analysis of oxygen transport to tumor tissue by microvascular networks. *Int J Radiat Oncol Biol Phys* **25** 481-489 (1993).

[97] Sham E, Durand E, Cell kinetics and repopulation mechanisms during multifraction irradiation of spheroids. *Radiother Oncol* **46** 201-297 (1998).

[98] Sham E, Durand RE, Cell kinetics and repopulation parameters of irradiated xenograft tumours in SCID mice: Comparison of two dose-fractionation regimes. *Eur J Cancer* **35** 850 (1999).

[99] Sham E, Durand RE, Repopulation characteristics and cell kinetic parameters resulting from multi-fraction irradiation of xenograft tumors in SCID mice. *Int J Radiat Oncol Biol Phys* **43** 617-622 (1999).

[100] Smith LG, Miller RC, Richards M, Brenner DJ, Hall EJ, Investigation of hyper-sensitivity to fractionated low-dose radiation exposure *Int J Radiat Oncol Biol Phys* **45** 187-191 (1999).

[101] Steel GG, Ed. Basic clinical radiobiology, 2nd edition. *Arnold, London* (1997).

[102] Tannock IF, Oxygen diffusion and the distribution of cellular radiosensitivity in tumors. *Br J Radiol* **45** 515-524 (1972).

[103] Terry NH, Meistrich ML, Roubein LD, Lynch PM, Dubrow RA, Rich TA, Cellular kinetics in rectal cancer. *Br J Cancer* **72** 435-441 (1995).

[104] Thames HD, Withers HR, Peters LJ, Fletcher GH, Changes in early and late radiation responses with altered dose fractionation: Implications for dose-survival relationships. *Int J Radiat Oncol Biol Phys* **8** 219-226 (1982).

[105] Thames HD, An incomplete-repair model for survival after fractionated and continuous irradiations. *Int J Biol* **47** 319-339 (1985).

[106] Thames HD, Hendry JH, Fractionation in Radiotherapy. Taylor & Francis, London (1987).

[107] Turesson I, Thames HD, Repair capacity and kinetics of human skin during fractionated radiotherapy: erythema, desquamation, and telangiectasia after 3 and 5 year's follow-up. *Radiother Oncol* **15** 169-188 (1989).

[108] Thames HD, Bentzen SM, Turesson I, Overgaard M, van den Bogaert W, Time-dose factors in radiotherapy: A review of the human data. *Radiother Oncol* **19** 219-235 (1990).

[109] Travis EL, Tucker SL, Isoeffect models and fractionated radiation therapy (Editorial). *Int J Radiat Oncol Biol Phys* **13** 283-287 (1987).

[110] Webb S, Nahum AE, A model for calculating tumour control probability in radiotherapy including the effects of inhomogeneuos distributions of dose and clonogenic cell density. *Phys Med Biol* **38** 653-666 (1993).

[111] Weinert TA, Hartwell LH. *Science* **241** 317-322 (1988).

[112] Weinert TA, DNA Damage and checkpoint pathways: Molecular anatomy and interactions with repair. *Cell* **94** 555-558 (1998).

[113] Wilson GD, Assessment of human tumour proliferation using BrdUrd - current status. *Acta Oncol* **30** 903-909 (1991).

[114] Wilson GD, Tpot and head and neck cancer: Where are we now? *Anticancer Res* **18** 4801-4806 (1998).

[115] Withers HR, The 4 Rs of radiotherapy. In: *Lett JT, Adler H eds., Advances in radiation biology* **5** 241 (1974).

[116] Withers HR, Mason K, Reid BO, Dubrvsky N, Barkley HT, Brown BW, Smathers JB, Response of mouse intestine to neutrons and $\gamma$ rays in relation to dose fractionation and division cycle. *Cancer* **34** 39-47 (1974).

[117] Withers HR, Taylor JM, Maciejewski B, Treatment volume and tissue tolerance. *Int J Radiat Oncol Biol Phys* **14** 751-759 (1988).

[118] Withers HR, Thames HD, Dose fractionation and volume effects in normal tissues and tumors. *Am J Clin Oncol* **11** 313-329 (1988).

[119] Taylor JM, Withers HR, Zixing H, A comparison of mathematical models for regeneration in acutely responding tissues. *Int J Radiat Oncol Biol Phys* **15** 1389-1400 (1988).

[120] Wouters BG, Brown JM, Cells at intermediate oxygen levels can be more important than the "hypoxic fraction" in determining tumor response to fractionated radiotherapy. *Radiat Res* **147** 541-550 (1997).

[121] Zätterström UK, Kallen A, Wennerberg J, Cell cycle time, growth fraction and cell loss in xenografted head and neck cancer. *in vivo* **5** 137-142 (1991).

## Danksagung

Mein Dank gilt an erster Stelle Frau Dr. Sabine Levegrün, die es mir ermöglicht hat, diese Arbeit zu verwirklichen. Dank schulde ich ihr auch für ihre wohlwollende Unterstützung, ihre konstruktive Kritik und ihre Diskussionsbereitschaft.

Herrn Professor Dr. Wolfgang Schlegel möchte ich für die Möglichkeit der Durchführung meiner Arbeit in seiner Abteilung danken, ebenso wie für seine Ermunterung, an Tagungen und Weiterbildungen teilzunehmen.

Herrn Professor Dr. Josef Bille danke ich für das Interesse an meiner Arbeit und die Bereitschaft, das Zweitgutachten zu übernehmen.

Herrn Dr. Peter Peschke danke ich für seine geduldigen Erklärungen der biologischen Grundlagen. Besonders erwähnen möchte ich seinen Enthusiasmus, der mich immer motiviert hat.

Herrn PD Dr. Dr. Jürgen Debus danke ich für neue Ideen und seine Aufmunterung, die Arbeit fortzusetzen.

Allen Mitarbeitern der Abteilung Schlegel danke ich für die angenehme Atmosphäre und die Hilfsbereitschaft bei der Beantwortung all meiner Fragen. Mein Dank gilt insbesondere Dr. Burkhard Groh, Dr. Andreas Mahr und Simeon Nill für die Hilfe bei der Installation allerlei Versionen von Linux und Windows. Darüberhinaus danke ich meinen Zimmerkollegen Christian Thieke und Christian Scholz für ihre Hilfsbereitschaft und Unterstützung.

Bei Christopher Popp und Oswald Harris King IV möchte ich mich herzlich für ihre Hilfe mit der englischen Sprache bedanken.

Andrea danke ich dafür, dass sie immer für mich da ist.